



Calhoun: The NPS Institutional Archive
DSpace Repository

Theses and Dissertations

1. Thesis and Dissertation Collection, all items

1990-03

Instantaneous Power Spectrum

Stitz, Elizabeth H.

Monterey, California. Naval Postgraduate School

<http://hdl.handle.net/10945/37553>

This publication is a work of the U.S. Government as defined in Title 17, United States Code, Section 101. Copyright protection is not available for this work in the United States.

Downloaded from NPS Archive: Calhoun



Calhoun is the Naval Postgraduate School's public access digital repository for research materials and institutional publications created by the NPS community. Calhoun is named for Professor of Mathematics Guy K. Calhoun, NPS's first appointed -- and published -- scholarly author.

Dudley Knox Library / Naval Postgraduate School
411 Dyer Road / 1 University Circle
Monterey, California USA 93943

<http://www.nps.edu/library>

DTIC FILE COPY

2

NAVAL POSTGRADUATE SCHOOL
Monterey, California

AD-A229 098



THESIS

DTIC
ELECTE
NOV 29 1990
S B D

INSTANTANEOUS POWER SPECTRUM

by

Elizabeth H. Stitz

March 1990

Thesis Advisor:

Ralph D. Hippenstiel

Approved for public release; distribution is unlimited

OP 11 28 508

Unclassified

security classification of this page

REPORT DOCUMENTATION PAGE

1a Report Security Classification Unclassified			1b Restrictive Markings		
2a Security Classification Authority			3 Distribution Availability of Report Approved for public release; distribution is unlimited.		
2b Declassification Downgrading Schedule					
4 Performing Organization Report Number(s)			5 Monitoring Organization Report Number(s)		
6a Name of Performing Organization Naval Postgraduate School		6b Office Symbol (if applicable) EC	7a Name of Monitoring Organization Naval Postgraduate School		
6c Address (city, state, and ZIP code) Monterey, CA 93943-5000			7b Address (city, state, and ZIP code) Monterey, CA 93943-5000		
8a Name of Funding Sponsoring Organization		8b Office Symbol (if applicable)	9 Procurement-Instrument Identification Number		
8c Address (city, state, and ZIP code)			10 Source of Funding Numbers		
			Program Element No	Project No	Task No
			Work Unit Accession No		
11 Title (Include security classification) INSTANTANEOUS POWER SPECTRUM					
12 Personal Author(s) Elizabeth H. Stitz					
13a Type of Report Master's Thesis		13b Time Covered From To		14 Date of Report (year, month, day) March 1990	
				15 Page Count 122	
16 Supplementary Notation The views expressed in this thesis are those of the author and do not reflect the official policy or position of the Department of Defense or the U.S. Government.					
17 Cosati Codes			18 Subject Terms (continue on reverse if necessary and identify by block number)		
Field	Group	Subgroup	Instantaneous Power Spectrum, spectral estimation, nonstationary signal analysis. (R)		
19 Abstract (continue on reverse if necessary and identify by block number)					
<p>The estimation of time varying spectra is a complicated one. The use of classical techniques coupled with the local stationarity assumption is met with only moderate success. Of the many time-frequency distribution functions used in the signal analysis, none present fully satisfactory spectra. The performance of the spectrogram, Instantaneous Power Spectra (IPS) the Wigner-Ville distribution (WD) and various aspects of the Rihaczek distribution (RD) for a variety of signal nonstationarities are compared. WD has the most narrow main-lobes but suffers from spectral cross-terms. IPS, the real part of the RD consistently shows a broadened main-lobe without cross-terms. The squared magnitude of the RD places sharp peaks along the crest of the main-lobe and is otherwise very similar to IPS. The imaginary part of the RD shows a sensitivity to discontinuous frequency changes i.e., frequency shift keying. Keywords: Electromagnetic Spectra, Theses —</p>					
20 Distribution Availability of Abstract <input checked="" type="checkbox"/> unclassified unlimited <input type="checkbox"/> same as report <input type="checkbox"/> DTIC users			21 Abstract Security Classification Unclassified		
22a Name of Responsible Individual Ralph D. Hippenstiel			22b Telephone (include Area code) (408) 646-2768		22c Office Symbol ECHi

DD FORM 1473, 84 MAR

83 APR edition may be used until exhausted
All other editions are obsolete

security classification of this page

Unclassified

Approved for public release; distribution is unlimited.

Instantaneous Power Spectrum

by

Elizabeth H. Stitz
Lieutenant, United States Navy
B.S., Jacksonville University, 1983

Submitted in partial fulfillment of the
requirements for the degree of

MASTER OF SCIENCE IN ELECTRICAL ENGINEERING

from the

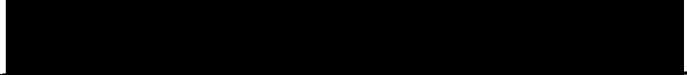
NAVAL POSTGRADUATE SCHOOL
March 1990

Author:




Elizabeth H. Stitz

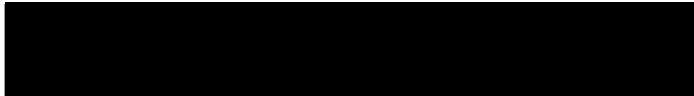
Approved by:



Ralph D. Hippenstiel, Thesis Advisor



Roberto Cristi, Second Reader



John P. Powers, Chairman,
Department of Electrical Engineering

ABSTRACT

The estimation of time varying spectra is a complicated one. The use of classical techniques coupled with the local stationarity assumption is met with only moderate success. Of the many time-frequency distribution functions used in the signal analysis, none present fully satisfactory spectra. The performance of the spectrogram, Instantaneous Power Spectra (IPS) the Wigner-Ville distribution (WD) and various aspects of the Rihaczek distribution (RD) for a variety of signal nonstationarities are compared. WD has the most narrow main-lobes but suffers from spectral cross-terms. IPS, the real part of the RD consistently shows a broadened main-lobe without cross-terms. The squared magnitude of the RD places sharp peaks along the crest of the main-lobe and is otherwise very similar to IPS. The imaginary part of the RD shows a sensitivity to discontinuous frequency changes i.e., frequency shift keying.



Accession For					
NTIS GRA&I	<input checked="" type="checkbox"/>				
DTIC TAB	<input type="checkbox"/>				
Unannounced	<input type="checkbox"/>				
Justification					
By _____					
Distribution/					
Availability Codes					
Dist	<table border="1" style="width: 100%; border-collapse: collapse;"> <tr> <th colspan="2" style="text-align: left; padding: 2px;">Avail and/or Special</th> </tr> <tr> <td style="width: 50%; height: 40px; vertical-align: bottom; padding: 5px;">A-1</td> <td style="width: 50%;"></td> </tr> </table>	Avail and/or Special		A-1	
Avail and/or Special					
A-1					

TABLE OF CONTENTS

I. INTRODUCTION	1
II. SPECTRAL ANALYSIS OF SIGNALS WITH STATIONARY CHARACTERISTICS	2
A. CLASSICAL TECHNIQUES	3
B. MODERN TECHNIQUES	5
III. SPECTRAL ANALYSIS OF SIGNALS WITH DYNAMIC CHARACTERISTICS	7
A. ADAPTING ESTABLISHED STATIONARY TECHNIQUES	7
1. Short-time Fourier Transform	7
2. Spectrogram	8
3. Correlator/Matched Filter	9
4. Autoregressive Modeling	10
B. TIME-DEPENDENT SPECTRAL TECHNIQUES	10
1. The Running Spectrum	11
a. Using Only the Past and Current Data	11
b. Using Only the Future and Current Data	14
c. Using All of the Data	14
2. Instantaneous Power Spectrum (IPS)	15
3. Rihaczek Distribution (RD)	16
4. Wigner-Ville Distribution (WD)	18
5. Time-varying Autoregressive Models	19
IV. COMPARISON OF T-F DISTRIBUTIONS	21
A. THEORETICAL RELATIONSHIPS	21
B. GENERAL PROPERTIES	22
C. RELATIVE PERFORMANCE	23
1. Experimental Analysis	23
2. Highlights of the Analysis	25
3. Test Case Results	35

a. Single-component, Analytic Sinusoid	35
b. Two-component, Analytic Signal	40
c. Single-component, Analytic, Linearly Chirped Signal	40
d. Two Parallel, Analytic, Linearly Chirped Signals	40
e. Single-component, Analytic, Quadratically Chirped Signal	53
f. Multi-component Analytic Signal	53
g. Complex FSK signal	53
D. ALTERNATE METHODS OF COMPUTING IPS	66
V. RECOMMENDATIONS AND CONCLUSIONS	69
APPENDIX A. COMPUTER CODE	71
1. Parameter File	71
2. Spectrogram	72
3. IPS	79
4. PWD	86
5. $ RD_y ^2$	94
APPENDIX B. CROSS IPS	102
APPENDIX C. CUMULANT	106
LIST OF REFERENCES	108
BIBLIOGRAPHY	111
INITIAL DISTRIBUTION LIST	113

LIST OF TABLES

Table 1. DISTRIBUTIONS AND CORRESPONDING KERNEL FUNCTIONS	22
Table 2. GENERAL PROPERTIES OF T-F DISTRIBUTIONS	24
Table 3. LINEAR OPERATIONS	25

LIST OF FIGURES

Figure 1. Behavior of the Spectrogram using an analytic sinusoid	8
Figure 2. Time-Frequency Distribution Models	12
Figure 3. Behavior of Page's distributions using an analytic sinusoid	14
Figure 4. Behavior of Levin's distribution for an analytic sinusoid	15
Figure 5. Behavior of IPS for an analytic sinusoid	16
Figure 6. Behavior of ImRD for an analytic sinusoid	19
Figure 7. Behavior of WD for an analytic sinusoid	20
Figure 8. Amplitude plots of a stationary analytic sinusoid	26
Figure 9. $ImRD_y$ for a stationary, analytic sinusoid	27
Figure 10. Contour plots of a single-component linear chirp	28
Figure 11. Contour plots of a single-component, stationary analytic sinusoid	29
Figure 12. Amplitude plots of a two-component stationary, analytic sinusoid	30
Figure 13. Graph depicting accuracy of stationary component placement	31
Figure 14. $ImRD_y$ for a two-component stationary, analytic sinusoid	31
Figure 15. Relative performance for a single-component linear chirp	32
Figure 16. Graph depicting accuracy of IPS in locating the instantaneous frequency	32
Figure 17. Behavior of IPS_y and PWD for 2 parallel linear chirps	33
Figure 18. $ImRD_y$ of two parallel linear chirps	33
Figure 19. A combination of stationary and nonstationary spectral components ..	34
Figure 20. Contour plots for a complex analytic FSK signal	35
Figure 21. Test signal 1: amplitude plots for Spectrogram, IPS_y and PWD	36
Figure 22. Test signal 1: contour plots for Spectrogram, IPS_y and PWD	37
Figure 23. Test signal 1: amplitude plots for $ RD_y ^2$, $ RD_x ^2$ and $ImRD_y$	38
Figure 24. Test signal 1: contour plots for $ RD_y ^2$, $ RD_x ^2$ and $ImRD_y$	39
Figure 25. Test signal 2: amplitude plots for Spectrogram, IPS_y and PWD	41
Figure 26. Test signal 2: contour plots for Spectrogram, IPS_y and PWD	42
Figure 27. Test signal 2: amplitude plots for $ RD_y ^2$, $ RD_x ^2$ and $ImRD_y$	43
Figure 28. Test signal 2: contour plots for $ RD_y ^2$, $ RD_x ^2$ and $ImRD_y$	44
Figure 29. Test signal 3: amplitude plots for Spectrogram, IPS_y and PWD	45
Figure 30. Test signal 3: contour plots for Spectrogram, IPS_y and PWD	46
Figure 31. Test signal 3: amplitude plots for $ RD_y ^2$, $ RL_y ^2$ and $ImRD_y$	47

Figure 32. Test signal 3: contour plots for $ RD_y ^2$, $ RD_x ^2$ and $ImRD_y$	48
Figure 33. Test signal 4: amplitude plots for Spectrogram, IPS_y and PWD	49
Figure 34. Test signal 4: contour plots for Spectrogram, IPS_y and PWD	50
Figure 35. Test signal 4: amplitude plots for $ RD_y ^2$, $ RD_x ^2$ and $ImRD_y$	51
Figure 36. Test signal 4: contour plots for $ RD_y ^2$, $ RD_x ^2$ and $ImRD_y$	52
Figure 37. Test signal 5: amplitude plots for Spectrogram, IPS_y and PWD	54
Figure 38. Test signal 5: contour plots for Spectrogram, IPS_y and PWD	55
Figure 39. Test signal 5: amplitude plots for $ RD_y ^2$, $ RD_x ^2$ and $ImRD_y$	56
Figure 40. Test signal 5: contour plots for $ RD_y ^2$, $ RD_x ^2$ and $ImRD_y$	57
Figure 41. Test signal 6: amplitude plots for Spectrogram, IPS_y and PWD	58
Figure 42. Test signal 6: contour plots for Spectrogram, IPS_y and PWD	59
Figure 43. Test signal 6: amplitude plots for $ RD_y ^2$, $ RD_x ^2$ and $ImRD_y$	60
Figure 44. Test signal 6: contour plots for $ RD_y ^2$, $ RD_x ^2$ and $ImRD_y$	61
Figure 45. Test signal 7: amplitude plots for Spectrogram, IPS_y and PWD	62
Figure 46. Test signal 7: contour plots for Spectrogram, IPS_y and PWD	63
Figure 47. Test signal 7: amplitude plots for $ RD_y ^2$, $ RD_x ^2$ and $ImRD_y$	64
Figure 48. Test signal 7: contour plots for $ RD_y ^2$, $ RD_x ^2$ and $ImRD_y$	65
Figure 49. IPS	67
Figure 50. Cross spectral analysis of a pulsed linear chirp	104
Figure 51. Cross spectral analysis for a Doppler-shifted linear pulse	105
Figure 52. The cumulant of various analytic signals	107

I. INTRODUCTION

The analysis of stationary spectra is a well-defined problem. Although from a theoretical point of view a true signal spectrum can only be defined in terms of infinite duration data, spectral estimates resulting from the analysis of finite duration data have proven very useful. In the classical estimation problem, one assumes that

- the data length is finite, and
- the random process from which it originates is at least wide-sense stationary.

Armed with these assumptions the behavior of spectra derived in this manner can be accurately predicted. The distortion incurred when analyzing a finite amount of data can be kept at a minimum given the specific estimation problem. But what happens if the signal is not at least wide sense stationary? Signals commonly encountered in the real world are not stationary; they vary in time. Either in amplitude or frequency content or possibly both, experimental data is rarely truly stationary. To better describe the variable random process, a time dependence must be included. All the theoretical results and even the practical application to finite duration data assume that ergodicity applies. Clearly a nonstationary signal is not an ergodic one, i.e., not one whose time average is equivalent to the mean realization.

In the analysis of nonstationary phenomena, there are a certain properties of the resulting spectrum which must be identical to the stationary analog. These properties include an all-positive spectrum and zero energy in the spectrum when the signal is not present. Further constraints must be applied to the spectral behavior along the time dimension, a problem unique to the analysis of nonstationary phenomena. There have been many attempts to adequately model the time-varying behavior of nonstationary spectra. In general it appears that each technique has some advantages and disadvantages. Some appear better-suited to the analysis of a certain class of signals. There has yet to be found a completely satisfactory description of the time dependent spectral estimation problem.

II. SPECTRAL ANALYSIS OF SIGNALS WITH STATIONARY CHARACTERISTICS

The Wiener-Khinchin theorem states that if $x(t)$ is a band limited, wide sense stationary process, then the power spectral density (PSD), is related to the autocorrelation function (ACF), through a Fourier transform

$$P_{xx}(f) = \int_{-\infty}^{\infty} R_{xx}(\tau) e^{-j2\pi f\tau} d\tau, \quad (1)$$

where $R_{xx}(\tau)$ is the ACF. Using the Fourier inversion formula,

$$R_{xx}(\tau) = \int_{-\infty}^{\infty} P_{xx}(f) e^{j2\pi f\tau} df, \quad (2)$$

and evaluating the correlation function at lag zero results in the average power in the process.

$$\lim_{T \rightarrow \infty} \frac{1}{2T} \int_{-T}^T E[|x(t)|^2] dt = \int_{-\infty}^{\infty} P_{xx}(f) df, \quad (3)$$

where E denotes statistical averaging and $2T$ represents the duration of observation. Equations (1) and (2) describe the relationship between the time dependent data and the frequency dependent power spectrum. Equation (3) describes the relationship between a signal's temporal density and its spectral density. The integrand to the left in (3) represents the instantaneous power of the process. The integrand to the right represents the power as a function of frequency. Both can be considered power density functions and both are non-negative everywhere. Because the ACF is always conjugate symmetric, the power spectral density is always real and the average power in the process is always real. [Ref. 1, 2]

Equation (1) can be rewritten,

$$P_{xx}(f) = \lim_{T \rightarrow \infty} E \left[\frac{1}{2T} \left| \int_{-T}^T x(t) e^{-j2\pi f t} dt \right|^2 \right], \quad (4)$$

which implies knowledge of the signal for all time. It is clear that in order to compute the true ACF or PSD, an infinite data set is required. Knowledge of an infinite number of realizations is also implied. These two theoretical constraints are impractical. Realistically one must deduce the power spectrum from a single, finite duration realization. This chapter examines a variety of estimation techniques, noting the specific advantages and limitations inherent in each.

A. CLASSICAL TECHNIQUES

The computation of a power spectrum from one, finite set of data serves as an estimate of the true PSD. One common estimation technique is the periodogram. It can be computed from the data as

$$\hat{P}_{per}(f) = \frac{1}{T} \left| \int_0^T x(t) e^{-j2\pi f t} dt \right|^2, \quad (5)$$

an estimate similar in form to (4), except that limiting and statistical averaging operations have been ignored. This estimate has the advantage of being both real and positive. Examination of the mean and variance of the periodogram spectral estimate best describes its deviation from the true PSD,

$$E[\hat{P}_{per}(f)] = \int_{-\infty}^{\infty} \text{sinc}^2[T(f - \sigma)] P_{xx}(\sigma) d\sigma, \quad (6)$$

where it is apparent that the periodogram represents a smeared version of the true PSD. The smoothing along the frequency axis is caused by the finite observation interval.

Increasing the observation interval T narrows the main lobe of the sinc^2 function, thereby minimizing the smoothing effect of the convolution in (6). The variance, on the other hand, is not so accommodating. [Ref. 3]

The variance of the periodogram spectral estimate for white Gaussian noise is a constant, with a standard deviation on the order of the mean. With so great a variance, the utility of the periodogram as described by (5) is questionable. One technique used to make this estimator more reliable is to compute an average periodogram. This has the effect of scaling down the variance by the number of terms in the average. In practice, since more than one realization is rarely available, this amounts to segmenting the data into shorter intervals, which causes a corresponding increase in the bias and loss of resolution of the estimate.

One variation of the averaged periodogram scheme requires a data window. Looking at smaller segments of the data, the window is applied in an overlapped fashion and subsequent processing results in a series of periodograms that tend to be correlated and hence statistically dependent. Consequently, the actual reduction in variance will generally be less than the number of terms in the average. Still another variation requires the data be prewhitened. This has the effect of reducing spectral bias, which is a problem compounded by the averaging process. [Ref. 3]

Increasing the data length increases the resolution of the periodogram. An improvement in variance can be realized if, instead of a periodogram, one uses a Blackman-Tukey spectral estimator. This estimator is derived from a biased ACF estimate,

$$\hat{R}_{xx}(\tau) = \frac{1}{2T} \int_{-T}^T x(t)x^*(t+\tau)dt, \quad (7)$$

where T is the duration of the data interval. Taking the Fourier transform of a windowed version of (7),

$$\begin{aligned} \hat{P}_{BT}(f) &= \int_{-\infty}^{\infty} w(\tau) \hat{R}_{xx} e^{-j2\pi f\tau} d\tau \\ &= \int_{-\infty}^{\infty} W(f-\sigma) \hat{P}_{per}(\sigma) d\sigma, \end{aligned} \quad (8)$$

leads to an improvement in variance. The type of window indicated by (8) should be capable of enhancing the spectral characteristics of interest [Ref. 4]. An unavoidable

loss in fine spectral detail is the price paid to improve the variance of the spectral estimate. Here $2L$ and T are the durations of the lag window and the total data observation respectively. The variance of the Blackman-Tukey estimator is

$$\text{Var}[\hat{P}_{BT}(f)] \approx \frac{3L}{2T} P_{xx}^2(f), \quad (9)$$

versus

$$\text{Var}[\hat{P}_{Per}(f)] \approx P_{xx}^2(f) \quad (10)$$

for the periodogram. [Ref. 3]

Classical techniques are reliable but have limited resolution and/or a poor variance. One assumes that the data is zero before and beyond the observation interval. This assumption causes the resulting spectral estimates to deviate from the true PSD. Using modern techniques, this type of error can be minimized. There are however, other limitations to consider.

B. MODERN TECHNIQUES

Modern spectral estimation techniques rely on linear filter theory. Parametric modeling provides the foundation for many modern spectral estimation procedures. Rather than assuming the data to be zero beyond some arbitrary interval, parametric models assume statistical knowledge of the underlying process. The data is assumed to be composed of sinusoids in white noise. The model should accurately estimate filter coefficients for some linear filter whose output, when driven by white noise, is the available time data and hence has a spectrum exactly like that of the signal in question. The power spectral density for such an output is

$$P_{xx}(f) = |H(f)|^2 \sigma_n^2. \quad (11)$$

It is assumed that the transfer function, $H(f)$, can be written as a rational polynomial and that the coefficients of the polynomial are the necessary filter coefficients with σ_n^2 the variance of the driving noise. Often the resonances of a particular random process are of interest. In this case an autoregressive (AR) model can be sufficient.

AR modeling of spectra is the most popular modeling method. By solving a set of linear equations, accurate estimates of the parameters can be determined. Selection of an AR model results in an all-pole filter, hence the apparent high resolution. Selection of model order, p , determines the number of poles in the filter, which determines the

number of peaks in the spectral estimate. Once the coefficients $\{a(i)\}_{i=1}^p$ are known, the AR spectral estimator becomes

$$\hat{P}_{AR}(f) = \frac{1}{\left| 1 + \sum_{i=1}^p a(i)e^{-j2\pi fi} \right|^2}. \quad (12)$$

The statistics of the AR spectral estimator are difficult to determine in closed form. Insight can be gained into its reliability by considering the following fundamental assumptions:

- the process to be modeled is truly an AR process,
- the process contains $\frac{p}{2}$ real sinusoids or p complex sinusoids, and
- the coefficients $\{a(i)\}_{i=1}^p$ are accurate.

The choice of model order obviously requires some knowledge of the signal's spectral content. The number of peaks in an AR spectrum, for complex-valued data, is equal to the model order, p . The spectrum, if the number of sinusoids truly present differs from p too much, can be unreliable. Furthermore, if the signal-to-noise ratio is poor, the estimate can be of poor quality. [Ref. 3]

Other parametric models may be more appropriate to the process under investigation. Moving average (MA) models are used when the valleys or zeros of a spectrum are important. Unfortunately, MA models require the solution to a set of nonlinear equations. Although not impossible, it is much more difficult to arrive at accurate parameter estimates. Still another alternative is to use a combination of AR and MA modeling, resulting in what is called an ARMA model.

The minimum variance spectral estimator (Capon's method) provides reasonable estimates without making any assumption about the data composition other than it originates from a wide-sense stationary random process. The classical periodogram spectral estimate can be interpreted as a bank of narrowband filters, all with identical passband characteristics. The minimum variance method is based on an adaptive passband characteristic with the advantage being the ability to adjust sidelobe levels and hence minimize spectral leakage. The resolution of this method lies somewhere between that of the periodogram and that enjoyed by AR estimates. [Ref. 3]

III. SPECTRAL ANALYSIS OF SIGNALS WITH DYNAMIC CHARACTERISTICS

A. ADAPTING ESTABLISHED STATIONARY TECHNIQUES

In Chapter II, classical spectral estimators were found to be limited by the interval of observation, limiting the spectral resolution. A finite duration signal permits only a finite duration correlation estimate, with increasingly poor estimates away from the zero lag. Modern spectral methods have apparent higher resolution but are sensitive to the signal-to-noise ratio (SNR). All the estimators discussed thus far assume the data to be at least wide-sense stationary. The analysis of nonstationary phenomena complicates the estimation problem.

A wide-sense nonstationary process is one whose statistics or parameters vary with time [Ref. 5]. The actual nonstationarities of a process may include fluctuating power magnitude, changing frequency content or a combination thereof. There remains the problem of a suitable representation, one which appropriately displays the fluctuation in time and frequency of the instantaneous energy in the signal. To adapt stationary estimation techniques to the nonstationary case, the concept of local stationarity is introduced. A process is considered locally stationary if, over a given interval of time, the process appears to be stationary. Determination of the optimum interval depends upon the most rapidly fluctuating nonstationarity present in the process. If the process is observed overly long, the temporal fluctuations will be smeared. If the interval is unnecessarily short, spectral detail will be lost. A discussion of the more popular methods of nonstationary estimation and their limitations follows.

1. Short-time Fourier Transform

Short-time Fourier analysis is a method whereby the observed signal is segmented into a number of shorter intervals. Each segment is Fourier transformed and then magnitude squared. The resulting spectra are interpreted as cross sections of the true instantaneous spectrum. These cross sections are pieced together sequentially to form an estimate of the true time-varying power spectrum [Ref. 5, 6]. This type of spectrum is called a waterfall display by the signal processing community. Processing sequential sections of data results in a very crude estimate of the nonstationarities as a function of time. Furthermore, using longer segments increases spectral detail but tends to average or broaden the time-dependent fluctuations. An overly short interval will

tend to enhance the detection of the time transient behavior of the process at the expense of spectral resolution.

2. Spectrogram

A modified version of the short-time Fourier transform estimation technique is the spectrogram. It is related in that it uses a real, finite duration, sliding window [Ref. 7] centered at time t . The spectrogram

$$\hat{P}_{Spectrogr.}(f,t) = \left| \int_{-\infty}^{\infty} x(\tau)w(\tau-t)e^{-j2\pi f\tau}d\tau \right|^2, \quad (13)$$

computes a classical estimate of the spectrum for each point in time rather than for contiguous blocks of data (see for example, Figure 1). Similar to the periodogram, this spectral estimate is real and positive everywhere. The reliability of the spectrogram hinges on its ability to represent the signal's energy in the time-frequency plane. Referring back to (3), any suitable time-frequency representation should reduce to $|x(t)|^2$ when the frequency dependence is removed. Likewise, the representation should reduce to $|X(f)|^2$ when the time dependency is removed. Taking a look at the spectrogram's behavior,

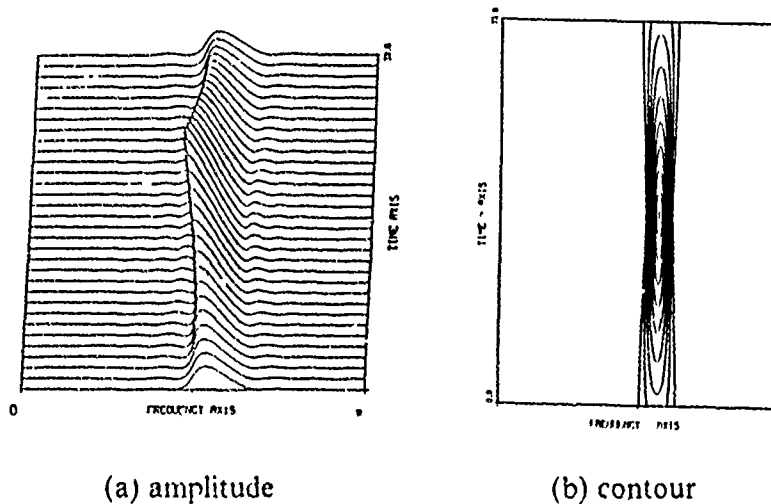


Figure 1. Behavior of the Spectrogram using an analytic sinusoid

$$\int_{-\infty}^{\infty} \hat{P}_{Spectrog.}(f,t) df = \int_{-\infty}^{\infty} |x(\tau)|^2 w^2(\tau - t) d\tau \quad (14)$$

and

$$\int_{-\infty}^{\infty} \hat{P}_{Spectrog.}(f,t) dt = \int_{-\infty}^{\infty} |X(\sigma)|^2 |W(f - \sigma)|^2 d\sigma \quad (15)$$

we note that the estimate is smeared not only in frequency but in time axis as well, a result of the sliding window operation. Another indicator of the spectrogram's reliability can be found by removing both the time and the frequency dependency. The equality expressed in (3) for stationary phenomena should have a nonstationary counterpart. Therefore the volume under the spectrogram should equal the average energy in the signal:

$$\int_{-\infty}^{\infty} \int_{-\infty}^{\infty} \hat{P}_{Spectrog.}(f,t) df dt = \int_{-\infty}^{\infty} \int_{-\infty}^{\infty} |x(\tau)|^2 w^2(\tau - t) d\tau dt. \quad (16)$$

The total signal energy requirement is satisfied only if the average energy of the window is equal to unity. The spectrogram represents a closer approximation of the instantaneous energy changes relative to the short-time Fourier transform; however, temporal smearing is now unavoidable. [Ref. 7, 8]

3. Correlator/Matched Filter

The spectrogram estimator can be implemented as a bank of bandpass filters,

$$\hat{P}_{Corr}(f_o, t) = \left| \int_{-\infty}^{\infty} x(\tau) h_{f_o}^*(t + \tau) d\tau \right|^2. \quad (17)$$

The signal is correlated with

$$h_{f_o}(t) = w(-t) e^{-j2\pi f_o t}, \quad (18)$$

centered at each frequency of interest, f_0 , and weighted according to some general lowpass characteristic, $w(-t)$. The output of each bandpass filter is then magnitude squared, creating an instantaneous energy representation of the signal as a function of time and center frequency. Since the signal is known, the general passband characteristic can be replaced by a matched filter. Commonly used in a radar environment, each filter tests for round trip time delay and Doppler shift. The filters possess finite bandwidth and hence spectral resolution finer than dictated by the filters is impossible. Similarly, resolution along the time axis is limited by the impulse response of the filters [Ref. 5].

4. Autoregressive Modeling

Autoregressive modeling can be adapted to fit slowly-varying spectral characteristics. How slowly the frequency fluctuations must occur depends on the actual process in question. In general, as the signal rotates away from the pole of the AR filter, broadening of the peak results. As the correlation function is time-dependent, suitable accuracy in the AR coefficients requires an embedded time dependence. This particular modification is discussed in a later section.

B. TIME-DEPENDENT SPECTRAL TECHNIQUES

Adapting stationary techniques to the nonstationary case is only marginally successful. There have been many attempts to describe the variation of signal energy, a function of both time and frequency, as a multivariable density. More appropriately, the simultaneous distribution of signal energy in time and frequency requires definition. Each technique has its merits, and each its own peculiarities. In 1966, a generalized phase-space distribution function was proposed [Ref. 9], which can be used to derive many of the more popular time-frequency representations. This generalized distribution function is

$$C(f, t) = \int_{-\infty}^{\infty} \int_{-\infty}^{\infty} \int_{-\infty}^{\infty} \Phi(v, \tau) x(t_1 + \frac{\tau}{2}) x^*(t_1 - \frac{\tau}{2}) e^{j2\pi(vt_1 - vt - f\tau)} dv dt_1 d\tau. \quad (19)$$

The advantage in using the generalized distribution (19) lies in the ability to define properties belonging to all representations derived in this manner. The distribution depends on the choice of $\Phi(v, \tau)$, referred to as the kernel of equation (19). An excellent presentation of the relationship between particular time-frequency distributions and (19) can be found in [Ref. 10] and is summarized below.

1. The Running Spectrum

a. Using Only the Past and Current Data

In 1952 C.H. Page [Ref. 11] derived a time-frequency presentation arguing that one has knowledge of the signal up to and including time t , but its future values are unknown. He defined a running transform, looking backwards over all previous data as

$$X_t^-(f) = \int_{-\infty}^t x(t_1) e^{-j2\pi f t_1} dt_1, \quad (20)$$

where the superscript $(-)$ indicates that the signal has been observed over the interval $(-\infty, t)$. By differentiating the squared magnitude of (20) with respect to time

$$P^-(f, t) = \frac{\delta}{\delta t} |X_t^-(f)|^2, \quad (21)$$

the running spectrum suggested by Page results. Substituting (20) into (21) and computing the partial derivative leads to the following alternate form

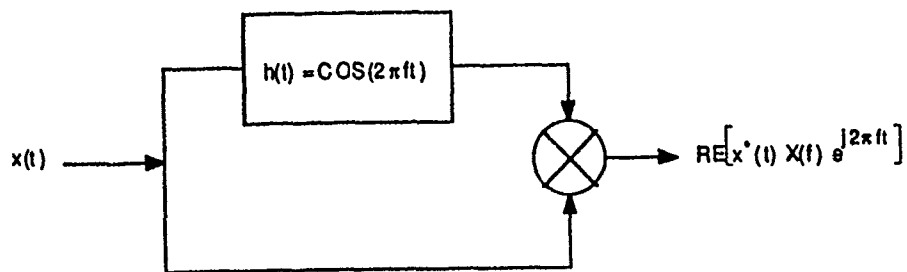
$$P^-(f, t) = 2\text{Re}[x^*(t)X_t^-(f)e^{j2\pi f t}]. \quad (22)$$

M.H. Ackroyd has argued [Ref. 5] that (22) is a finite duration approximation relative to the physical measurement of a true time-varying energy distribution. He suggests that the true time-varying spectrum for a real-valued signal can be expressed as

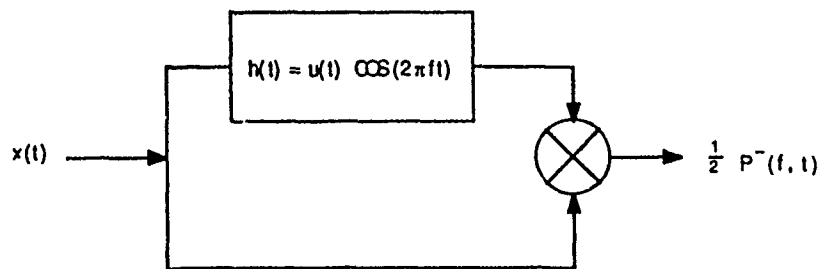
$$x(t)\text{Re}[X(f)e^{j2\pi f t}] = x(t) \int_{-\infty}^{\infty} x(\tau) \cos(2\pi f(t - \tau)) d\tau, \quad (23)$$

the product of the response of a linear filter driven by the signal and the signal itself. The implementation suggested by (23) is shown in Figure 2 (a). It requires an infinitely narrow filter with a noncausal impulse response. To deal with the causality issue, the impulse response is modified by a unit step function,

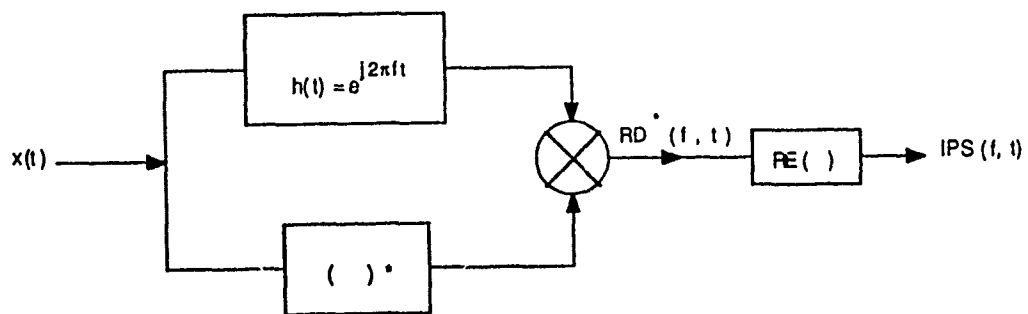
$$\begin{aligned} x(t) \int_{-\infty}^{\infty} x(\tau) u(t - \tau) \cos(2\pi f(t - \tau)) d\tau &= x(t) \int_{-\infty}^t x(\tau) \cos(2\pi f(t - \tau)) d\tau \\ &= x(t) \text{Re}[X_t^-(f) e^{j2\pi f t}] \\ &= \frac{1}{2} P^-(f, t), \end{aligned} \quad (24)$$



(a) Ideal



(b) Page



(c) IPS

Figure 2. Time-Frequency Distribution Models

which is a scaled version of (22). Figure 2 (b) suggests a practical means of measuring a time-dependent spectrum. For ease of comparison, Figure 2 (c) shows the implementation of a distribution discussed on pages 14-15. The distribution of a signal's energy as proposed by Page is limited in spectral resolution; i.e., limited by the finite bandwidth of the filter. It represents an improvement over the spectrogram which was found to be smeared in both the time and frequency directions.

Page's distribution can be generated from the generalized equation (19) using the kernel function

$$\Phi(v, \tau) = e^{j\pi v |\tau|}, \quad (25)$$

which allows one to write (21) in yet another form.

$$\begin{aligned} P^-(f, t) &= \int_{-\infty}^{\infty} \int_{-\infty}^{\infty} \int_{-\infty}^{\infty} e^{j\pi v |\tau|} x(t_1 + \frac{\tau}{2}) x^*(t_1 - \frac{\tau}{2}) e^{j2\pi(v t_1 - v t - f\tau)} dv dt_1 d\tau \\ &= \int_{-\infty}^{\infty} \int_{-\infty}^{\infty} x(t_1 + \frac{\tau}{2}) x^*(t_1 - \frac{\tau}{2}) \left[\int_{-\infty}^{\infty} e^{j2\pi v (t_1 + \frac{|\tau|}{2} - t)} dv \right] e^{-j2\pi f\tau} dt_1 d\tau \\ &= \int_{-\infty}^{\infty} x(t_1 + \frac{\tau}{2}) x^*(t_1 - \frac{\tau}{2}) \delta(t_1 + \frac{|\tau|}{2} - t) e^{-j2\pi f\tau} dt_1 d\tau \\ &= \int_{-\infty}^0 x^*(t) x(t + \tau) e^{-j2\pi f\tau} d\tau + \int_0^{\infty} x(t) x^*(t - \tau) e^{-j2\pi f\tau} d\tau \\ &= 2 \operatorname{Re}[x^*(t) X_t^-(f) e^{j2\pi f t}]. \end{aligned} \quad (26)$$

Equation (26) can be interpreted as the Fourier transform of an estimate of the true time-varying ACF, where

$$\begin{aligned} \hat{R}(t, \tau) &= x^*(t) x(t + \tau) \quad \text{for } -\infty < \tau < 0 \\ &= x(t) x^*(t - \tau) \quad \text{for } 0 < \tau < \infty. \end{aligned} \quad (27)$$

The behavior of this distribution can be seen in Figure 3 (a). As time increases, the amplitude of the signal continually increases and the true frequency location becomes more localized.

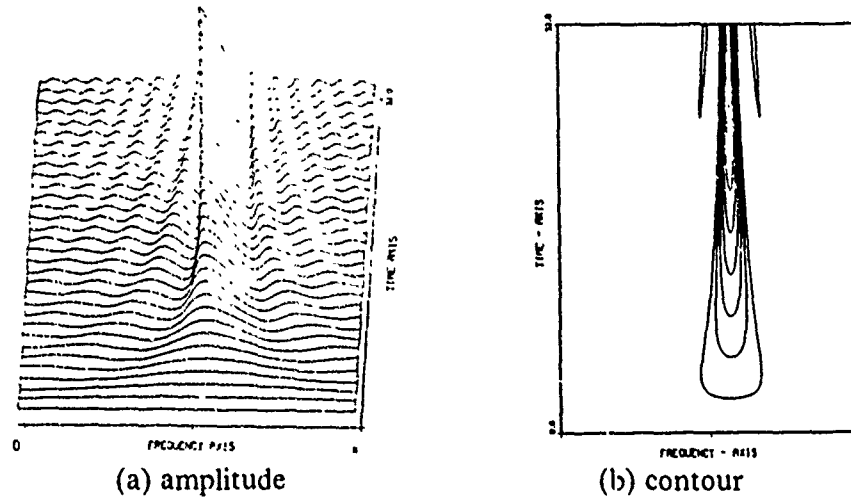


Figure 3. Behavior of Page's distributions using an analytic sinusoid

b. Using Only the Future and Current Data

In 1967, M.J. Levin [Ref. 12] extended the concept of a running transform to include

$$X_t^+(f) = \int_t^\infty x(t_1) e^{-j2\pi f t_1} dt_1, \quad (28)$$

where the superscript (+) indicates only those data values occurring at or later than time t are to be considered. The equivalent to (22) is

$$\begin{aligned} P^+(f, t) &= -\frac{\delta}{\delta t} |X_t^+(f)|^2 \\ &= 2 \operatorname{Re}[x^*(t) X_t^+(f) e^{j2\pi f t}], \end{aligned} \quad (29)$$

and the corresponding kernel function is

$$\Phi(v, \tau) = e^{-j\pi v |\tau|}. \quad (30)$$

The behavior of this future term can be seen in Figure 4. Maximum frequency localization occurs early in the distribution, decreasing continually as time progresses.

c. Using All of the Data

Assigning equal weight to the past and future terms Levin defined the instantaneous power spectrum (IPS) as the average of the two running spectra,

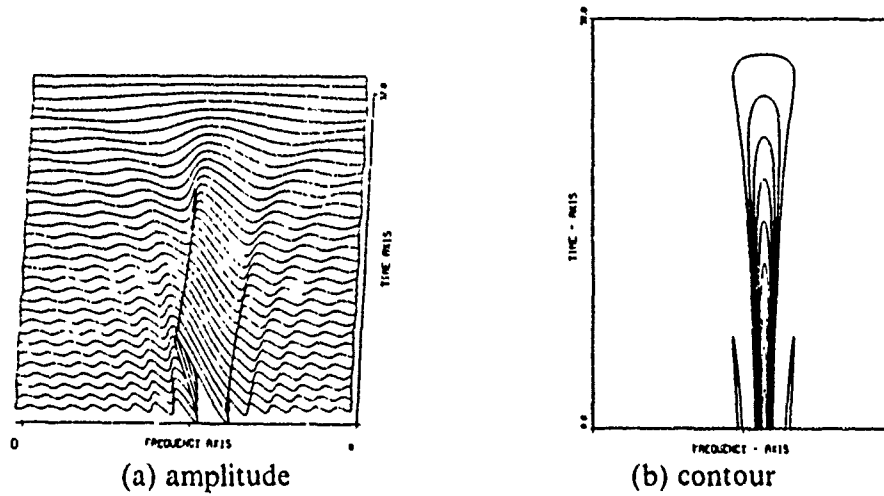


Figure 4. Behavior of Levin's distribution for an analytic sinusoid

$$\begin{aligned}
 IPS(f,t) &= \frac{1}{2} [X_t^+(f) + X_t^-(f)] \\
 &= \text{Re}\{x^*(t)e^{j2\pi ft}[P_t^+(f) + P_t^-(f)]\} \\
 &= \text{Re}[x^*(t)X(f)e^{j2\pi ft}].
 \end{aligned} \tag{31}$$

Figure 2 (c) suggests a method whereby the IPS may be generated. IPS, like Page's distribution, requires a noncausal infinitely narrow bandwidth filter. Modifying the impulse response in order to create a realizable filter [Ref. 13, 14] causes both temporal and spectral smoothing, [Ref. 15, pp. 26-28]. The two terms of IPS can be interpreted as follows. The past term contains information of the energy and energy flow to create the signal up to time t . The future term contains the information about the energy and energy flow of the signal after time t [Ref. 6].

2. Instantaneous Power Spectrum (IPS)

IPS can be derived from the generalized time-frequency distribution using the kernel function:

$$\Phi(\nu, \tau) = \cos(\pi\nu\tau). \tag{32}$$

This kernel, $\cos \pi\nu\tau$, can be formed by taking one half the sum of the kernels for the past and future running spectra. Substituting (32) into (19) and simplifying gives

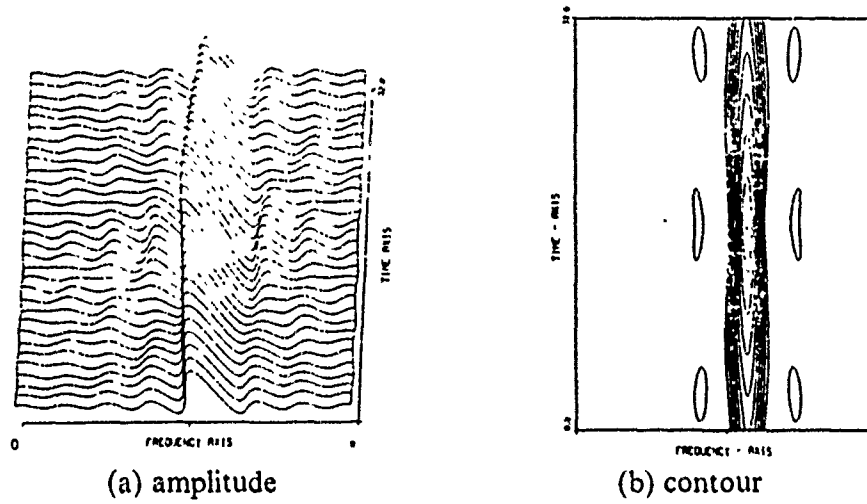


Figure 5. Behavior of IPS for an analytic sinusoid

$$\begin{aligned}
 IPS(f, t) &= \int_{-\infty}^{\infty} \int_{-\infty}^{\infty} \int_{-\infty}^{\infty} \cos \pi v \tau x(t_1 + \frac{\tau}{2}) x^*(t_1 - \frac{\tau}{2}) e^{j2\pi(vt_1 - vt - f\tau)} dv dt_1 d\tau \\
 &= \frac{1}{2} \int_{-\infty}^{\infty} (x(t) x^*(t - \tau) + x^*(t) x(t + \tau)) e^{-j2\pi f\tau} d\tau \\
 &= \text{Re} [x(t) X^*(f) e^{-j2\pi f t}]
 \end{aligned} \tag{33}$$

It is important to note that the terms in the integrand of (33) do not bear a direct relationship to the past and future spectra defined previously by (31). In this form, each term in the sum spans all the data and therefore contains contributions from both running spectra [Ref. 15]. The ACF estimate as defined by IPS is

$$\hat{R}_{IPS}(t, \tau) = \frac{1}{2} (x(t) x^*(t - \tau) + x^*(t) x(t + \tau)) \quad \text{for } -\infty < \tau < \infty. \tag{34}$$

By comparing Figure 3 and Figure 4, the behavior of IPS as shown in Figure 5, demonstrates an improvement in end-point resolution where the main ridge is most narrow at the center of the duration.

3. Rihaczek Distribution (RD)

Derived from physical considerations [Ref. 5,16], the complex energy or Rihaczek distribution (RD) is

$$RD(f, t) = x(t)X^*(f)e^{-j2\pi ft}. \quad (35)$$

Since the real part of a complex function is equal to the real part of the complex conjugate of that function, it is obvious the IPS as defined in (31) is equivalent (33), the real part of (35). This relationship is depicted in figure 2 (c). As yet, there is no satisfactory interpretation of the imaginary part of the Rihaczek distribution (ImRD), although its computation leads to an increase in spectral localization over that of IPS for certain signals. A closer look at the behavior of IPS and RD can be found in Chapter IV.

There exists a relationship between the spectrogram estimate and the RD. Rewriting (13)

$$\begin{aligned} \hat{P}_{Spectrogr.}(f, t) &= \left| \int_{-\infty}^{\infty} x(\tau)w(\tau - t)e^{-j2\pi f\tau} d\tau \right|^2 \\ &= \int_{-\infty}^{\infty} x(\tau)w(\tau - t)e^{-j2\pi f\tau} \int_{-\infty}^{\infty} x^*(t_1)w^*(t_1 - \tau)e^{j2\pi ft_1} dt_1 d\tau \\ &= \int_{-\infty}^{\infty} x(\tau)w(\tau - t)e^{-j2\pi f\tau} \int_{-\infty}^{\infty} X^*(\sigma)W^*(f - \sigma)e^{j2\pi(f - \sigma)t} d\sigma d\tau \quad (36) \\ &= \int_{-\infty}^{\infty} \int_{-\infty}^{\infty} x(\tau)X^*(\sigma)e^{-j2\pi\sigma\tau} w(\tau - t)W^*(f - \sigma)e^{j2\pi(f - \sigma)(\tau - t)} d\sigma d\tau \\ &= \int_{-\infty}^{\infty} \int_{-\infty}^{\infty} RD_x(\sigma, \tau) RD_w(f - \sigma, \tau - t) d\sigma d\tau, \end{aligned}$$

where $RD(f, t)$ is defined by (35). Equation (36) shows the spectrogram to be the 2-D convolution of the RD of the data with the RD of the window function. [Ref. 6, 15]

The complex energy distribution can be generated from (19) using the kernel function

$$\Phi(v, \tau) = e^{j\pi v\tau}. \quad (37)$$

Substituting (37) into (36) results in

$$\begin{aligned}
RD(f, t) &= \int_{-\infty}^{\infty} \int_{-\infty}^{\infty} \int_{-\infty}^{\infty} e^{j\pi v \tau} x(t_1 + \frac{\tau}{2}) x^*(t_1 - \frac{\tau}{2}) e^{j2\pi(v t_1 - v t - f \tau)} dv dt_1 d\tau \\
&= \int_{-\infty}^{\infty} \int_{-\infty}^{\infty} x(t_1 + \frac{\tau}{2}) x^*(t_1 - \frac{\tau}{2}) \left[\int_{-\infty}^{\infty} e^{j2\pi v(t_1 + \frac{\tau}{2} - t)} dv \right] e^{-j2\pi f \tau} dt_1 d\tau \\
&= \int_{-\infty}^{\infty} x(t_1 + \frac{\tau}{2}) x^*(t_1 - \frac{\tau}{2}) \delta(t_1 + \frac{\tau}{2} - t) e^{-j2\pi f \tau} dt_1 d\tau \\
&= \int_{-\infty}^{\infty} x(t) x^*(t - \tau) e^{-j2\pi f \tau} d\tau \\
&= x(t) \lambda^*(f) e^{-j2\pi f t}.
\end{aligned} \tag{38}$$

Equation (38) can also interpreted as the Fourier transform of an ACF estimate, where

$$\hat{R}(t, \tau) = x(t) x^*(t - \tau) \quad \text{for } -\infty < \tau < \infty. \tag{39}$$

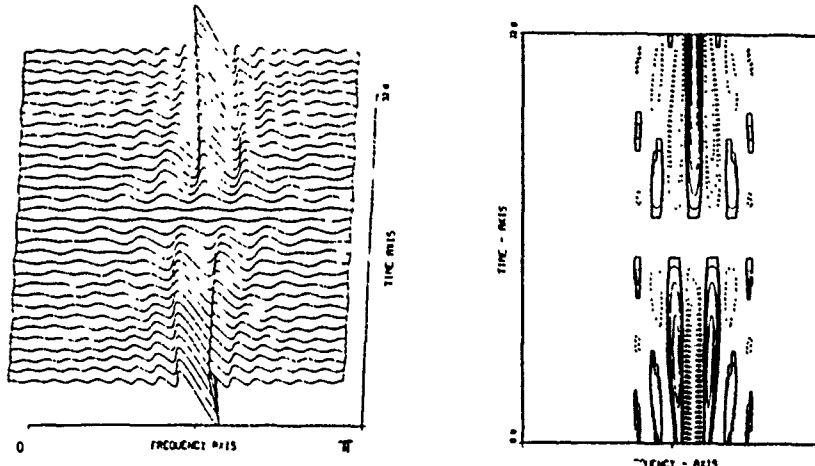
Because RD is complex, this ACF estimate cannot be an even function of the shift variable, τ . This suggests that it is the nonstationarities of a process which lead to an ACF which is partially odd. The behavior of this particular distribution is shown in Figures 5 and 6. Figure 5 shows the behavior of IPS for an analytic sinusoid. IPS is equivalent to the real part of the RD. The imaginary part, shown in Figure 6 (a) and (b), demonstrates an improved sensitivity to rapid changes in signal energy as a function of frequency. The behavior of the RD is discussed in more detail in Chapter IV.

4. Wigner-Ville Distribution (WD)

Originally introduced by Wigner in a quantum mechanical context [Ref. 17] and extended to signal analysis applications by Ville [Ref. 18], the Wigner-Ville distribution (WD) is another valid representation of a signal's energy as a function of both time and frequency. The WD can be generated from (19) using

$$\Phi(v, \tau) = 1 \tag{40}$$

as the kernel function. Substituting (40) into (19) results in



(a) amplitude of imaginary part

(b) contour of imaginary part

Figure 6. Behavior of ImRD for an analytic sinusoid

$$\int_{-\infty}^{\infty} x^* \left(t - \frac{\tau}{2} \right) x \left(t + \frac{\tau}{2} \right) e^{-j2\pi f\tau} d\tau. \quad (41)$$

The WD can be interpreted as the Fourier transform of an ACF estimate defined by

$$\hat{R}_{WD}(t, \tau) = x^* \left(t - \frac{\tau}{2} \right) x \left(t + \frac{\tau}{2} \right) \quad \text{for } -\infty < \tau < \infty. \quad (42)$$

Since the WD is always real, this ACF estimate possesses even symmetry about the point of zero lag. An example of the WD is shown in Figure 7.

5. Time-varying Autoregressive Models

An appropriate AR model for time-varying spectra contains an embedded time dependency. In so doing, the model would be able to track a spectral peak minimizing the effects of broadening. Rewriting equation (12) to reflect this time dependence,

$$\hat{P}_{AR}(f, t) = \frac{1}{\left| \sum_{l=0}^P a_l(t) e^{-j2\pi f t} \right|^2}. \quad (43)$$

where the coefficients are given by

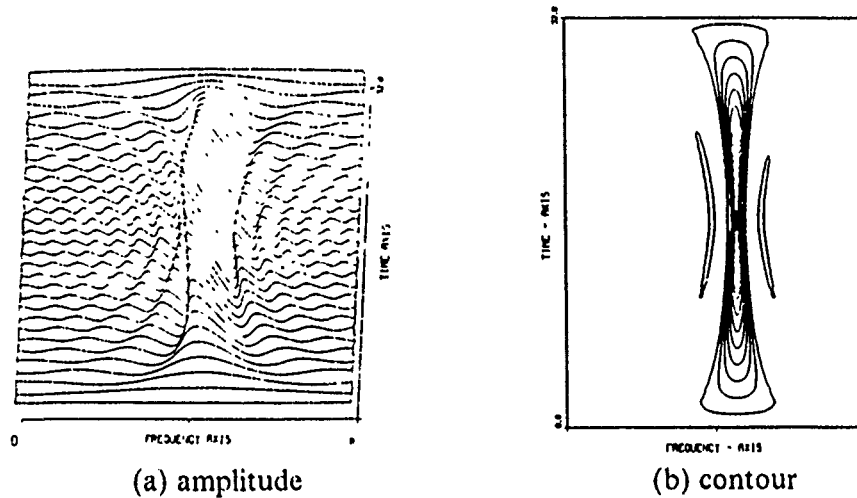


Figure 7. . Behavior of WD for an analytic sinusoid

$$a_i(t) = \sum_{k=0}^K a_{k,i} \phi_k(t). \quad (44)$$

The $\{a_{i,k}\}_{k=0}^K$ represent the weights of a sum of ortho-normal basis functions. An appropriate selection of ortho-normal basis set ideally uses some *a priori* knowledge of the spectrum under investigation. The time-varying AR model order is $(K + 1)P$, requiring the estimation of $(K + 1)$ times more coefficients relative to the stationary analog. Whether one can accurately model the process with a manageable number of coefficients will depend on the particular process at hand.

IV. COMPARISON OF T-F DISTRIBUTIONS

A. THEORETICAL RELATIONSHIPS

Equation (36) shows that the spectrogram can be represented as the 2-D convolution of the RD of the signal with the RD of the window. A similar expression can be derived relating the spectrogram to the WD. Both RD and WD can be derived from the generalized distribution formula (19), as can many other t-f representations. It turns out that any particular distribution, $C(f, t)$, whose kernel function satisfies

$$\Phi(v, \tau) \Phi(-v, \tau) = 1, \quad (45)$$

can be related to the spectrogram in the following way [Ref. 10],

$$\hat{P}_{Spectrograph}(f, t) = \int_{-\infty}^{\infty} \int_{-\infty}^{\infty} C_x(v, \tau) C_w(f - v, \tau - t) dv d\tau, \quad (46)$$

where C_x and C_w are the generalized distribution functions of the signal and window respectively. The spectrogram itself, can be represented through the generalized equation using a kernel function

$$\Phi(v, \tau) = \int_{-\infty}^{\infty} w(t + \frac{\tau}{2}) w^*(t - \frac{\tau}{2}) e^{j2\pi(-v)t} dt. \quad (47)$$

The right side of the equality in equation (47) is the ambiguity function (AF) of the window, $w(t)$ [Ref. 6]. For clarity, the AF is defined as [Ref. 8]

$$\begin{aligned} \chi_{xx}(v, \tau) &= \int_{-\infty}^{\infty} x(t) x^*(t + \tau) e^{-j2\pi vt} dt \\ &= \int_{-\infty}^{\infty} x(t_1 - \frac{\tau}{2}) x^*(t_1 + \frac{\tau}{2}) e^{-j2\pi vt_1} dt_1 \\ &= \left[\int_{-\infty}^{\infty} x(t_1 + \frac{\tau}{2}) x^*(t_1 - \frac{\tau}{2}) e^{j2\pi vt_1} dt_1 \right]^*. \end{aligned} \quad (48)$$

So far, we have seen that a relationship exists between the spectrogram and certain other distribution functions (46), and that the spectrogram can be generated using a modified form of the AF as its kernel. In fact, all the distributions discussed thus far can be related through the AF. Rewriting (19) in a slightly different form,

$$\begin{aligned}
 C(f,t) &= \int_{-\infty}^{\infty} \int_{-\infty}^{\infty} \int_{-\infty}^{\infty} \Phi(v, \tau) x(t_1 + \frac{\tau}{2}) x^*(t_1 - \frac{\tau}{2}) e^{j2\pi(vt_1 - vt - f\tau)} dv dt_1 d\tau \\
 &= \int_{-\infty}^{\infty} \int_{-\infty}^{\infty} \left[\Phi(v, \tau) \int_{-\infty}^{\infty} x(t_1 + \frac{\tau}{2}) x^*(t_1 - \frac{\tau}{2}) e^{j2\pi vt_1} dt_1 \right] e^{-j2\pi(vt + f\tau)} dv d\tau \quad (49) \\
 &= F_{v, \tau} [\Phi(v, \tau)] *_{f, t} F_{v, \tau} \left[\int_{-\infty}^{\infty} x(t_1 + \frac{\tau}{2}) x^*(t_1 - \frac{\tau}{2}) e^{j2\pi vt_1} dt_1 \right],
 \end{aligned}$$

where the generalized distribution is shown to be the 2-D convolution of the double Fourier transform of the kernel with the double Fourier transform of the complex conjugate of the AF. Table 1 lists the distributions discussed thus far, along with their respective kernels.

Table 1. DISTRIBUTIONS AND CORRESPONDING KERNEL FUNCTIONS

Distributions	$C(f,t)$	Kernel - $\Phi(v, \tau)$
Spectrogram	$\left \int_{-\infty}^{\infty} x(\tau) w(\tau - t) e^{-j2\pi f\tau} d\tau \right ^2$	$\int_{-\infty}^{\infty} w(t + \frac{\tau}{2}) w^*(t - \frac{\tau}{2}) e^{-j2\pi v\tau} d\tau$
Page	$\frac{\delta}{\delta t} X_t^- ^2$	$e^{j\pi v} \frac{ v }{2}$
Levin	$-\frac{\delta}{\delta t} X_t^- ^2$	$e^{-j\pi v} \frac{ v }{2}$
IPS	$Re [x(t) X^*(f) e^{-j2\pi f t}]$	$\cos \pi v \tau$
RD	$x(t) X^*(f) e^{-j2\pi f t}$	$e^{-j\pi v \tau}$
WD	$\int_{-\infty}^{\infty} x(t + \frac{\tau}{2}) x^*(t - \frac{\tau}{2}) e^{-j2\pi f \tau} d\tau$	1

B. GENERAL PROPERTIES

Comparing Figure 1 and Figures 3 through 7, it is apparent that the particular kernel function has a tremendous influence on the particular properties of the resulting

distribution. From a spectral point of view, an appropriate t-f spectral representation, hence appropriate kernel function, should ensure certain properties. These properties and corresponding kernel restrictions, if any, are listed in Table 2 below. [Ref. 10, 15, 19, 20, 21]

Of the many distributions discussed, none possess all the desired characteristics. The choice of a particular t-f representation depends on the application at hand. For practical applications, the properties ascribed to the various distributions in Table 2 must be re-evaluated. When using windowed data, the resulting WD is referred to as the pseudo-Wigner distribution (PWD). Similarly modified versions of IPS and RD are indicated by the subscript (y), where $y \equiv x(t)w(t)$ is the product of the data with some window function. Considering the linear operation of filtering, predictable distortion of the signal's true spectrum is encountered. In Table 3 a summary of the effects of four linear operations as they relate to time-dependent spectra is given. [Ref. 10, 15, 19]

C. RELATIVE PERFORMANCE

In the previous section it was shown that the spectrogram is related to certain generalized distributions through a 2-D convolution. It was further shown that any generalized distribution is the 2-D convolution of the double Fourier transform of the kernel function with the double Fourier transform of the complex conjugate of the ambiguity function (AF). All these inter-relationships are interesting. By looking at the relative performance of certain t-f distributions, insight into the benefits and disadvantages characteristic of a specific representation are easily seen. The distributions compared in this section are:

- Spectrogram
- IPS_y
- $ImRD_y$, the imaginary part of RD_y
- 2 linear, magnitude combinations of the real and imaginary parts of RD_y
- PWD,

where the subscript (y) indicates the use of windowed data.

1. Experimental Analysis

Seven test signals, in the absence of noise, were considered. What follows is a brief description of the true time frequency behavior of the analytic signals and a list of the particular processing parameters of the digital implementations. Unless otherwise specified, all data is 128 points in duration, using a 1024 point FFT algorithm. Two

Table 2. GENERAL PROPERTIES OF T-F DISTRIBUTIONS

Properties		kernel constraints	Distributions					
	$x(t) \rightarrow C(f, t)$		1	2	3	4	5	6
Zero energy	$x(t_0) = 0 \rightarrow C(f, t_0) = 0$			x	x	x	x	x
	$X(f_0) = 0 \rightarrow C(f_0, t) = 0$			x	x	x	x	
Time shift	$x(t - t_0) \rightarrow C(f, t - t_0)$	$\Phi(v, \tau)$ must be independent of absolute time and frequency						
Freq. shift	$x(t) e^{j2\pi f_0 t} \rightarrow C(f - f_0, t)$		x	x	x	x	x	x
Positive	$C(f, t) \geq 0 \quad \forall f, t$	$F_{v, \tau}[\Phi(v, \tau)] \geq 0$	x					
Real	$C(f, t) = C^*(-f, t)$	$\Phi(v, \tau) = \Phi^*(-v, -\tau)$	x	x	x	x		x
Marginal in t	$\int_{-\infty}^{\infty} C(f, t) df = x(t) ^2$	$\Phi(v, 0) = 1 \quad \forall v$		x	x	x	x	x
Marginal in f	$\int_{-\infty}^{\infty} C(f, t) dt = X(f) ^2$	$\Phi(0, \tau) = 1 \quad \forall \tau$		x	x	x	x	x
Group delay	$\frac{\int_{-\infty}^{\infty} t C(f, t) dt}{ X(f) ^2} = T_s$	$\Phi(0, \tau) = 0 \quad \forall \tau$ and $\frac{\delta}{\delta \tau} \Phi(v, \tau) _{\tau=0} = 0$				x		x
Instantaneous frequency ¹	$\frac{\int_{-\infty}^{\infty} f C(f, t) df}{ x(t) ^2} = f_i$	$\Phi(v, 0) = 0 \quad \forall v$ and $\frac{\delta}{\delta v} \Phi(v, \tau) _{v=0} = 0$				x		x
Legend:	1 \equiv Spectrogram, 2 \equiv Page, 3 \equiv Levin, 4 \equiv IPS, 5 \equiv RD, 6 \equiv WD							

1 Analytic signals only

Table 3. LINEAR OPERATIONS

	signal	Fourier transform	Distributions		
Ideal	$x(t)$	$X(f)$	$IPS_x(f,t)$	$RD_x(f,t)$	$WD_x(f,t)$
time shift	$x(t - t_0)$	$X(f)e^{-j2\pi ft_0}$	$IPS_x(f,t - t_0)$	$RD_x(f,t - t_0)$	$WD_x(f,t - t_0)$
modulation	$x(t)e^{j2\pi f_0 t}$	$X(f - f_0)$	$IPS_x(f - f_0,t)$	$RD_x(f - f_0,t)$	$WD_x(f - f_0,t)$
windowing	$x(t)w(t)$	$X(f) * W(f)$	$Re [RD_x(f,t) * RD_w(f,t)]$	$RD_x(f,t) * RD_w(f,t)$	$WD_x(f,t) * WD_w(f,t)$
filtering	$x(t) * h(t)$	$X(f)W(f)$	$Re [RD_x(f,t) * RD_h(f,t)]$	$RD_x(f,t) * RD_h(f,t)$	$WD_x(f,t) * WD_h(f,t)$

different Hamming window functions are used depending on the type of spectra analyzed, stationary, non-stationary, or a combination of both. Except for the spectrogram, all distributions have been smoothed in the time direction using a 5-cell box-car average, centered at the time of interest. The test signals used were:

1. Single component., analytic sinusoid computed as $e^{j2\pi \frac{36.3}{128} n}$, where $1 \leq n \leq 128$, using a 127 point Hamming window,
2. Two component., analytic signal computed as $e^{j2\pi \frac{36.3}{128} n} + e^{j2\pi \frac{38.0}{128} n}$, where $1 \leq n \leq 128$, using a 127 point Hamming window,
3. Single component, analytic linearly chirped signal computed as $e^{j2\pi \frac{n}{128} (5.0 - 10(\frac{n}{128}))}$, where $1 \leq n \leq 128$, using a 55 point Hamming window,
4. Two parallel., analytic., linearly chirped signals computed as $e^{j2\pi \frac{n}{128} (5.0 - 10(\frac{n}{128}))} + e^{j2\pi \frac{n}{128} (15.0 - 10(\frac{n}{128}))}$, where $1 \leq n \leq 128$, using a 55 point Hamming window,
5. Single component, analytic, quadratically chirped signal computed as $e^{j2\pi \frac{n}{128} (5.0 - 10(\frac{n}{128})^2)}$, where $1 \leq n \leq 128$, using a 55 point Hamming window,
6. Multi-component signal comprised of a stationary sinusoid, a linearly chirped and a quadratically chirped component computed as $e^{j2\pi \frac{55.0}{128} n} + e^{j2\pi \frac{n}{128} (25.0 - 10(\frac{n}{128}))} + e^{j2\pi \frac{n}{128} (2.0 - 15(\frac{n}{128})^2)}$, where $1 \leq n \leq 128$, using a 55 point Hamming window,
7. Frequency shift keyed (FSK) signal computed as $e^{j2\pi \frac{10.2}{128} n}$, for $1 \leq n < 24$ and $56 \leq n \leq 128$, and $e^{j2\pi \frac{40.3}{128} n}$ for $24 \leq n < 56$, using a 55 point Hamming window.

2. Highlights of the Analysis

To judge the accuracy of component placement along the frequency axis, the performance of *IPS*, is compared to that of the spectrogram in Figure 8. Using a stationary, single component, analytic signal both spectra have good end-point resolution.

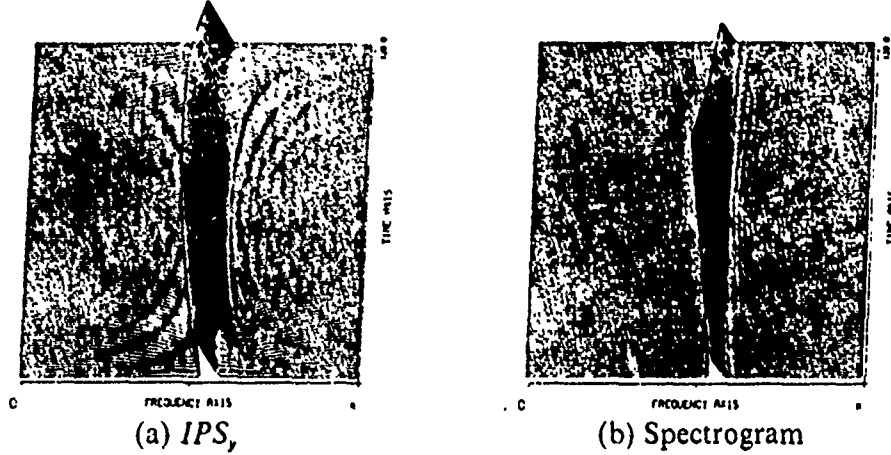


Figure 8. Amplitude plots of a stationary analytic sinusoid

Where the spectrogram presents a stationary spectral ridge with increasing amplitude near the center of the *t-f* plane, *IPS*, shows a fairly constant amplitude, stationary spectral ridge which is wider by comparison. Equation (36) describes the spectrogram as a 2-D convolution of the RD of the signal and the RD of the window. The apparent superior resolution of the spectrogram over *IPS*, the real part of the RD, indicates that the imaginary part of the RD contains some important spectral information. The imaginary part is formed as

$$\text{ImRD}(f, t) = \frac{1}{2} \int_{-\infty}^{\infty} (x(t) x^*(t - \tau) - x^*(t) x(t + \tau)) e^{-j2\pi f\tau} d\tau. \quad (50)$$

Using the kernel function

$$\Phi(v, \tau) = j \sin \pi v \tau, \quad (51)$$

equation (50) can be derived from (19). It is obvious that the kernel for the RD is the sum of the kernels for *IPS* and *ImRD*. As to the behavior of *ImRD*, a windowed version of (50), demonstrates an improved sensitivity to spectral change relative to PWD and

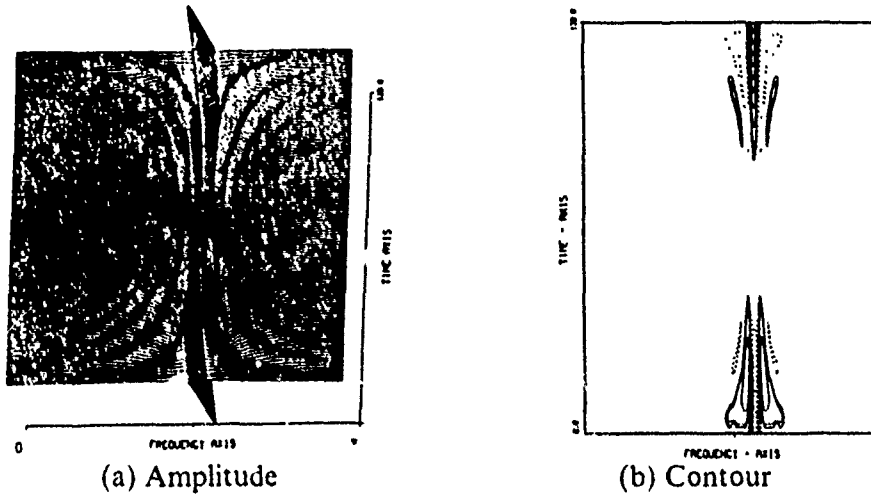


Figure 9. $ImRD_y$ for a stationary, analytic sinusoid

IPS_y , which is shown in Figure 9. In particular, using a single-component, linearly chirped signal, the zero crossings of $ImRD_y$ occur near the true frequency location. In Figure 10, the relative performance between PWD, IPS_y and $ImRD_y$ for a single-component, linearly chirped, analytic signal can be compared. One can see that $ImRD_y$ has an improvement in resolution over that of IPS_y , comparable to that achieved by PWD. Where both IPS_y and PWD rely on the sharpness of the spectral ridge for resolution, $ImRD_y$ relies on the zero crossings.

The $ImRD_y$ has large values near the time of frequency change, with the amplitude approaching zero otherwise. This behavior is clearly demonstrated in Figure 9 where a single component stationary signal is shown to have a nonzero imaginary spectra, greatest in amplitude near the beginning and end of the life of the signal. In Figure 8 (a), IPS_y presents a spectral ridge which, although rounded at the endpoints, grows increasingly more narrow toward the center of time. By forming a linear combination of IPS_y and $ImRD_y$, an overall improvement in spectral resolution for some signals can be achieved. One such linear combination is

$$|RD_y(f,t)|^2 = |IPS_y(f,t)|^2 + |ImRD_y(f,t)|^2. \quad (52)$$

Another combination can be formed taking the difference of magnitudes,

$$|RD_y(f,t)|_-^2 \equiv |IPS_y(f,t)|^2 - |ImRD_y(f,t)|^2. \quad (53)$$

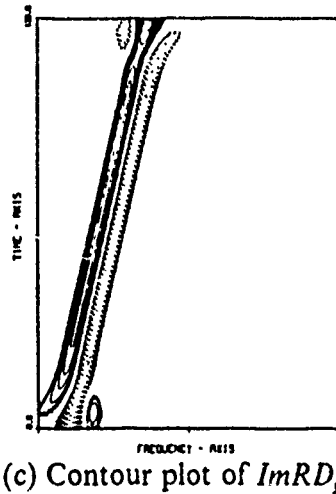
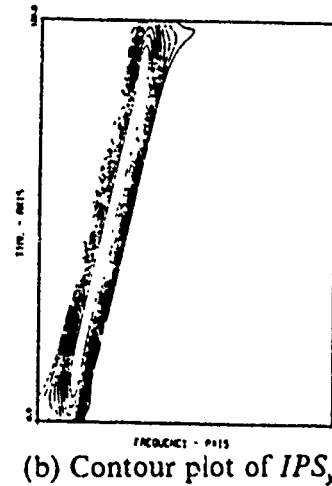
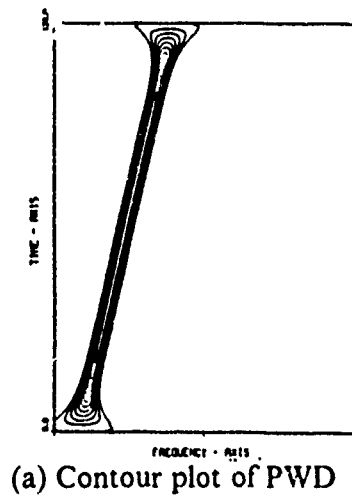


Figure 10. Contour plots of a single-component linear chirp

Equation (52) results in a nonnegative spectrum. Equation (53), unfortunately, can have negative values.

For stationary data, $|RD_1|^2$ represents an improvement in the end-point resolution relative to IPS_1 , as can be seen in Figure 11. When two stationary components are present IPS_1 , $ImRD_1$, and both linear combinations produce modulated spectra. The modulation effect is related to the difference frequency. PWD produces a spectrum having cross-terms midway between the true components. The cross-terms are also related to the difference frequency. The relative behavior of IPS_1 , $|RD_1|^2$ and PWD for

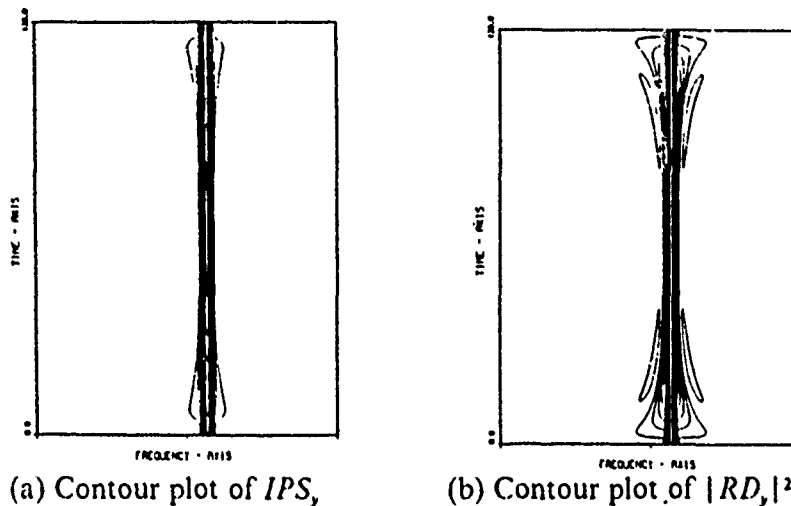


Figure 11. Contour plots of a single-component, stationary analytic sinusoid

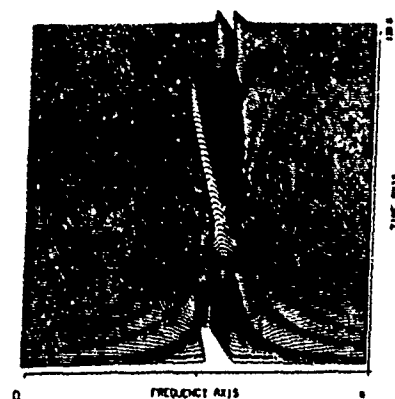
a two-component analytic signal is shown in Figure 12. Using 128 point data sets at a sampling frequency of 128, classical analysis predicts component resolution where the separation is at least 0.89 Hz [Ref. 4]. $IPS,$ is capable of resolving two components separated by at least 1.25 Hz. $|RD,|^2$ and PWD are able to resolve two components separated by at least 0.6 Hz, an improvement over classical analysis. Figure 13 is a graph depicting the relative location of the spectral peaks as a function of frequency and time. $IPS,$, after an initial settling, consistently places the spectral peaks demonstrating a bias which is not symmetric. $|RD,|^2$, similar to $IPS,$, consistently places the spectral peaks but with a symmetric bias. PWD succeeds in making the nearest approximation to the true component locations demonstrating a bias which is not symmetric. The placement of these spectral peaks does not appear to settle at one location as appears to be the case for the Rihaczek-derived distributions; however in a mean-squared error comparison, PWD appears to be superior.

The $ImRD,$ is also capable of resolving two closely-spaced, narrow-band, stationary components. Instead of searching for spectral peaks, $ImRD,$ characteristically detects the zero crossings which yield information in this spectrum. In Figure 14, the behavior of $ImRD,$ using two closely-spaced stationary sinusoids can be seen.

To study the behavior of any spectral estimator of nonstationary phenomena we begin by considering a single-component, linearly chirped, analytic test signal. The relative performance of $IPS,$, $ImRD,$ and PWD was discussed previously, see also Figure 10. The behavior of the two linear magnitude combinations can be seen in Fig-



(a) Amplitude plot of PWD



(b) Amplitude plot of IPS_x



(c) Amplitude plot of $|RD_x|^2$

Figure 12. Amplitude plots of a two component stationary, analytic sinusoid

ure 15. Forming the difference, $|RD_x|^2$ creates a spectral ridge comparable in width to IPS_x , but with a better defined peak. Detection using $|RD_x|^2$ should be thus be improved. Forming the sum, $|RD_x|^2$ completely resolves IPS into its past and future terms, the distributions defined by Page and Levin. Component location using $|RD_x|^2$ requires detection of the minimum occurring between the two resolved ridges, making detection using $|RD_x|^2$ questionable. In the presence of noise, the separation IPS_x into component parts will lead to difficulty in interpretation. The ability of IPS_x to properly locate the instantaneous frequency for a linear chirped signal is shown in Figure 16. The lo-

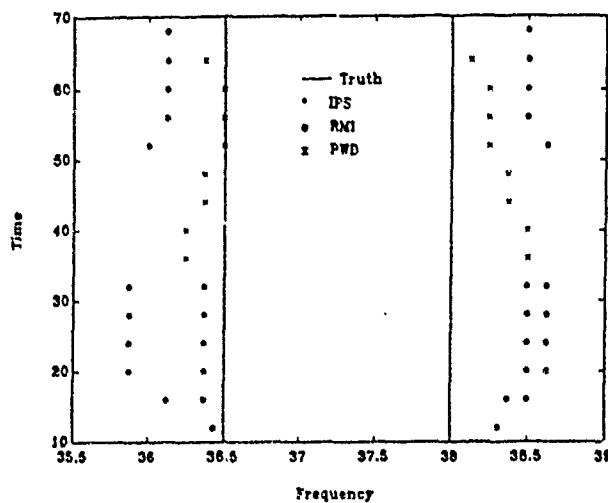


Figure 13. Graph depicting accuracy of stationary component placement

cation of the peaks in IPS , coincide with the true instantaneous spectral locations for a slow chirp. Early in the spectrum, when the future term is dominant, IPS , tends to place the instantaneous frequency higher than truth. On the other hand, late in the spectra when the past term is dominant, IPS , tends to place the instantaneous frequency lower than truth. Doubling the chirp rate results in a greater frequency ambiguity as seen by the two terms which compose IPS . Looking at Figure 16, this is demonstrated by the apparent random placement by IPS , of the spectral peaks, neither the future nor past term seems to be favored as the maximum peak location.

Next, a test signal composed of two, parallel, linearly chirped, analytic signals is considered. The spectra resulting from IPS , and PWD is shown in Figure 17. Similar

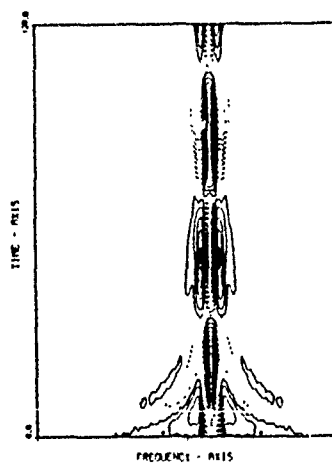


Figure 14. $ImRD$, for a two-component stationary, analytic signal

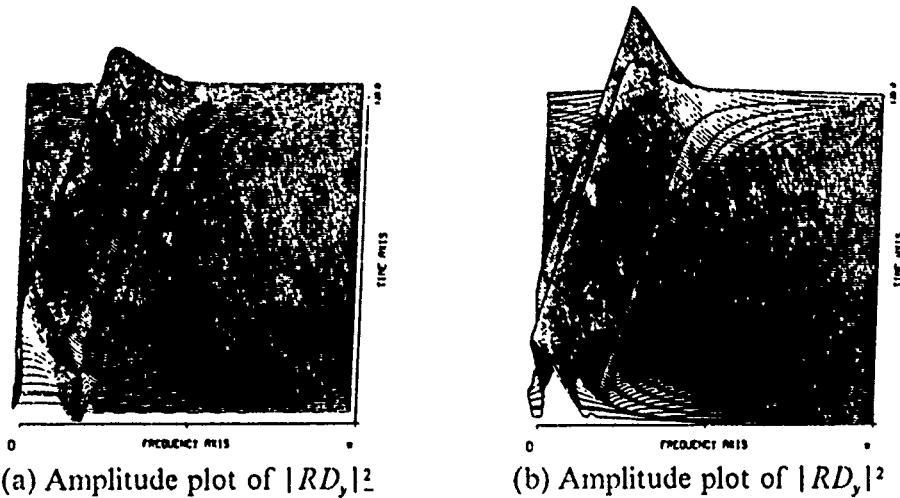


Figure 15. Relative performance for a single-component linear chirp

to the stationary, two-component case, modulation and cross-terms fluctuating at the difference frequency are present in IPS_y and PWD, respectively. Neither of the two linear combinations of magnitudes of the component parts of the Rihaczek distribution, was able to improve on the resolution achieved by IPS_y . Moving from the peaks to the valleys, $ImRD_y$ can be seen to discriminate between the two chirps as a function of the zero crossings. This is demonstrated in Figure 18 where a pattern of zero crossings allows the eye to discern the two components.

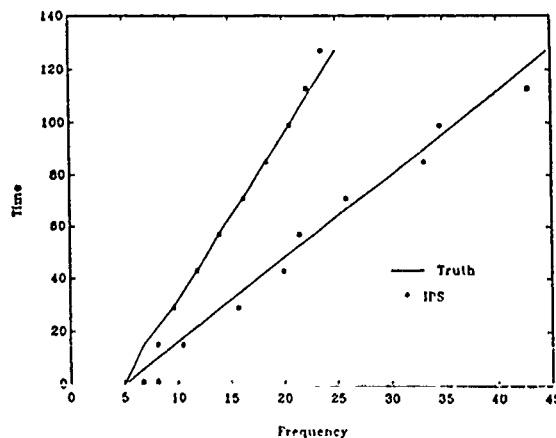
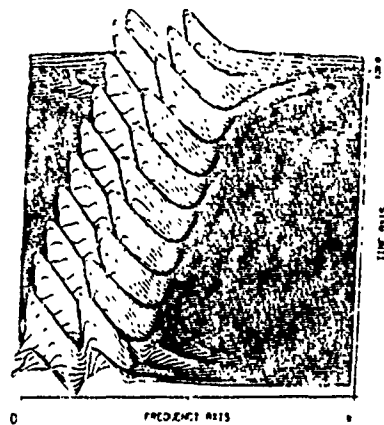


Figure 16. Graph depicting accuracy of IPS in locating the instantaneous frequency



(a) Amplitude plot of IPS_y



(b) Amplitude plot of PWD

Figure 17. Behavior of IPS_y and PWD for 2 parallel linear chirps

Examination of the spectra for more complicated signal suggests a relative ranking in terms of resolution among the different power distributions discussed thus far. The test signal is composed of a high frequency stationary component and two chirped components, one a linear chirp and the other a quadratic chirp. Considering first those spectra which estimate frequency location as the point of maximum power, PWD produces the most narrow ridges; see Figure 19 (a). It suffers from poor end-point resolution and spectral cross-terms. $|RD_y|^2$, seen in Figure 19 (b), produces well-defined periodic peaks along the instantaneous frequency path of the nonstationary components. The stationary component ridge is broadened, with the modulation effect most

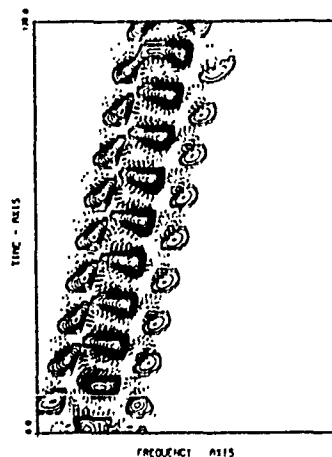
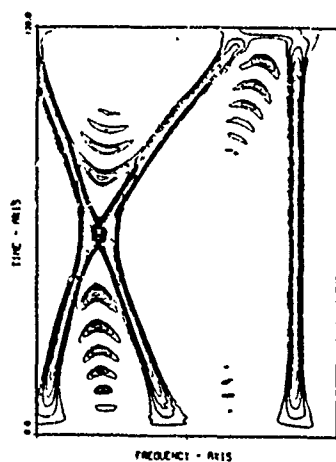
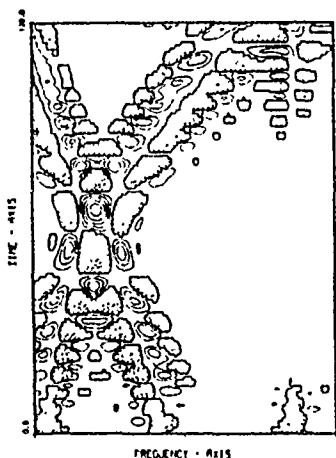


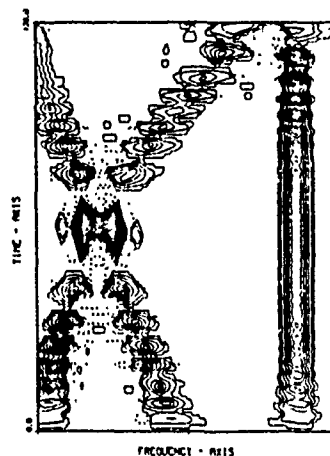
Figure 18. $ImRD_y$ of two parallel linear chirps



(a) PWD



(c) $ImRD_y$



(b) $|RD_y|^2$

Figure 19. A combination of stationary and nonstationary spectral components

apparent near the end-points. $|RD_y|^2$ would be difficult to interpret as it resolves the past and future terms for the nonstationary components. Looking for the zeros, $ImRD_y$, accurately describes the location of the nonstationary components, but provides little information during parts of the stationary signals existence. Again, Figure 19 (c) requires pattern recognition to be able to discern the individual, dynamic components.

Considering a pulsed spectra, such as in FSK modulation, $|RD_y|^2$ presents a narrow ridge with good resolution throughout the duration of each pulse. The ridge width for each pulse in the PWD spectral description is dependent upon the pulse du-

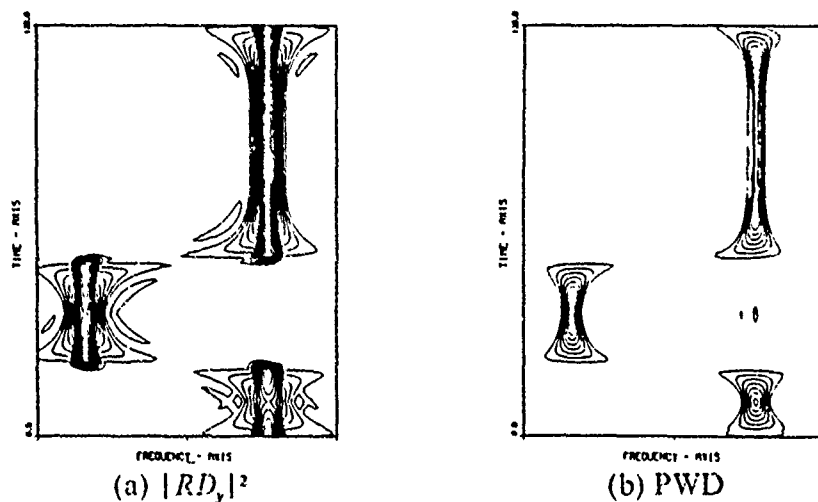


Figure 20. Contour plots for a complex analytic FSK signal

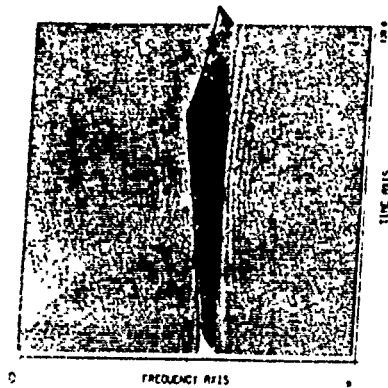
ration. The longest pulse showing the most narrow ridge, one which is slightly more narrow than what is found with $|RD_y|^2$. These two spectra are shown in Figure 20. PWD has a slow build up and decay at the ends of each pulse. There appears to be a trade-off between the width of a spectral ridge and end-point resolution.

3. Test Case Results

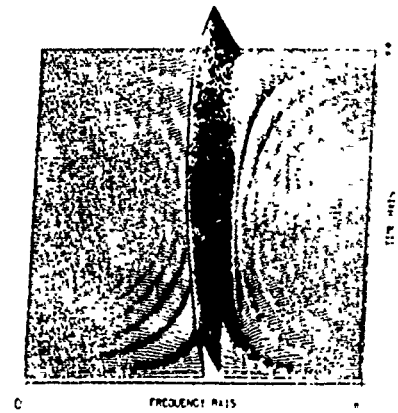
Figures of the spectral distributions resulting from the six t-f representations are contained in this section. They are ordered by the type of test signal under analysis.

a. Single-component, Analytic Sinusoid

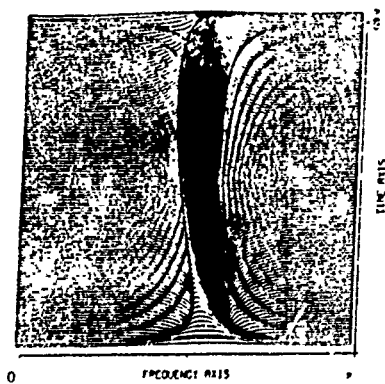
Using the spectrogram as the reference, the resolution ability of five additional t-f distributions is compared in Figure 21 - Figure 24. PWD presents a well-defined spectral ridge near mid-plane, but suffers from a sluggish built-up and decay. IPS_y presents a wider main-lobe relative to PWD which is compensated somewhat by an increase in end-point resolution. $|RD_y|^2$ provides the best end-point resolution, maintaining constant amplitude throughout the plane. $|RD_y|^2$ proves to be more sluggish than PWD and $ImRD_y$ demonstrates an improved response near the time of spectral change.



(a) Spectrogram



(b) IPS_y



(c) PWD

Figure 21. Test signal 1: amplitude plots for Spectrogram, IPS_y , and PWD

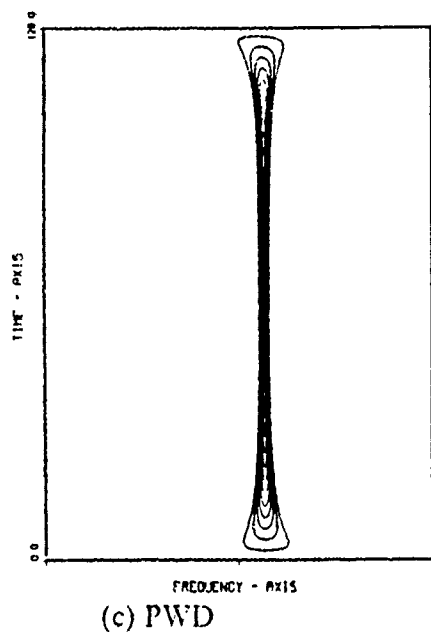
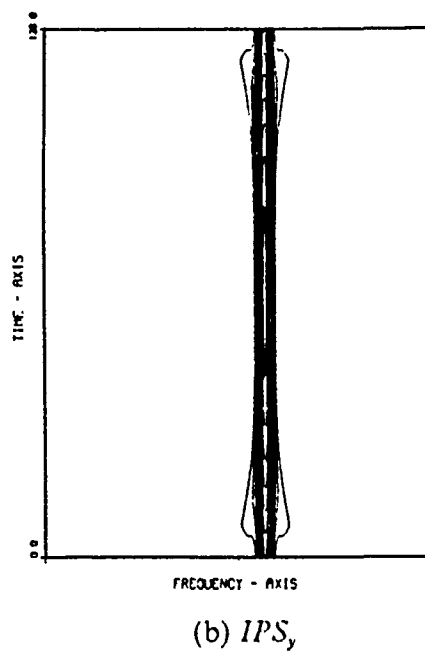
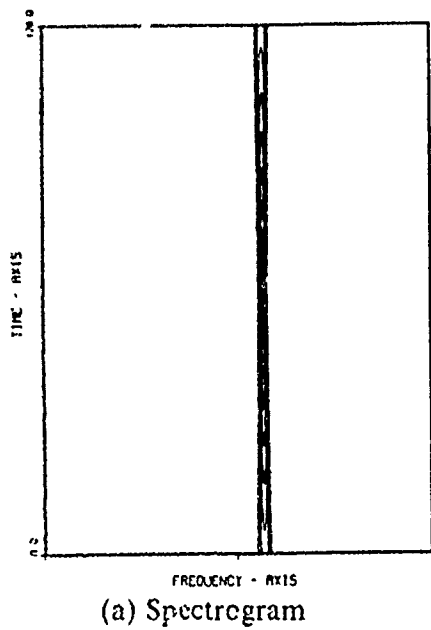
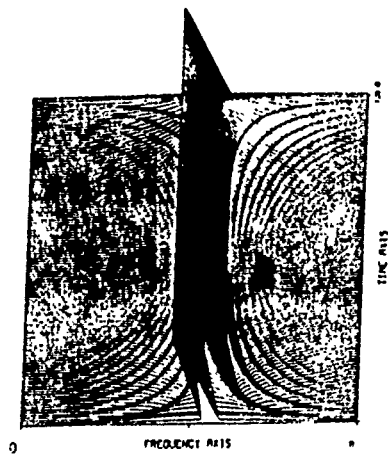
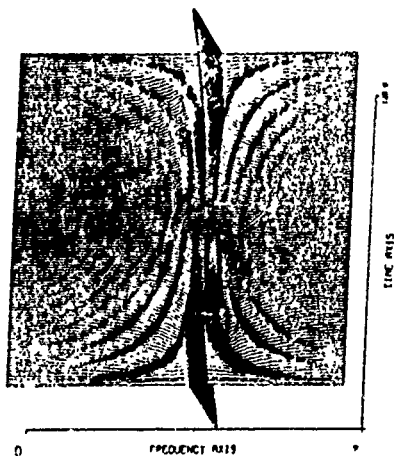


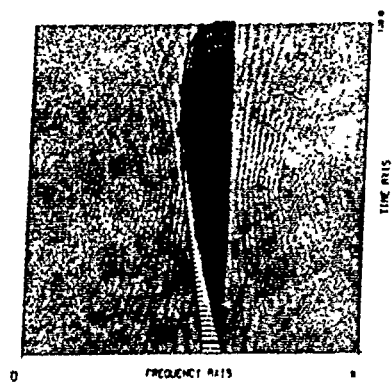
Figure 22. Test signal 1: contour plots for Spectrogram, IPS_y , and PWD



(a) $|RD_y|^2$

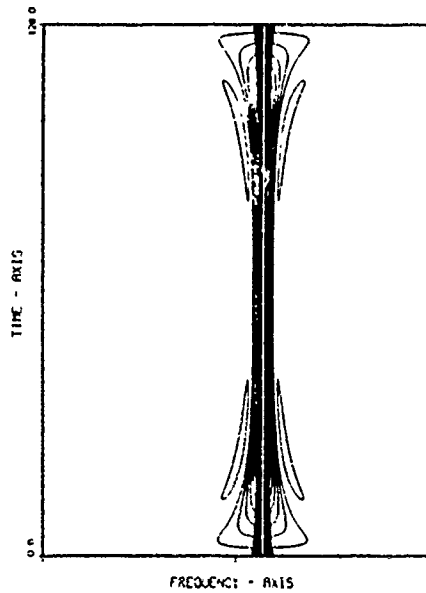


(c) $ImRD_y$

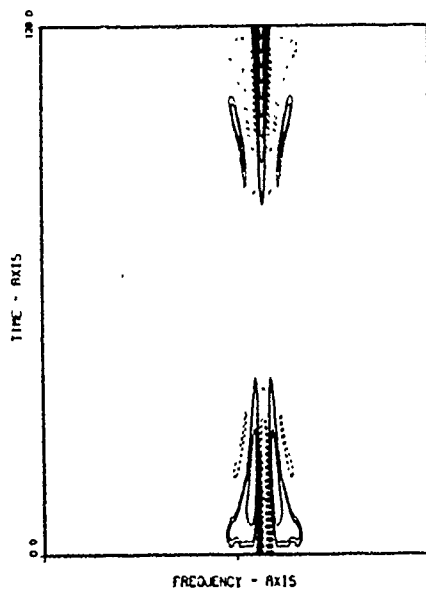


(b) $|RD_x|^2$

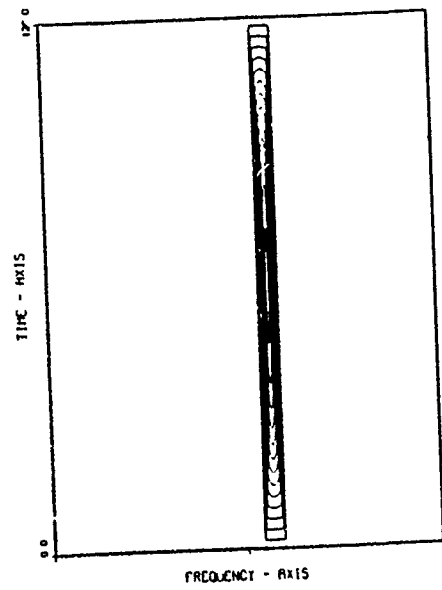
Figure 23. Test signal 1: amplitude plots for $|RD_y|^2$, $|RD_x|^2$ and $ImRD_y$



(a) $|RD_y|^2$



(c) $ImRD_y$



(b) $|RD_x|^2$

Figure 24. Test signal 1: contour plots for $|RD_y|^2$, $|RD_x|^2$ and $ImRD_y$

b. Two-component, Analytic Signal

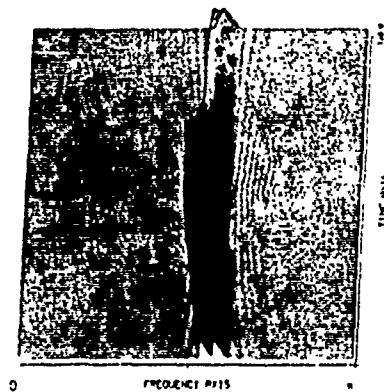
The spectrogram and all five t-f distributions shown in Figure 25 through Figure 28 display a distorted spectrum. This distortion exists for a minimal time in the spectrogram estimate. In the case of IPS_y and PWD, the distortion is related to the difference frequency. IPS_y shows modulation of each component; PWD contains additional peaks oscillating at the difference frequency. The modulation effect characteristic of Rihaczek-derived distributions makes the spectra using $|RD_y|^2$ and $ImRD_y$ extremely difficult to interpret. $|RD_y|^2$ suffers also from the modulation effect; however, this magnitude combination enhances resolution relative to IPS_y , making it easier to detect the presence of two components.

c. Single-component, Analytic, Linearly Chirped Signal

The inadequacy of assuming local stationarity is clearly demonstrated in Figure 29 (a) and Figure 30 (a) for the spectrogram, where the slope of the instantaneous frequency line is distorted and broadened near the end-points. Both IPS_y and PWD shown in Figure 29 (b) and (c), and Figure 30 (b) and (c) maintain a better approximation to the instantaneous frequency slope near the end-points. Characteristically, IPS_y presents a broadened spectral ridge whereas PWD decays to zero at the start and stop of the chirp. Looking at the spectrum created by $|RD_y|^2$, Figure 31 (a) and Figure 32 (a), the future and past terms which make up the RD are clearly visible. Although $|RD_y|^2$ is an all-positive distribution possessing many desirable properties, this characteristic resolution quality makes it difficult to interpret more complicated spectra. The two remaining Rihaczek-related distributions represent improvements over the ability of IPS_y to pinpoint the instantaneous frequency as a function of time. $|RD_y|^2$ in Figure 31 (b) and in Figure 32 (b) shows a spectral ridge more narrow than that for PWD. $ImRD_y$, while accurately locating the instantaneous frequency, requires the detection of zero crossings. For particular detection schemes information thus provided may be appropriate.

d. Two Parallel, Analytic, Linearly Chirped Signals

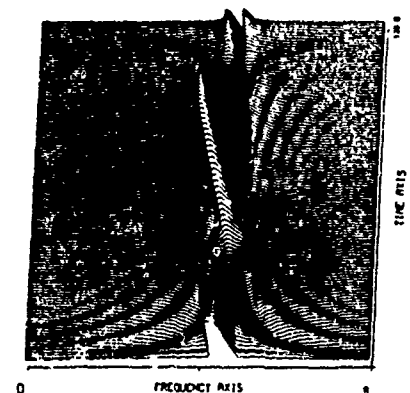
For this test signal, the spectrogram spectral estimates shown in Figure 33 (a) and Figure 34 (a) is unacceptable. The comments made previously concerning the distortion in the spectra when two closely spaced, parallel, stationary components can also be applied to this nonstationary case (see Figure 33 - Figure 36). In the case of PWD, not only are cross-terms oscillating between the true components present but the spectral ridges themselves show the effects of modulation. $|RD_y|^2$ and $ImRD_y$ do not show promise as estimation tools for closely-spaced frequency components. It is



(a) Spectrogram



(c) PWD



(b) IPS_y

Figure 25. Test signal 2: amplitude plots for Spectrogram, IPS_y , and PWD

interesting to note however, that $|RD_y|^2$ resolve the past and future terms for each component similar to the behavior shown in Figure 31 (a). $|RD_y|^2$ shows very sharp peaks along the modulated instantaneous frequency lines of the two linear chirps. Because these peaks are the largest peaks in the plane, $|RD_y|^2$ from a practical view point, appears to be more suited toward the analysis of this type of signal than PWD where the cross terms periodically represent the dominant peak.

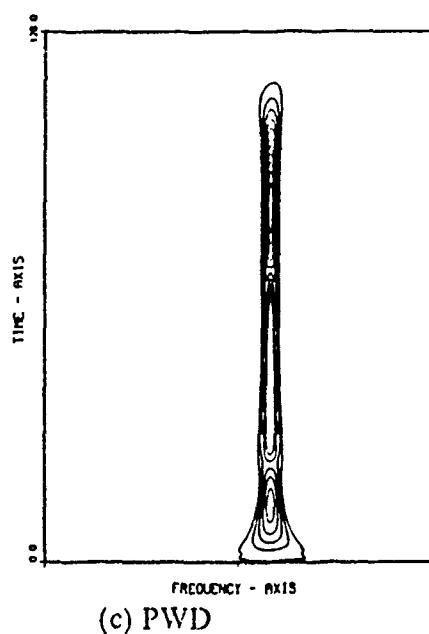
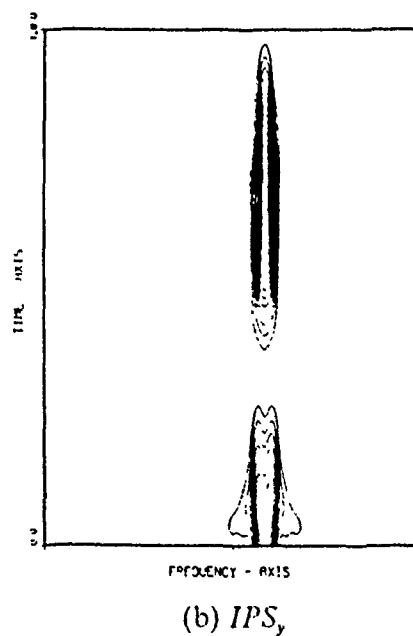
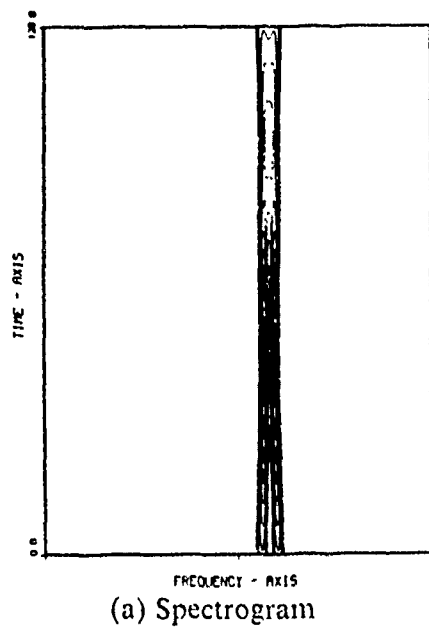
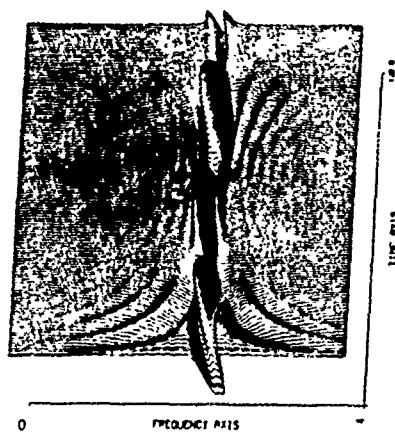


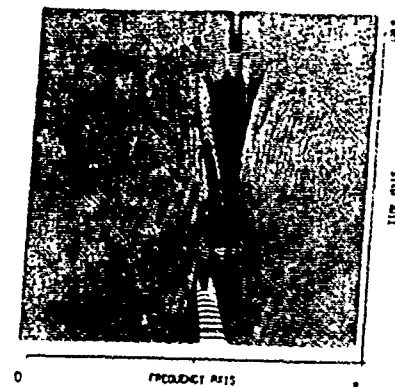
Figure 26. Test signal 2: contour plots for Spectrogram, IPS_y , and PWD



(a) $|RD_y|^2$

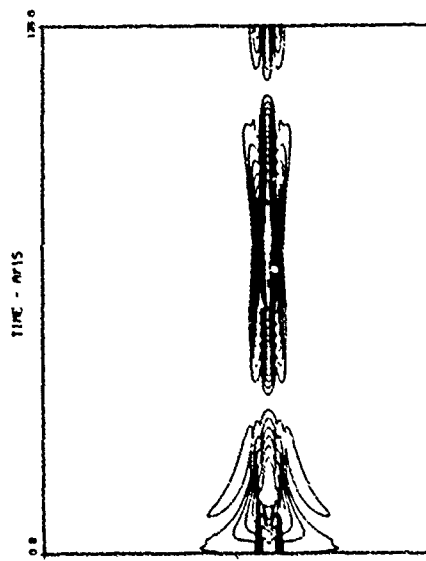


(c) $ImRD_y$

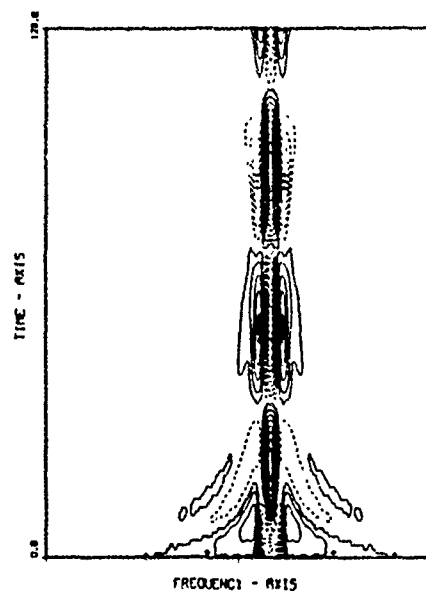


(b) $|RD_y|^2$

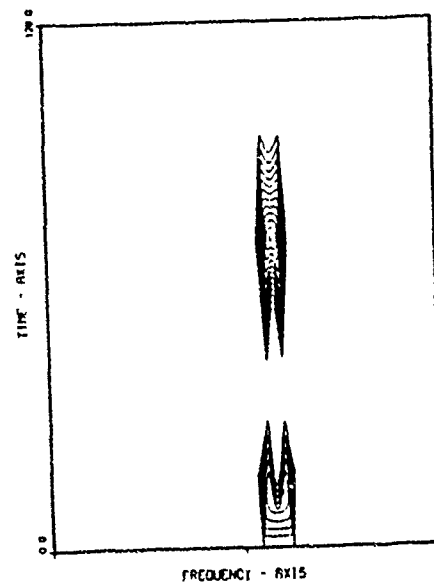
Figure 27. Test signal 2: amplitude plots for $|RD_y|^2$, $|RD_y|^2$ and $ImRD_y$



(a) $|RD_y|^2$



(c) $ImRD_y$



(b) $|RD_y|^2$

Figure 28. Test signal 2: contour plots for $|RD_y|^2$, $|RD_y|^2$ and $ImRD_y$.

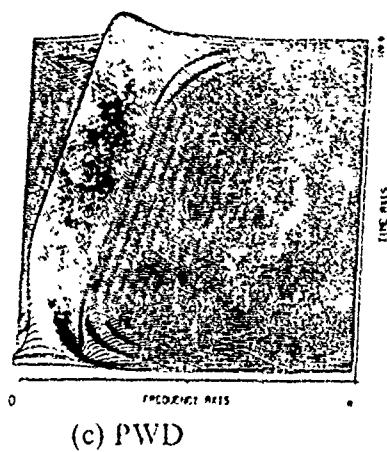
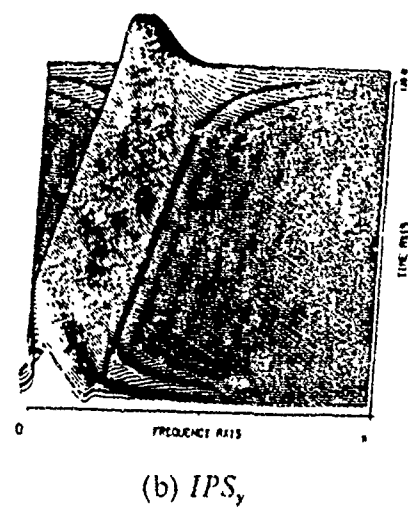
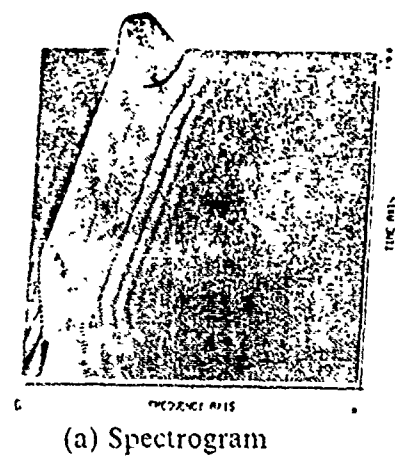


Figure 29. Test signal 3: amplitude plots for Spectrogram, IPS_y , and PWD

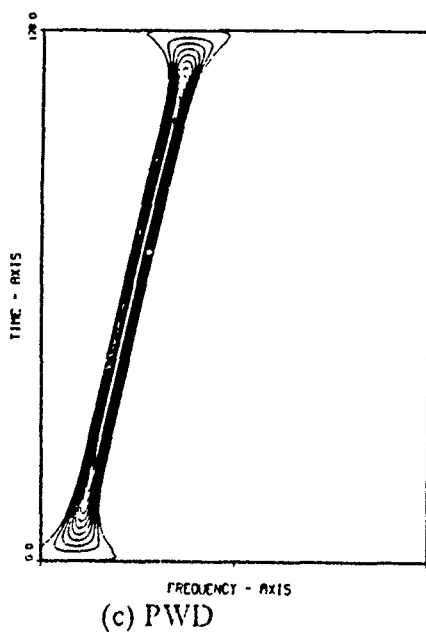
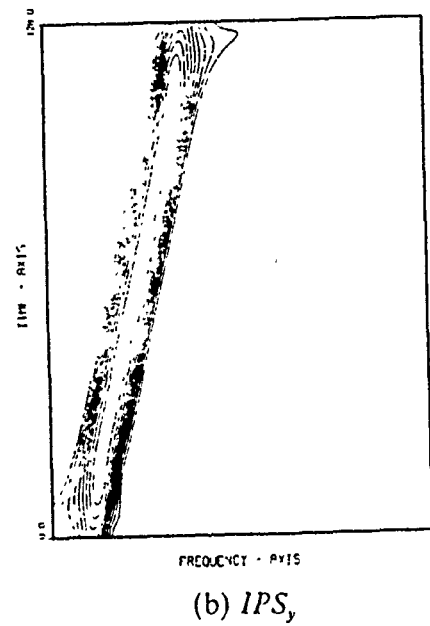
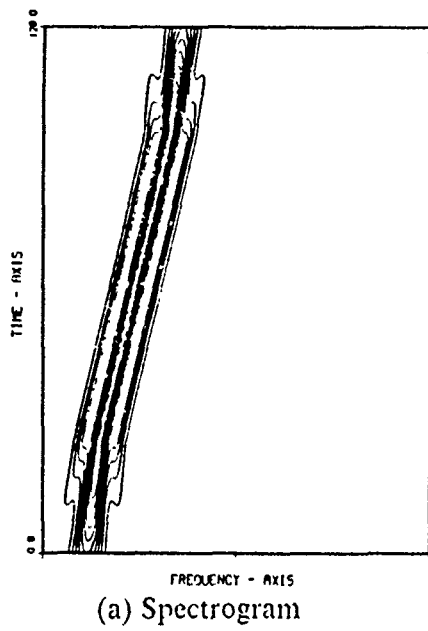
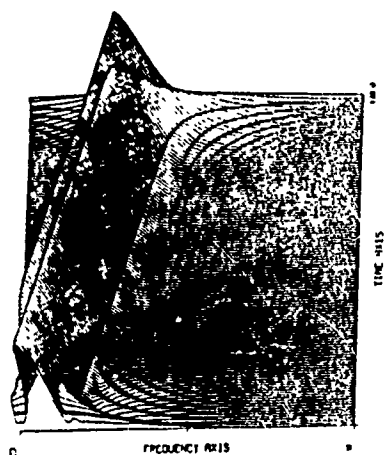
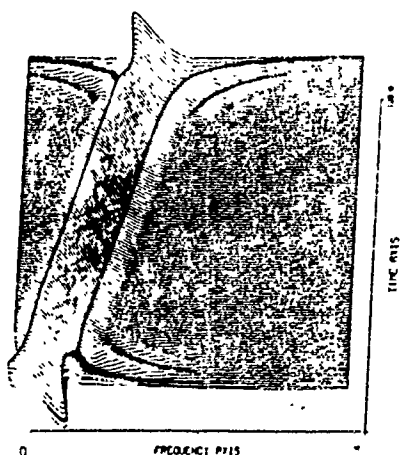


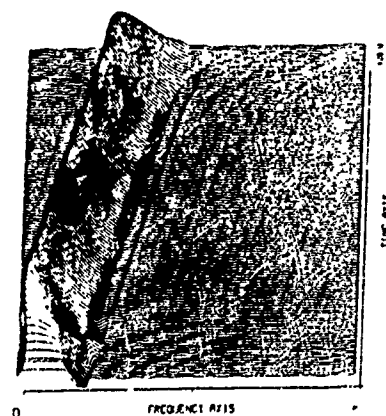
Figure 30. Test signal 3: contour plots for Spectrogram, IPS_y , and PWD



(a) $|RD_y|^2$

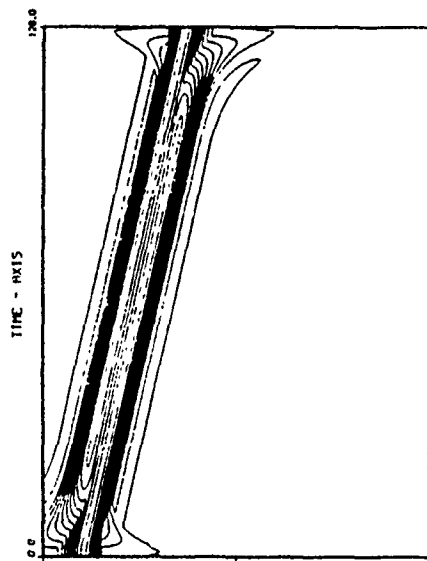


(c) $ImRD_y$

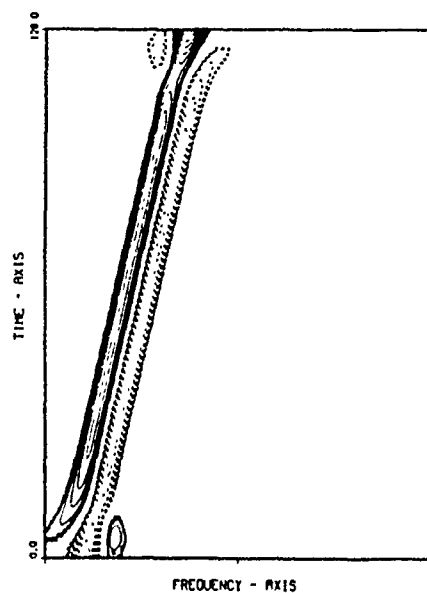


(b) $|RD_y|^2$

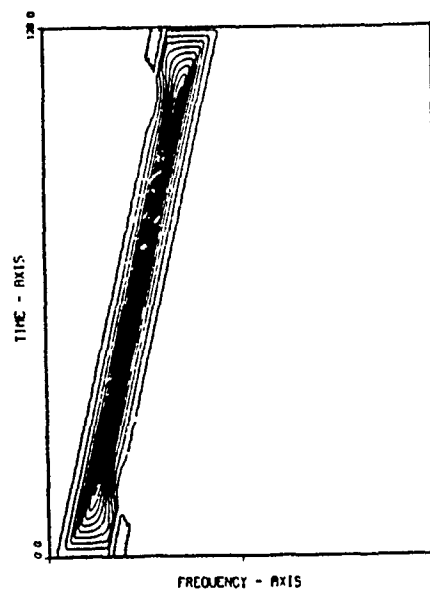
Figure 31. Test signal 3: amplitude plots for $|RD_y|^2$, $|RD_y|^2$ and $ImRD_y$



(a) $|RD_y|^2$

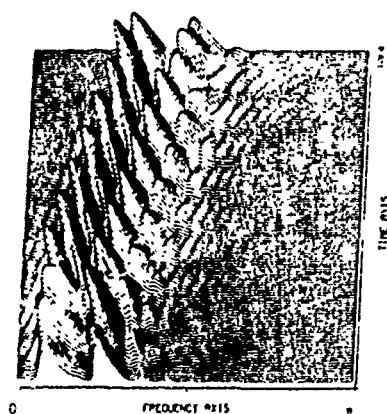


(c) $ImRD_y$

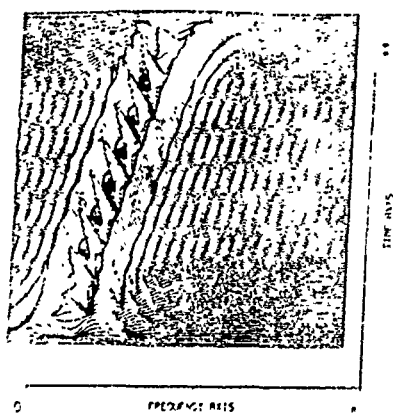


(b) $|RD_y|^2$

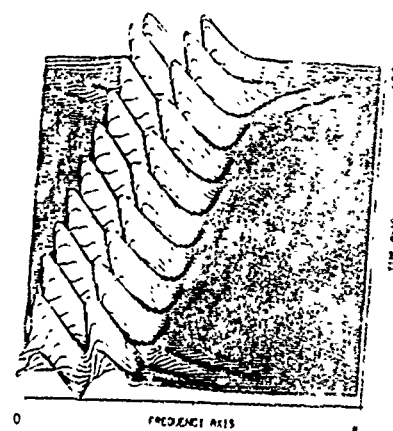
Figure 32. Test signal 3: contour plots for $|RD_y|^2$, $|RD_y|^2$ and $ImRD_y$



(a) Spectrogram

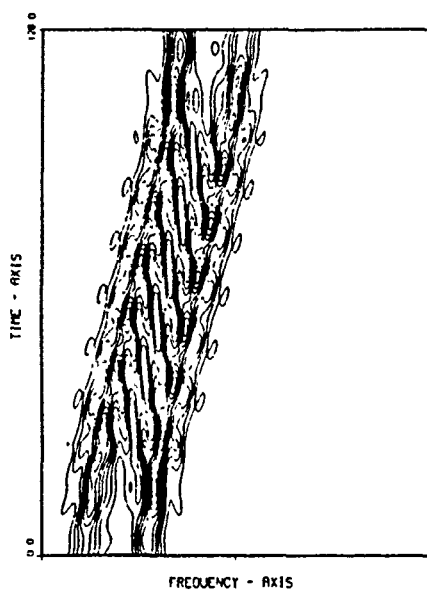


(c) PWD

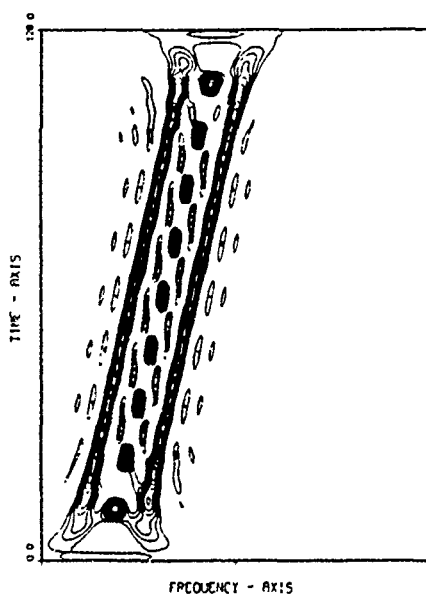


(b) IPS_y

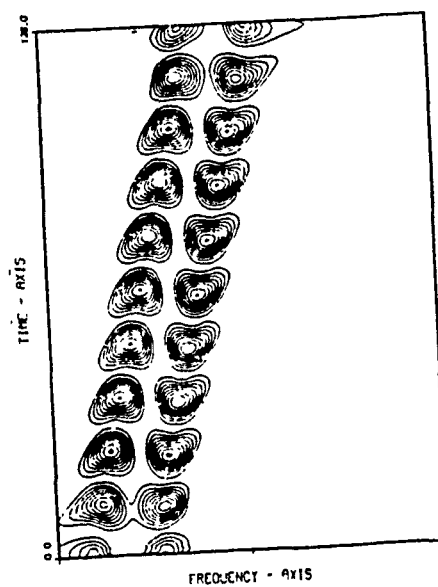
Figure 33. Test signal 4: amplitude plots for Spectrogram, IPS_y , and PWD



(a) Spectrogram



(c) PWD



(b) IPS_y

Figure 34. Test signal 4: contour plots for Spectrogram, IPS_y and PWD

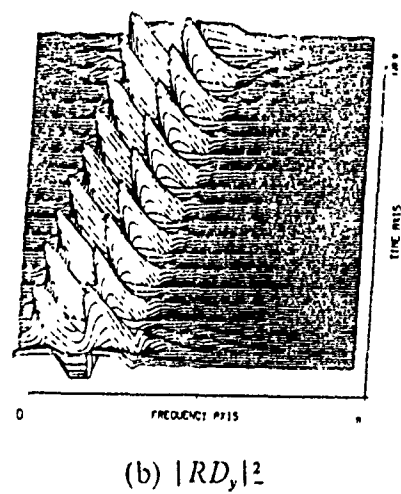
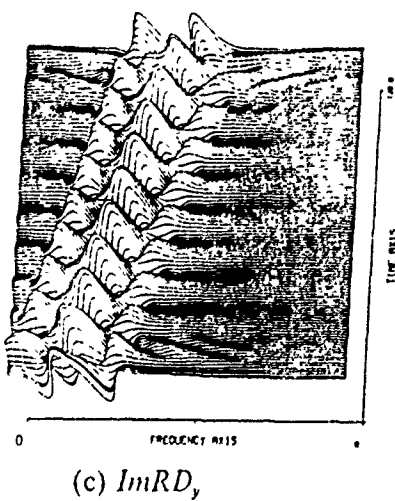
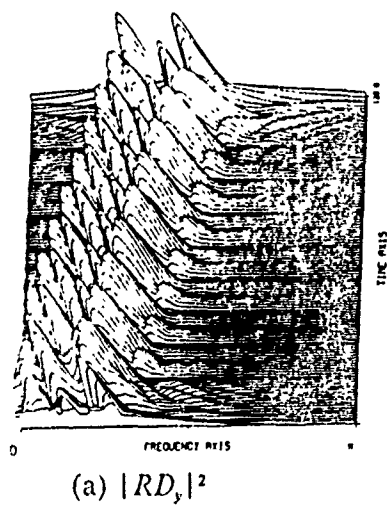
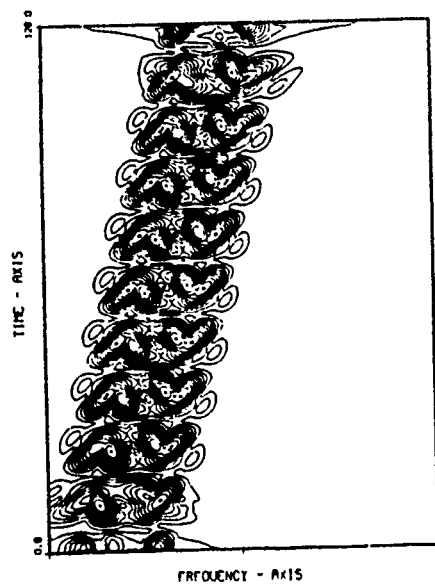
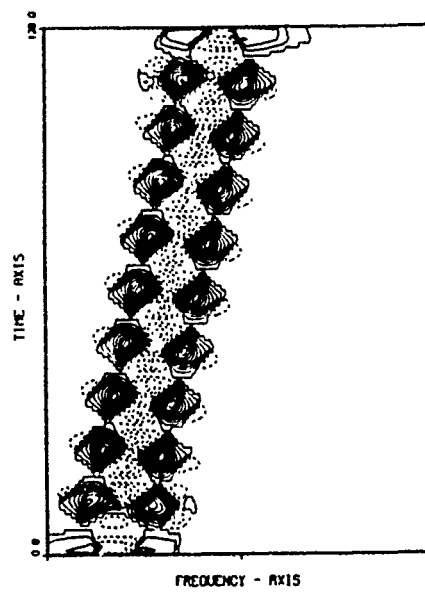


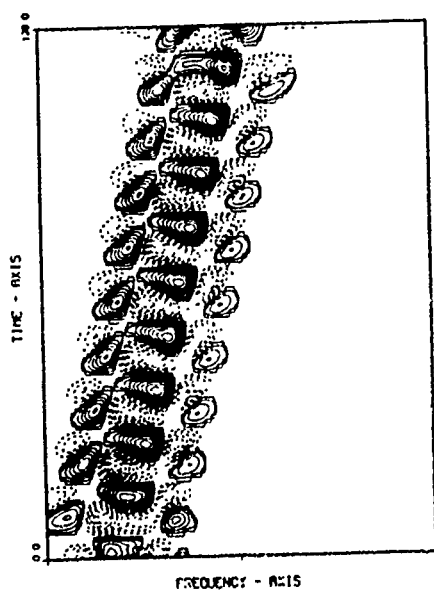
Figure 35. Test signal 4: amplitude plots for $|RD_y|^2$, $|RD_y|^2$ and $ImRD_y$



(a) $|RD_y|^2$



(b) $|RD_y|^2$



(c) $ImRD_y$

Figure 36. Test signal 4: contour plots for $|RD_y|^2$, $|RD_y|^2$ and $ImRD_y$

e. Single-component, Analytic, Quadratically Chirped Signal

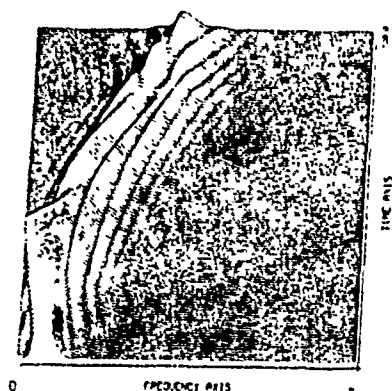
The ability of the spectrogram and these 5 t-f distributions to accurately display more rapid spectral dynamics can be compared in Figure 37 to Figure 40. Not surprisingly, the spectrogram presents a poor estimate. IPS_y demonstrates a spectral ridge which tends to broaden as a function of time, making it difficult to ascertain the actual instantaneous frequency curve. PWD, although zero at the end-points, tracks the chirp closely presenting a ridge along the line of instantaneous frequency as narrow as that found for the linear chirp. $|RD_y|^2$ appears to provide the most narrow ridge. Both PWD and $|RD_y|^2$ show amplitude modulation along the peak of the curve. As to the remaining spectra, $|RD_x|^2$ and $ImRD_y$ behave in a manner similar to the case of the linear chirp and thus do not appear particularly suited to this class of signal.

f. Multi-component Analytic Signal

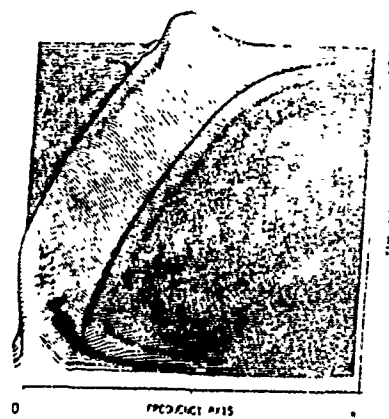
How the various spectral estimation techniques perform when confronted with a mixture of stationary and nonstationary dynamics is demonstrated in Figure 41 through Figure 44. This test signal is composed a high frequency stationary component and two chirped components, a linear chirp and a quadratic chirp. Their relative performance suggests a ranking in terms of desirability as an estimator of continuously changing spectral components. The spectrogram is predictably, the worst, followed by $|RD_y|^2$ and $ImRD_y$ in ascending order of desirability. Only IPS_y , $|RD_x|^2$ and PWD present spectra which closely resemble the true signal components. All three show a broadened ridge for the stationary component relative to the single stationary component case examined previously. This results from using a shorter window. As expected, $|RD_x|^2$ sharpens the modulation peaks found in its own spectrum and that of IPS_y . A comparison of $|RD_x|^2$ and PWD is also quite characteristic. The price paid for increased end-point resolution and elimination of the spectral cross-terms is a broadening of the spectral ridge and the appearance of modulation along the crest of the spectral ridges.

g. Complex FSK signal

In contrast to the continuously-varying frequency dynamics of the previous test case, a very different order of desirability is suggested in the case of pulsed spectral dynamics. Comparison of Figure 45 - Figure 48 shows $|RD_y|^2$ to possess superior end-point resolution ability coupled with a rapid build-up and decay of the spectral ridge relative to the true pulse dynamics. IPS_y and $|RD_x|^2$ produce similar spectra; however, the end-point build up is slower. $ImRD_y$, with its heightened sensitivity to detect spectral change appears to be an excellent indicator of the time and location of frequency



(a) Spectrogram



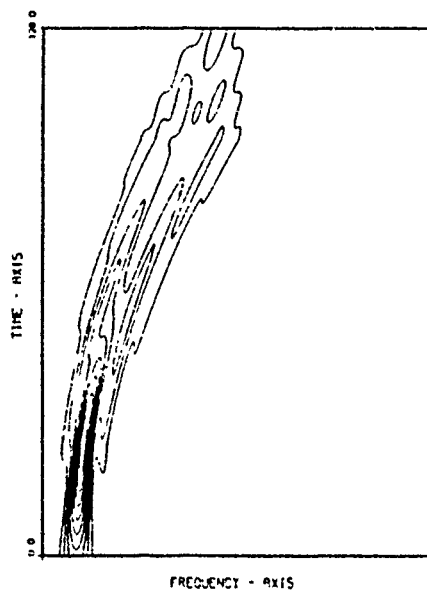
(b) IPS_x



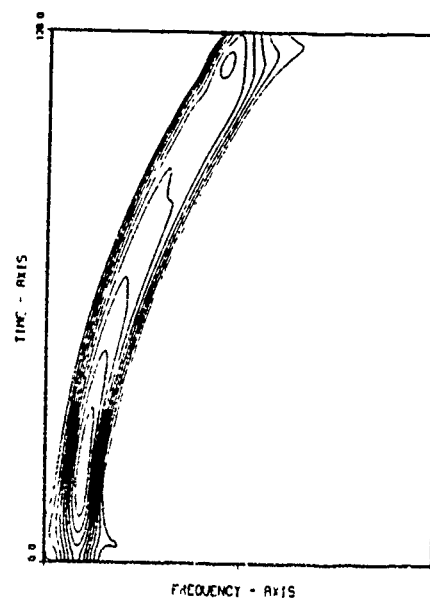
(c) PWD

Figure 37. Test signal 5: amplitude plots for Spectrogram, IPS_x , and PWD

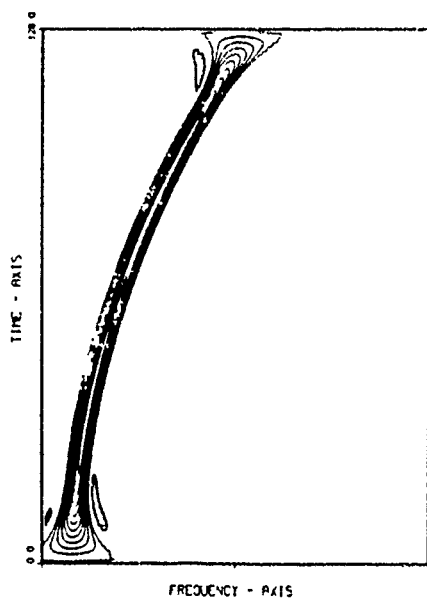
change. PWD presents a sluggish build-up and decay, with the width of each spectral ridge dependent on the duration of the pulse. Furthermore, cross-terms can be seen between the two higher frequency pulses.



(a) Spectrogram

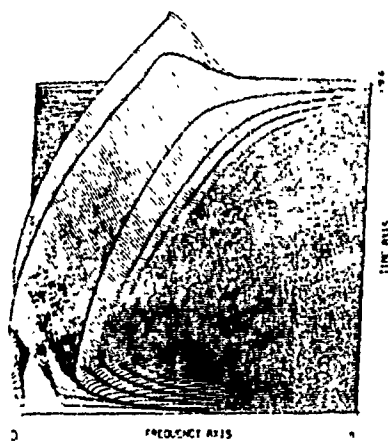


(b) IPS_y



(c) PWD

Figure 38. Test signal 5: contour plots for Spectrogram, IPS_y and PWD



(a) $|RD_y|^2$

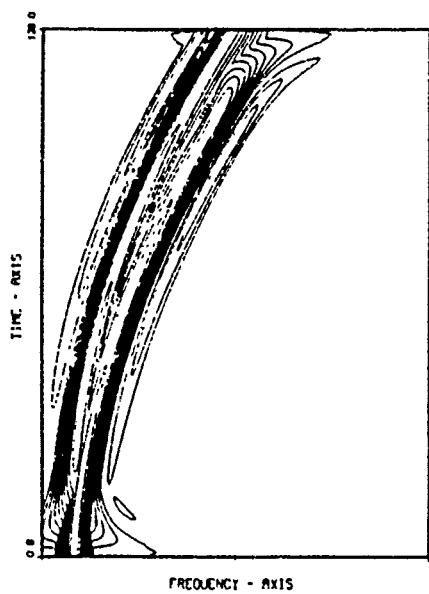


(c) $ImRD_y$

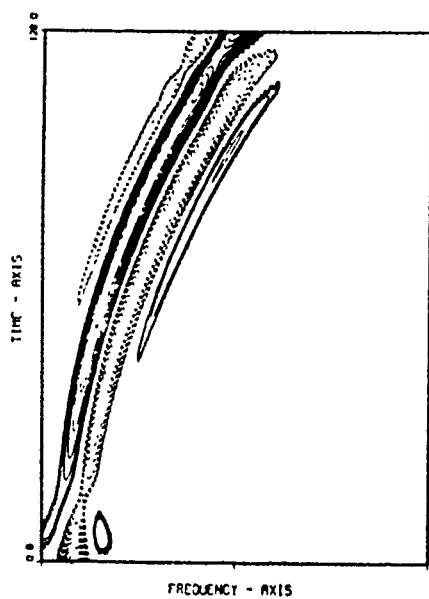


(b) $|RD_y|^2$

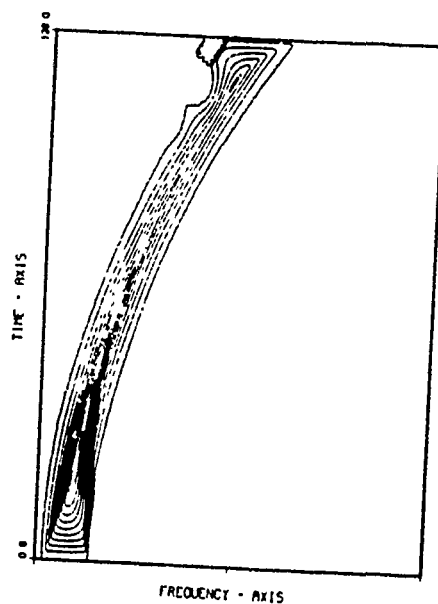
Figure 39. Test signal 5: amplitude plots for $|RD_y|^2$, $|RD_y|^2$ and $ImRD_y$



(a) $|RD_y|^2$

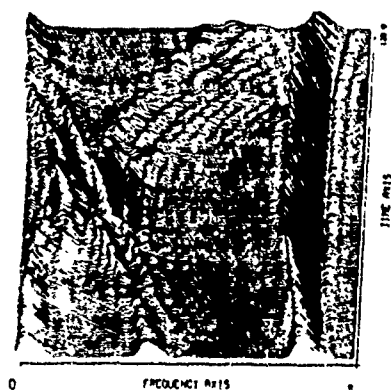


(c) $ImRD_y$



(b) $|RD_y|^2$

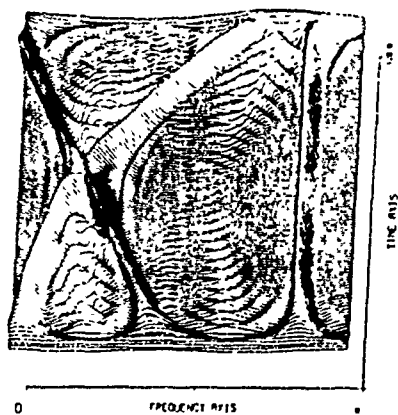
Figure 40. Test signal 5: contour plots for $|RD_y|^2$, $|RD_y|^2$ and $ImRD_y$



(a) Spectrogram



(b) IPS_y



(c) PWD

Figure 41. Test signal 6: amplitude plots for Spectrogram, IPS_y , and PWD

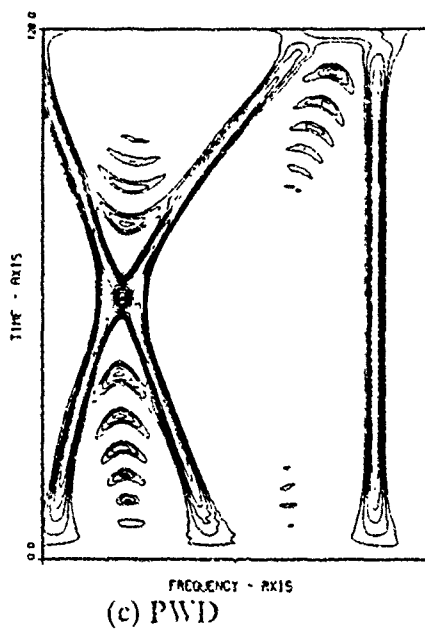
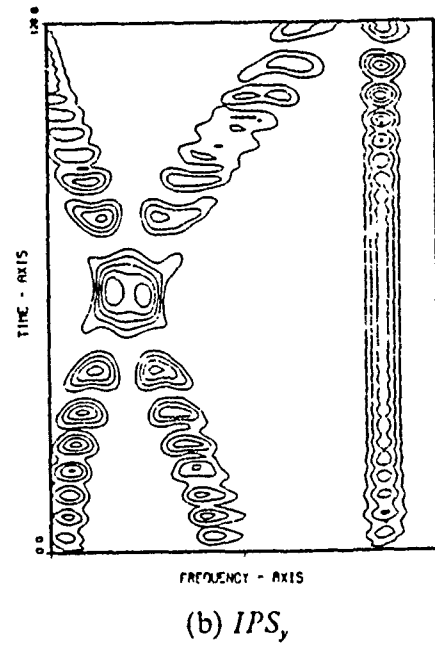
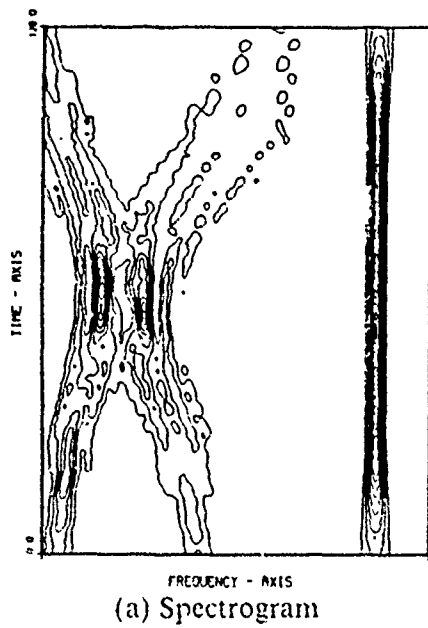
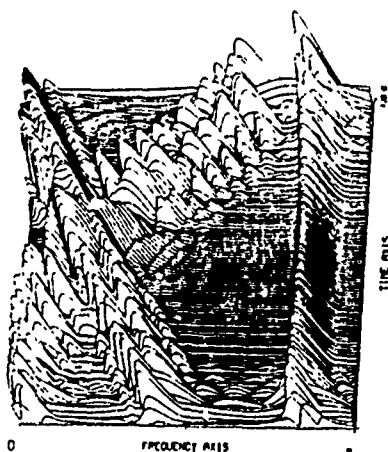
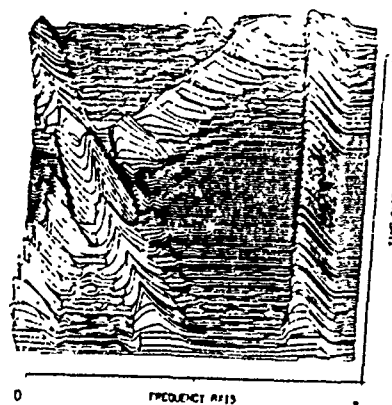


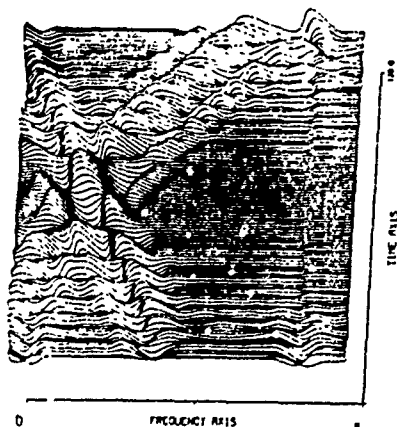
Figure 42. Test signal 6: contour plots for Spectrogram, IPS_y , and PWD



(a) $|RD_r|^2$

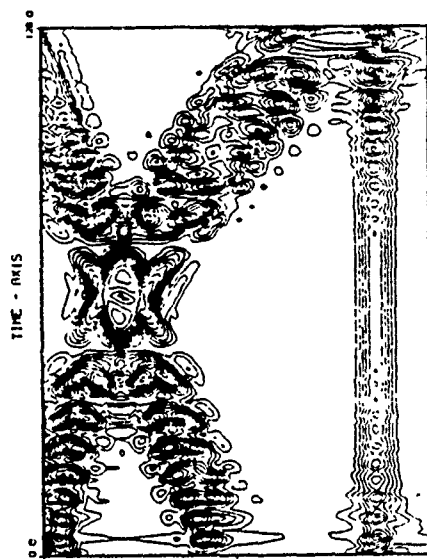


(b) $|RD_i|^2$

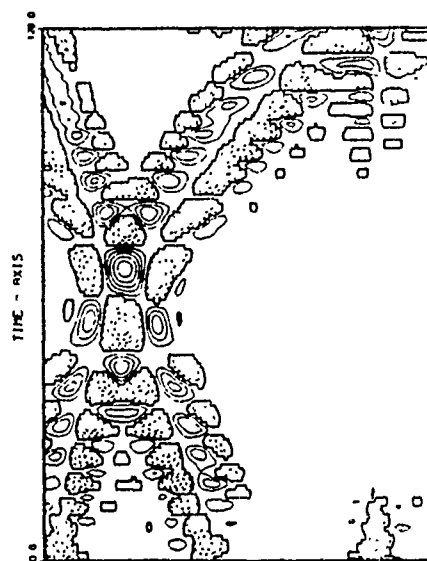


(c) $ImRD_r$

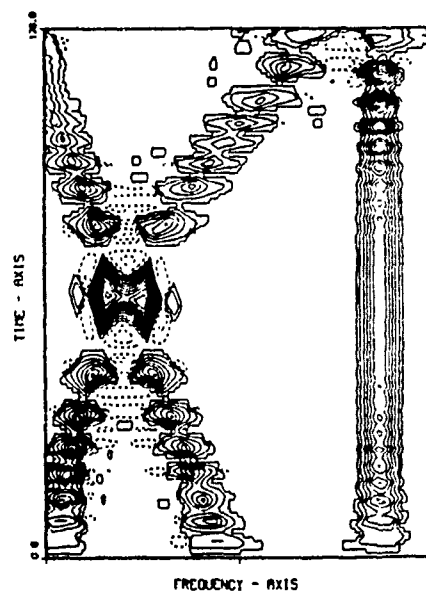
Figure 43. Test signal 6: amplitude plots for $|RD_r|^2$, $|RD_i|^2$ and $ImRD_r$



(a) $|RD_y|^2$

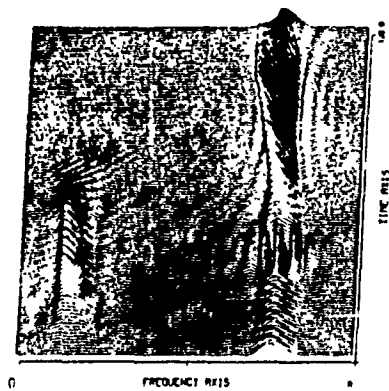


(c) $ImRD_y$

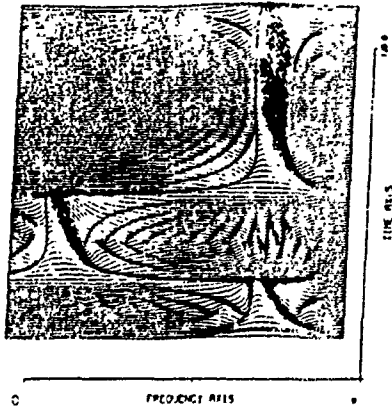


(b) $|RD_y|^2$

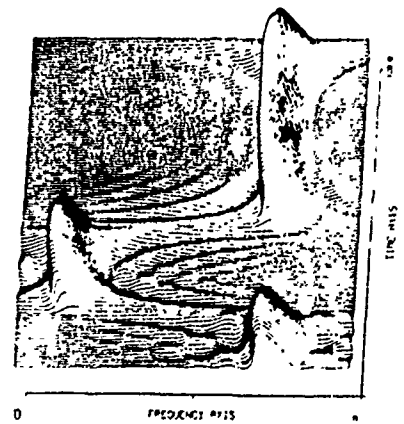
Figure 44. Test signal 6: contour plots for $|RD_y|^2$, $|RD_y|^2$ and $ImRD_y$



(a) Spectrogram



(c) PWD



(b) IPS_t

Figure 45. Test signal 7: amplitude plots for Spectrogram, IPS_t , and PWD

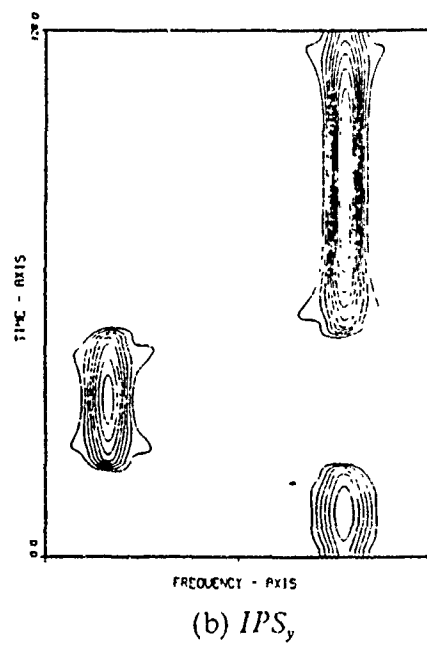
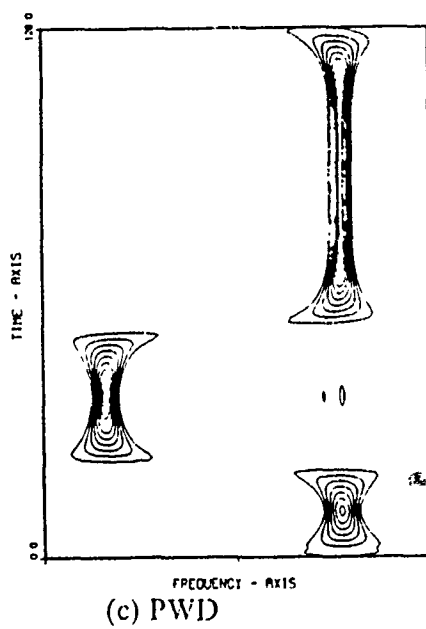
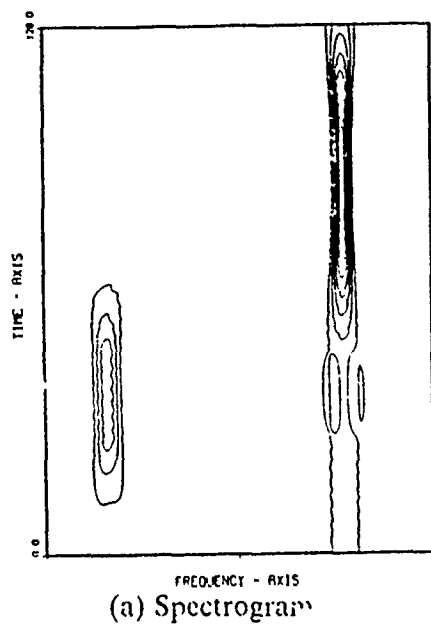


Figure 46. Test signal 7: contour plots for Spectrogram, IPS_y , and PWD

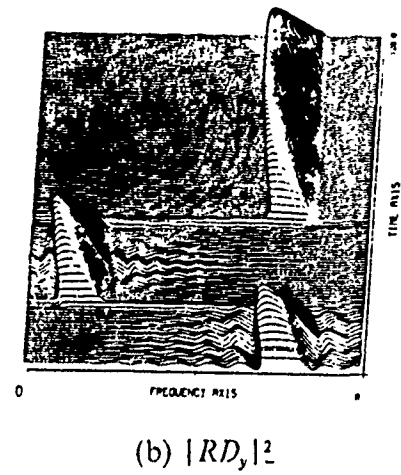
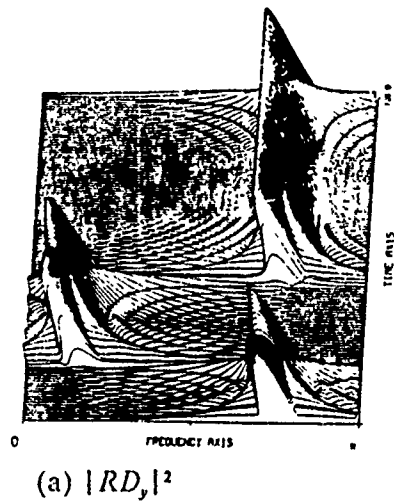
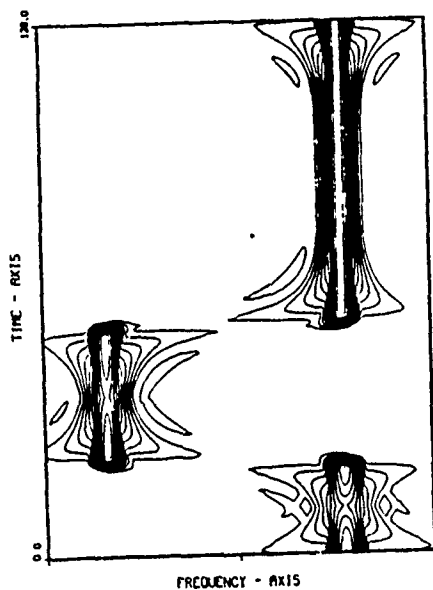
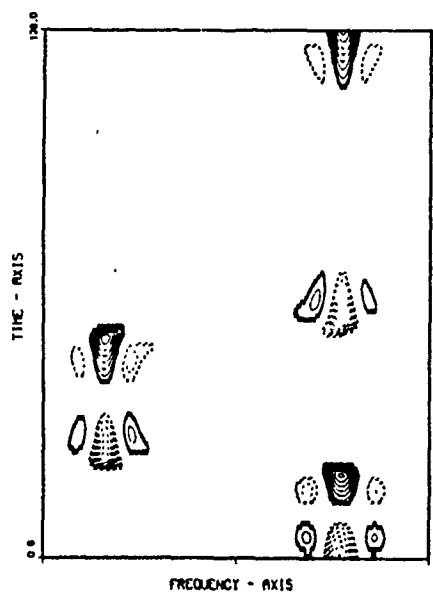


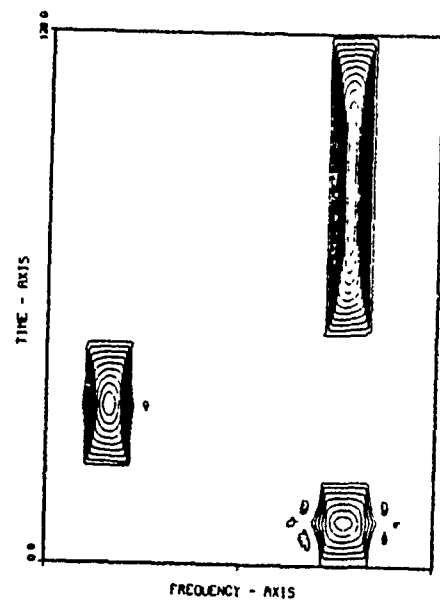
Figure 47. Test signal 7: amplitude plots for $|RD_y|^2$, $|RD_y|^2$ and $ImRD_y$



(a) $|RD_y|^2$



(c) $ImRD_y$



(b) $|RD_y|^2$

Figure 48. Test signal 7: contour plots for $|RD_y|^2$, $|RD_y|^2$ and $ImRD_y$

D. ALTERNATE METHODS OF COMPUTING IPS

Equation (33), the defining equation for IPS, can be rewritten as the Fourier transform of an ACF estimate (34), namely

$$\begin{aligned} IPS(f, t) &= \int_{-\infty}^{\infty} \hat{R}_{IPS}(\tau, t) e^{-j2\pi f\tau} d\tau \\ &= \frac{1}{2} \int_{-\infty}^{\infty} (x(t)x^*(t-\tau) + x^*(t)x(t+\tau)) e^{-j2\pi f\tau} d\tau. \end{aligned} \quad (54)$$

IPS for finite-duration discrete signals is

$$IPS(\theta, n) = \frac{\Delta T}{2} \sum_{k=-\infty}^{\infty} (x(n)x^*(n-k) + x^*(n)x(n+k)) e^{-j\theta k}, \quad (55)$$

where the signal sequence $x(n)$ is finite and zero outside the known samples, and ΔT is a constant. Equation (55) can be expressed as [Ref. 15]

$$\frac{2}{\Delta T} IPS(\theta, n) - |x(n)|^2 = |X(\theta)|^2 - |X_2(\theta)|^2, \quad (56)$$

where

$$\begin{aligned} X(\theta) &= \sum_{r=-\infty}^{\infty} x(r) e^{-j\theta r} \\ X_2(\theta) &= \sum_{\substack{r=-\infty \\ r \neq n}}^{\infty} x(r) e^{-j\theta r}. \end{aligned} \quad (57)$$

For use later in the derivation, let the Fourier transform of the point of interest be

$$\begin{aligned} D(\theta) &= x(n) e^{-j\theta n} \\ |D(\theta)|^2 &= |x(n)|^2. \end{aligned} \quad (58)$$

By neglecting $|x(n)|^2$ in (56) a modified version of IPS is defined. The behavior of this modified IPS for a single-component, analytic sinusoid is shown in Figure 49 (a). Comparing this with an unwindowed version of IPS for the identical data sequence in

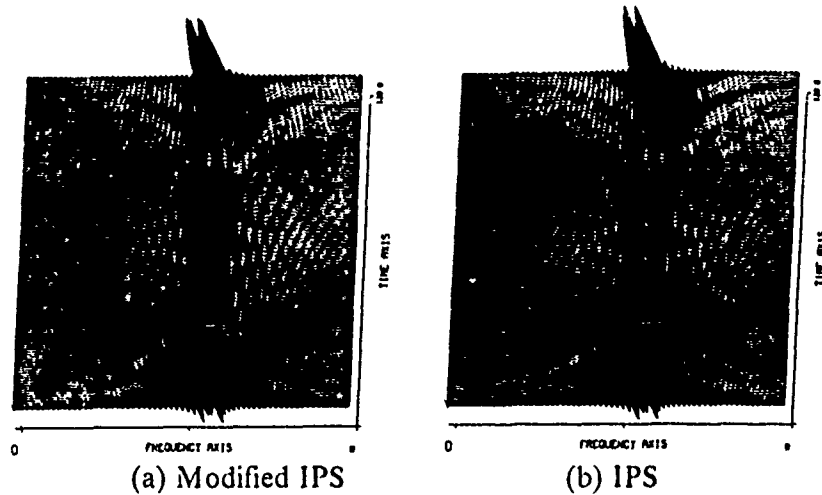


Figure 49. IPS

Figure 49 (b), shows the two methods of computing IPS to be very similar. The greatest difference can be seen when comparing maximum amplitudes. Modified IPS is on the order of 10^{-3} and IPS is on the order of 10. Both methods were computed using a five-cell-box-car averaging procedure along the t axis.

The question arises concerning the implementation of modified IPS using a window function. One method of windowing can be written as

$$IPS(\theta, n) = \frac{\Delta T}{2} \sum_{k=-\infty}^{\infty} (x(n)x^*(n-k) + x^*(n)x(n+k))w(k) e^{-j\theta k}. \quad (59)$$

Applying the definitions in (57),

$$\begin{aligned} IPS(\theta, n) &= \frac{\Delta T}{2} \{x(n)e^{-j\theta n}(X^*(\theta)_\theta^* W(\theta)) + x^*(n)e^{j\theta n}(X(\theta)_\theta^* W(\theta))\} \\ &= \frac{\Delta T}{2} \{D(\theta)(X^*(\theta)_\theta^* W(\theta)) + D^*(\theta)(X(\theta)_\theta^* W(\theta))\} \\ &= \frac{\Delta T}{2} \left\{ D(\theta) \sum_{p=-\infty}^{\infty} X^*(p) W(\theta - p) + D^*(\theta) \sum_{p=-\infty}^{\infty} X(p) W(\theta - p) \right\}, \end{aligned} \quad (60)$$

where $*$ denotes convolution in the frequency variable. Moving everything inside the summation sign and substituting $X_i^*(p) + D^*(p)$ for $X^*(p)$ and $X^*(\theta) - X_i^*(\theta)$ for $D^*(\theta)$ gives

$$\begin{aligned}
IPS(\theta, n) &= \frac{\Delta T}{2} \sum_{p=-\infty}^{\infty} (X_z^*(p) + D^*(p)) D(\theta) W(\theta - p) \\
&\quad + \frac{\Delta T}{2} \sum_{p=-\infty}^{\infty} (X^*(\theta) - X_z^*(\theta)) X(p) W(\theta - p) \\
&= \frac{\Delta T}{2} \sum_{p=-\infty}^{\infty} [D(\theta) X_z^*(p) + D(\theta) D^*(p)] W(\theta - p) \\
&\quad + \frac{\Delta T}{2} \sum_{p=-\infty}^{\infty} [X^*(\theta) X(p) - X_z^*(\theta) X(p)] W(\theta - p).
\end{aligned} \tag{61}$$

A straight-forward relationship between IPS and the spectral contribution of any single point in the data set is given by equation (56). Equation (61) defines an analogous relationship between (57) and (59). Unfortunately, this relationship is not so straight-forward and requires additional analysis to determine the benefits, if any, to be gained from processing data in this manner.

V. RECOMMENDATIONS AND CONCLUSIONS

The comparative behavior of the spectrogram, IPS, WD and three novel t-f distributions was explored in Chapter IV. Of the three, $ImRD$, proves to be particularly sensitive to discontinuous changes in frequency. This characteristic behavior may be useful in certain detection applications. When confronted with more complicated spectra, one containing closely-spaced stationary components or continuously-varying nonstationary components, $ImRD$, does not appear particularly useful. Similarly $|RD|^2$ provides an improvement in end-point resolution when used for the estimation of stationary or pulsed spectra. Taking the square root of $|RD|^2$ results in a t-f distribution, denoted by $|RD(f,t)|$, which satisfies many of the desirable properties listed in Table 2. In particular $|RD(f,t)|$:

1. Satisfies both zero energy requirements
2. Obeys the time and frequency shift properties
3. Is positive and real for all time and frequencies.

How well $|RD|^2$ can track a rapidly fluctuating pulsed signal, similar to something found in frequency hopped communications, is an area worth investigating.

For detection of continuously changing spectral dynamics, $|RD|^2$ appears to be a viable processing scheme, however the performance of this estimator in noise needs still to be examined. Using $|RD|^2$ as an estimator is not without problems. Unlike $|RD|$, taking the square root of $|RD|^2$ does not produce an estimator which satisfies the marginal requirements. It does however comply with the zero energy and time frequency shift properties desirable for time-dependent estimation problems. Used with stationary spectra $|RD|^2$ appears to improve the resolution of closely spaced components beyond that currently achieved by classical methods. For stationary spectra, $|RD|^2$ is a biased estimator, i.e., the true spectral peaks occur at a given fixed offset from their true frequency location. PWD also provides a resolution improvement; however the estimate it provides never settles down to one frequency location. For short duration data $|RD|^2$ may prove superior in the detection of multiple stationary components.

In addition to the experimental results presented in Chapter IV, IPS , demonstrates a 3-dB noise advantage relative to PWD [Ref. 15]. Coupled with superior end-point

resolution IPS may be the desirable method in practical analysis problems. All the results presented were derived from noise-free data sequences using digital implementations (see Appendix A). Because $ImRD$, $|RD|^2$ and $|RD|^2$ all show advantages when applied to the appropriate signal type, analysis of their noise performance is an open issue. As they are derived from the RD, as is IPS, it is likely that they enjoy a similar robustness.

Looking to practical applications of IPS, a brief discussion of performance in a multi-sensor environment can be found in Appendix B. The initial results look promising, but more extensive research needs to be conducted. A second practical application scheme involves the use of a cumulant or third-order moment. Typically associated with the sonar environment, this scheme seeks to take advantage of the fact that the odd moments of a zero-mean, gaussian noise process are identically zero. An initial investigation using IPS to compute cumulants can be found in Appendix C.

In general, WD produces very narrow spectral ridges but suffers from poor end-point resolution and spectral artifacts. IPS provides an improvement over these shortcomings at the cost of spectral broadening. Recently appearing in the literature is another t-f distribution [Ref. 10, 22]. Defined by H.I. Choi and W.J. Williams, this t-f distribution minimizes the effects of the spectral cross-terms. Closer examination of the resultant spectra, which uses the kernel function

$$\Phi(v, \tau) = e^{-\frac{\pi v^2 \tau^2}{2\sigma}},$$

where σ is a constant, shows that the spectral ridges are broadened, similar in behavior to IPS. In classical estimation, i.e., the periodogram, one maximizes spectral resolution using nothing but the raw finite data set. The price paid is a large, slow roll-off sidelobe structure that can mask a true component. In time-frequency distributions, i.e., in the generalized phase-space equation (19), one maximizes spectral detail using a constant kernel of unit amplitude. The price paid is poor end-point resolution and spectral artifacts across time and frequency. In the classical analog, using any other window results in improved sidelobe behavior at a corresponding loss in detail along the frequency axis. IPS, the Rihaczek derived distributions and the distribution suggested by Choi and Williams all improve or eliminate the disturbing spectral cross terms characteristic of WD. The price paid is loss in spectral detail.

APPENDIX A. COMPUTER CODE

To conserve space only the read file and four of the si. Fortran codes have been included. Data was generated and read by the basic programs as required. The data generation file is not included here. The read file allows easy change of processing parameters. Further, IPS_y and $ImRD_y$ are generated by code that differs in a minus sign in line code. IPS_y requires a plus sign; $ImRD_y$ requires a minus sign. Similarly $|RD_y|^2$ and $|RD_y|^2$ are simply related. The location of the sign change is indicated in the respective algorithms. Graphics are produced using DISSPLA.

1. Parameter File

1	1	031	039	08	MODE	PLTR	BWLEN	EWLEN	WINC
HAMMING WINDOW (\$'					WTYPE				
B					CONTR				
IPS: \$'					TTL				
FS=1/128, 40 POINTS OF DATA\$'					SIGNAL				
5 CELL TIME SMOOTHING\$'					TSMTH				

2. Spectrogram

```

C**      THIS FORTRAN FILE COMPUTES THE SPECTROGRAM OF      ***
C**      A DATA SEQUENCE                                     ***
C
C
C      INPUT DATA SEQUENCE IS READ USING FILEDEF 4, AS THE COMPLEX
C      ARRAY DATA(L).
C
C      L IS THE LENGTH OF THE DATA SEQUENCE AND IS ADJUSTED FROM THE
C      PARAMETER STATEMENT.  L MUST NOT EXCEED 128.
C
C      ANALYSIS PARAMETERS ARE READ USING FILEDEF 41.  THE PARAMETERS
C      ARE:
C
C          ARGUMENT TYPE      ALLOWED VAULUES
C
C      MODE - I1              1    PLOT 0 TO PI
C                             2    PLOT PI TO PI
C
C      PLTR - I1              0    SHERPA LASER PRINTER
C                             1    IMB79 GRAPHICS TERMINAL
C
C      BWLEN- I3              3    DIGIT INITIAL WINDOW LENGTH,
C                             MUST BE AN ODD INTEGER
C      EWLEN- I3              3    DIGIT FINAL WINDOW LENGTH
C      WINC - I2              2    DIGIT WINDOW INCREMENT, MUST
C                             BE AN EVEN INTEGER
C
C      WTYPE- A19             19   CHARACTER STRING USED IN THE
C                             PLOT HEADER DISCRIBING THE
C                             WINDOW USED.  THE CURRENT
C                             WINDOW LENGTH IS AUTOMATICALLY
C                             INCLUDED
C
C      CONTR- A1              1    CHARACTER STRING INDICATING
C                             TYPE OF PLOT DESIRED
C
C                             A    AMPLITUDE PLOT ONLY
C                             C    CONTOUR PLOT ONLY
C                             B    BOTH AMPLITUDE AND CONTOUR
C
C      TTL - A43              43   CHARACTER STRING USED IN THE
C                             HEADING WHICH DESCRIBES THE
C                             ALGORITHM AND THE CLASS OF
C                             SIGNAL USED
C
C      SIGNAL- A43            43   CHARACTER STRING DESCRIBING
C                             TEST SIGNAL
C
C      OUT  REAL
C           OUTPUT ARRAY OF DIMENSION 512 BY L
C
C      COEF COMPLEX
C           ARRAY OF DATA AFTER IT HAS BEEN WEIGHTED WITH A
C           SLIDING WINDOW FUNCTION.

```

```

C
C      FT      COMPLEX
C              ARRAY OF THE 1024 POINT TRANSFORM COEF
C
C      Z      INTEGER
C              LENGTH OF CURRENT WINDOW
C
C      M      INTEGER
C              MID-POINT OF THE CURRENT WINDOW
C
C      AMAX    REAL
C              MAXIMUM AMPLITUDE, USED TO SCALE VERTICAL AXIS
C
C      AMIN    REAL
C              MINIMUM AMPLITUDE, USED TO SCALE VERTICAL AXIS
C
C*****
C      PARAMETER(L= 32)
C              INTEGER I,J,N,M,MODE,Z,BWLEN,EWLEN,WINC,PLTR
C              REAL OUT(512,L),AMAX,AMIN
C              CHARACTER WTYPE*19,TTL*43,SIGNAL*43,CONTR*1
C              COMPLEX DATA(L),FT(1024),COEF(1024)
C              CALL EXCMS('FILEDEF 4 DISK TEST IN A (PERM')
C              CALL EXCMS('FILEDEF 41 DISK PARAM IN A (PERM')
C
C----- READ IN PARAMETER LIST -----
C      READ(41,400)MODE,PLTR,BWLEN,EWLEN,WINC,WTYPE,CONTR,TTL,
C      + SIGNAL
C      400  FORMAT (1X,I1,3X,I1,3X,I3,3X,I3,3X,I2/1X,A19/1X,A1/1X,A43/
C      + 1X,A43)
C-----
C
C----- TEST TO ENSURE WINDOW LENGTH IS APPROPRIATE -----
C      I=L-1
C      IF ((BWLEN .GT. I) .OR. (EWLEN .GT. I)) THEN
C          WRITE(*,69)
C          GO TO 99
C      ENDIF
C      I=MOD(BWLEN,2)
C      K=MOD(WINC,2)
C      IF (I .EQ. 0) THEN
C          IF (K .EQ. 1) THEN
C              WRITE(*,68)
C              GO TO 99
C          ELSE
C              WRITE(*,67)
C              GO TO 99
C          ENDIF
C      ENDIF
C      69  FORMAT (1X,'WINDOW LENGTH EXCEEDS LENGTH OF THE DATA')
C      68  FORMAT (1X,'WINDOW INCREMENT MUST BE EVEN')
C      67  FORMAT (1X,'INITIAL WINDOW LENGTH MUST BE ODD')
C-----

```

```

C
C----- PLOTTING DEVICE CALL -----
      IF (PI.TR .EQ. 0) THEN
        CALL COMPRS
      ELSE
        CALL IBM79
      ENDIF
C-----
C
      PI=4*ATAN(1.)
      READ(4,*)(DATA(I),I=1,L)
C
C
      DO 111 Z=BWLEN,EWLEN,WINC
      M=(Z-1)/2
      CALL ANGLE(0.0)
      AMAX=0
      AMIN=AMAX
      DC 10 J=1,L
        DO 20 N=-M,M
          IF ( ((I+N) .GE. 1) .AND. ((I+N) .LE. L) ) THEN
            COEF(M+N+1)=DATA(I+N)
            + *(0.54+0.46*COS(2*PI*N/(2*M)))
          ELSE
            COEF(M+N+1)=(0.,0.)
          ENDIF
20      CONTINUE
        DO 30 N=2*M+2,1024
          COEF(N)=(0.,0.)
30      CONTINUE
      CALL FFT(1024,COEF,FT)
      IF ( MODE.EQ. 2) THEN
        DO 40 N=1,513,2
          OUT( INT((N+1)/2+255),I)=ABS(FT(N))**2/(2*M+1)
          IF (OUT( INT((N+1)/2+255),I) .GT. AMAX) THEN
            AMAX=OUT( INT((N+1)/2+255),I)
          ENLTF
          IF (OUT( INT((N+1)/2+255),I) .LT. AMIN) THEN
            AMIN=OUT( INT((N+1)/2+255),I)
          ENDIF
40      CONTINUE
        DO 50 N=515,1024,2
          OUT( INT((N-1)/2-256),I)=ABS(FT(N))**2/(2*M+1)
          IF (OUT( INT((N-1)/2-256),I) .GT. AMAX) THEN
            AMAX=OUT( INT((N-1)/2-256),I)
          ENDIF
          IF (OUT( INT((N-1)/2-256),I) .LT. AMIN) THEN
            AMIN=OUT( INT((N-1)/2-256),I)
          ENDIF
50      CONTINUE
      ELSE
        DO 51 N=1,512
          OUT(N,I)=ABS(FT(N))**2/(2*M+1)
          IF (OUT(N,I) .GT. AMAX) THEN
            AMAX=OUT(N,I)
          ENDN

```



```

      DIMENSION RARRAY(2),IARRAY(1)
C
C THIS ROUTINE MAKES NEGATIVE CONTOURS DASHED AND THE ZERO LINE HEAVIER.
C
      CALL RESET('DASH')
      IF (RARRAY(1) .GE. 0.) GC TO 10
      CALL DASH
10  RARRAY(2) = 1.
      IARRAY(1) = 1
      IF (RARRAY(1) .EQ. 0.) IARRAY(1) = 2
      RETURN
      END
C
CS S S S S S S S S S S S S S S S S S S S S S S S S S S S S S S S S S S S
C
C *****
C *
C *      CALL FFT(N,XTMP,X)
C *
C *      X - OUTPUT COMPLEX ARRAY CONTAINING FFT (1024)
C *      N - NUMBER OF POINTS
C *      XTMP - COMPLEX ARRAY CONTAINING DATA SAMPLES
C *      (starting at 1,up to 1024)
C *****
C
      SUBROUTINE FFT(N,XTMP,X)
      COMPLEX X(1024),XTMP(1024),WTFAC,TMP
      M=INT(LOG10(FLOAT(N))/LOG10(2.))+0.5)
      EN = N
      PI = 4.0*ATAN(1.0)
      DO 10 K=0,N-1
        NEWADR = 0
        MADDR = K
        DO 20 I=0,M-1
          LRMNDR = MOD(MADDR,2)
          NEWADR = NEWADR + LRMNDR*2**(M-1-I)
          MADDR = MADDR/2
20      CONTINUE
        X(NEWADR+1) = XTMP(K+1)
10     CONTINUE
      DO 50 L=1,M
        ISPACE = 2**L
        S = N/ISPACE
        IWIDTH = ISPACE/2
        DO 40 J=0,(IWIDTH-1)
          R = S*J
          ALPHA = 2.*PI*R/EN
          WTFAC = CMPLX( COS(ALPHA), -SIN(ALPHA))
          DO 30 ITOP=J,N-2,ISPACE
            IBOT = ITOP + IWIDTH
            TMP = X(IBOT+1)*WTFAC
            X(IBOT+1) = X(ITOP+1) - TMP
            X(ITOP+1) = X(ITOP+1) + TMP
30          CONTINUE
40        CONTINUE
50      CONTINUE

```

```

FFT00130
FFT00140
FFT00210
FFT00270
FFT00320
FFT00330
FFT00340
FFT00350
FFT00360
FFT00370
FFT00380
FFT00390
FFT00400
FFT00410
FFT00530
FFT00610
FFT00620
FFT00630
FFT00670
FFT00720
FFT00730
FFT00740
FFT00750
FFT00800
FFT00810
FFT00820
FFT00830
FFT00840
FFT00850
FFT00860

```

RETURN
END

FFT01000
FFT01010

3. IPS

```

C**      THIS FORTRAN FILE COMPUTES THE IPS OF A DATA SEQUENCE      ***
C
C      INPUT DATA SEQUENCE IS READ USING FILEDEF 4, AS THE COMPLEX
C      ARRAY X(N).
C
C      N IS THE LENGTH OF THE DATA SEQUENCE AND IS ADJUSTED FROM THE
C      PARAMETER STATEMENT.  N MUST NOT EXCEED 128.
C
C      ANALYSIS PARAMETERS ARE READ USING FILEDEF 41.  THE PARAMETERS
C      ARE:
C
C          ARGUMENT TYPE      ALLOWED VAULUES
C
C      MODE - I1              1  PLOT 0 TO PI
C                             2  PLOT PI TO PI
C
C      PLTR - I1              0  SHERPA LASER PRINTER
C                             1  IMB79 GRAPHICS TERMINAL
C
C      BWLEN- I3              3 DIGIT INITIAL WINDOW LENGTH,
C                             MUST BE AN ODD INTEGER
C      EWLEN- I3              3 DIGIT FINAL WINDOW LENGTH
C      WINC - I2              2 DIGIT WINDOW INCREMENT, MUST
C                             BE AN EVEN INTEGER
C
C      WTYPE- A19             19 CHARACTER STRING USED IN THE
C                             PLOT HEADER DISCRIBING THE
C                             WINDOW USED.  THE CURRENT
C                             WINDOW LENGTH IS AUTOMATICALLY
C                             INCLUDED
C
C      CONTR- A1              1 CHARACTER STRING INDICATING
C                             TYPE OF PLOT DESIRED
C
C                             A  AMPLITUDE PLOT ONLY
C                             C  CONTOUR PLOT ONLY
C                             B  BOTH AMPLITUDE AND CONTOUR
C
C      TTL - A43              43 CHARACTER STRING USED IN THE
C                             HEADING WHICH DESCRIBES THE
C                             ALGORITHM AND THE CLASS OF
C                             SIGNAL USED
C
C      SIGNAL- A43            43 CHARACTER STRING DESCRIBING
C                             TEST SIGNAL
C
C      TSMTH- A25             25 CHARACTER STRING DESCRIBING
C                             TYPE OF TIME SMOOTHING USED
C
C      OUT  REAL
C           OUTPUT ARRAY OF DIMENSION 512 BY N
C
C      SAMP COMPLEX

```

```

C          SHIFTED VERSION OF X          *
C          *                             *
C      SAM  COMPLEX                      *
C          SHIFTED AND CONJUGATED VERSION OF X *
C          *                             *
C      C    COMPLEX                      *
C          ARRAY OF SUM OF PRODUCTS OF DIMENSION 1 BY 1025 *
C          POSITIONS 1 - 512 ARE CONJUGATE SYMMETRIC WITH *
C          POSITIONS 514 - 1025.  POSITION 513 = (0.,0.) *
C          *                             *
C      FT   COMPLEX                      *
C          ARRAY OF THE 1024 POINT TRANSFORM C *
C          *                             *
C      Z    INTEGER                      *
C          LENGTH OF CURRENT WINDOW *
C          *                             *
C      M    INTEGER                      *
C          MID-POINT OF THE CURRENT WINDOW *
C          *                             *
C      AMAX REAL                        *
C          MAXIMUM AMPLITUDE, USED TO SCALE VERTICAL AXIS *
C          *                             *
C      AMIN REAL                        *
C          MINIMUM AMPLITUDE, USED TO SCALE VERTICAL AXIS *
C          *                             *
C      NX   HORIZONTAL DIMENSION OF OUT WHICH IS ALWAYS 512 *
C          *                             *
C      DATA CAN BE OUTPUT USING FILEDEF 61.  POINTS OF INTEREST MUST *
C          BE DEFINED IN THE APPROPRAITE SECTION OF CODE.  BECAUSE *
C          OF SPACE CONSTRAINTS, THE DATA OUTPUT FILE IS WRITTEN TO *
C          THE B DISK. *
C*****
C
C      PARAMETER(M= 64)
C      COMPLEX X(N),C(1025),SAMP,SAM,FT(1024)
C      REAL OUT(512,N),AMAX,AMIN
C      INTEGER NX,K,I,J,MODE,Z,M,BWLEN,EWLEN,WINC,PLTR
C      CHARACTER WTYPE*19,TTL*43,SIGNAL*43,TSMTH*25,CONTR*1
C      CALL EXCMS('FILEDEF 4 DISK TEST IN (PERM')
C      CALL EXCMS('FILEDEF 41 DISK PARAM IN (PERM')
C      CALL EXCMS('FILEDEF 61 DISK DATA OUT B (PERM')
C
C----- READ IN PARAMETER LIST -----
C      READ(41,400)MODE,PLTR,BWLEN,EWLEN,WINC,WTYPE,CONTR,TTL,
C      + SIGNAL,TSMTH
C      400  FORMAT (1X,I1,3X,I1,3X,I3,3X,I3,3X,I2/1X,A19/1X,A1/1X,A43
C      + /1X,A43/1X,A25)
C-----
C
C----- TEST TO ENSURE WINDOW LENGTH IS APPROPRIATE -----
C      I=N-1
C      IF ((BWLEN .GT. I) .OR. (EWLEN .GT. I)) THEN
C          WRITE(*,69)
C          GO TO 99
C      ENDIF

```

```

        I=MOD(BWLEN,2)
        K=MOD(WINC,2)
        IF (I .EQ. 0) THEN
            IF (K .EQ. 1) THEN
                WRITE(*,68)
                GO TO 99
            ELSE
                WRITE(*,67)
                GO TO 99
            ENDIF
        ENDIF
69    FORMAT (1X,'WINDOW LENGTH EXCEEDS LENGTH OF THE DATA')
68    FORMAT (1X,'WINDOW INCREMENT MUST BE EVEN')
67    FORMAT (1X,'INITIAL WINDOW LENGTH MUST BE ODD')
C-----
C
C-----PLOTTING DEVICE CALL -----
        IF (PLTR.EQ.0)THEN
            CALL COMPRS
        ELSE
            CALL IBM79
        ENDIF
C-----
C
C
        PI=4*ATAN(1.)
        NX=512
        READ (4,*)(X(J),J=1,N)
        DO 111 Z= BWLEN,EWLEN,WINC
        600    WRITE(61,600)TTL,SIGNAL,TSMTH,WTYPE,Z
            FORMAT (1X,A43/1X,A43/1X,A25/1X,A19,I3,' POINTS')
            CALL ANGLE(0.,0.)
            M=(Z-1)/2
            AMAX=0.
            AMIN=AMAX
            DO 10 I=1,N
                DO 20 K=0,512
                    SAMP=(0.,0.)
                    SAM=SAMP
                    IF ( (I+K) .LE. N ) THEN
                        SAMP=X(I+K)
                    ENDIF
                    IF ( (I-K) .GT. 0 ) THEN
                        SAM=CONJG(X(I-K))
                    ENDIF
C
C+ - + - + - + - + - + - + - + - + - + - + - + - + - + - +
C+--+--+ sum of product is IPS      difference of product is IMRD -+--+
            IF (K .LE. M) THEN
                C(K+1)=(X(I)*SAM + CONJG(X(I))*SAMP)
                +      *(0.54+0.46*CO;(2*PI*K/(2*M)))
            ELSE
                C(K+1)=0
            ENDIF
C+ - + - + - + - + - + - + - + - + - + - + - + - + - + - +
C

```

```

20      C(1024-K+1)=CONJG(C(K+1))
      CONTINUE
      C(513)=(0.,0.)
      CALL FFT(1024,1,FT)
      DO 40 K=1,MODE*12,MODE
      IF (REAL(FT(K)) .GT. AMAX) THEN
          AMAX=REAL(FT(K))
      ENDIF
      IF (REAL(FT(K)) .LT. AMIN) THEN
          AMIN=REAL(FT(K))
      ENDIF
      IF ( (K .LT. 514) .AND. (MODE .EQ. 2) ) THEN
          OUT(INT((K+1)/2+255),I)=REAL(FT(K))
      ELSE
          IF ( MODE .EQ. 2 ) THEN
              OUT(INT((K+1)/2-257),I)=REAL(FT(K))
          ELSE
              OUT(K,I)=REAL(FT(K))
          ENDIF
      ENDIF
40      CONTINUE
10      CONTINUE
C-----FOR TIME SMOOTHING PURPOSES -----
      DO 48 K=1,512
      DO 46 I=1,N-2
          OUT(K,I)=(OUT(K,I)+OUT(K,I+1)+OUT(K,I+2))/3
46      CONTINUE
      DO 47 I=N,3,-1
          OUT(K,I)=(OUT(K,I)+OUT(K,I-1)+OUT(K,I-2))/3
47      CONTINUE
C
C----- DATA OUTPUT -----
      IF((K.GE.208).AND.(K.LT.370))THEN
C          IF(((K.GE.120).AND.(K.LT.140)).OR.((K.GE.370).AND.
C      + (K.LT.390)))THEN
          WRITE(61,601)
          DO 81 I=1,N-1,14
              WRITE(61,602)K,I,OUT(K,I)
81          CONTINUE
          ENDIF
601      FORMAT ('FREQ BIN=',8X,'TIME BIN=',7X,'AMPLITUDE=')
602      FORMAT (10X,I4,13X,I4,14X,E14.7)
C-----
C
48      CONTINUE
C-----
C
C----- PLOTTING -----
      IF(CONTR.EQ.'C')THEN
          GO TO 50
      ENDIF
      CALL BSHIFT (-0.2,-.25)
      CALL AREA2D(8,9)
      CALL VOLM3D(10,10,8)
      CALL HEADIN(TTL,100,1.,3)
      CALL HEADIN(SIGNAL,100,1.,3)

```


[illegible]

4. PWD

```

C** THIS FORTRAN FILE COMPUTES THE PWD OF A DATA SEQUENCE ****
C
C INPUT DATA SEQUENCE IS READ USING FILEDEF 4, AS THE COMPLEX
C ARRAY X(N).
C
C N IS THE LENGTH OF THE DATA SEQUENCE AND IS ADJUSTED FROM THE
C PARAMETER STATEMENT. N MUST NOT EXCEED 128.
C
C ANALYSIS PARAMETERS ARE READ USING FILEDEF 41. THE PARAMETERS
C ARE:
C
C ARGUMENT TYPE ALLOWED VAULUES
C
C MODE - I1 1 PLOT 0 TO PI
C 2 PLOT PI TO PI
C
C PLTR - I1 0 SHERPA LASER PRINTER
C 1 IMB79 GRAPHICS TERMINAL
C
C BWLEN- I3 3 DIGIT INITIAL WINDOW LENGTH,
C MUST BE AN ODD INTEGER
C EWLEN- I3 3 DIGIT FINAL WINDOW LENGTH
C WINC - I2 2 DIGIT WINDOW INCREMENT, MUST
C BE AN EVEN INTEGER
C
C WTYPE- A19 19 CHARACTER STRING USED IN THE
C PLOT HEADER DISCRIBING THE
C WINDOW USED. THE CURRENT
C WINDOW LENGTH IS AUTOMATICALLY
C INCLUDED
C
C CONTR- A1 1 CHARACTER STRING INDICATING
C TYPE OF PLOT DESIRED
C
C A AMPLITUDE PLOT ONLY
C C CONTOUR PLOT ONLY
C B BOTH AMPLITUDE AND CONTOUR
C
C TTL - A43 43 CHARACTER STRING USED IN THE
C HEADING WHICH DESCRIBES THE
C ALGORITHM AND THE CLASS OF
C SIGNAL USED
C
C SIGNAL- A43 43 CHARACTER STRING DESCRIBING
C TEST SIGNAL
C
C TSMTH- A25 25 CHARACTER STRING DESCRIBING
C TYPE OF TIME SMOOTHING USED
C
C OUT REAL
C OUTPUT ARRAY OF DIMENSION 512 BY N
C
C SAMP COMPLEX

```



```

C          SHIFTED VERSION OF X          *
C                                          *
C      SAM    COMPLEX                     *
C          SHIFTED AND CONJUGATED VERSION OF X *
C                                          *
C      C      COMPLEX                     *
C          ARRAY OF SUM OF PRODUCTS OF DIMENSION 1 BY 1025 *
C          POSITIONS 1 - 512 ARE CONJUGATE SYMMETRIC WITH *
C          POSITIONS 514 - 1025.  POSITION 513 = (0.,0.) *
C                                          *
C      FT     COMPLEX                     *
C          ARRAY OF THE 1024 POINT TRANSFORM C *
C                                          *
C      Z      INTEGER                     *
C          LENGTH OF CURRENT WINDOW *
C                                          *
C      M      INTEGER                     *
C          MID-POINT OF THE CURRENT WINDOW *
C                                          *
C      AMAX   REAL                       *
C          MAXIMUM AMPLITUDE, USED TO SCALE VERTICAL AXIS *
C                                          *
C      AMIN   REAL                       *
C          MINIMUM AMPLITUDE, USED TO SCALE VERTICAL AXIS *
C                                          *
C      NX     HORIZONTAL DIMENSION OF OUT WHICH IS ALWAYS 512 *
C                                          *
C      DATA CAN BE OUTPUT USING FILEDEF 61.  POINTS OF INTEREST MUST *
C      BE DEFINED IN THE APPROPRAITE SECTION OF CODE.  BECAUSE *
C      OF SPACE CONSTRAINTS, THE DATA OUTPUT FILE IS WRITTEN TO *
C      THE B DISK. *
C*****
C
C      PARAMETER(N= 64)
C      COMPLEX X(512),C(1025),SAMP,SAM,FT(1024)
C      REAL OUT(512,N),AMAX,AMIN
C      INTEGER NX,K,I,J,MODE,Z,M,BWLEN,EWLEN,WINC,PLTR
C      CHARACTER WTYPE*19,TTL*43,SIGNAL*43,TSMTH*25,CONTR*1
C      CALL EXCMS('FILEDEF 4 DISK TEST IN (PERM')
C      CALL EXCMS('FILEDEF 41 DISK PARAM IN (PERM')
C      CALL EXCMS('FILEDEF 61 DISK DATA OUT B (PERM')
C
C----- READ IN THE PARAMETER LIST -----
C      READ(41,400)MODE,PLTR,BWLEN,EWLEN,WINC,WTYPE,CONTR,TTL,
C      + SIGNAL,TSMTH
C      400  FORMAT(1X,I1,3X,I1,3X,I3,3X,I3,3X,I2/1X,A19/1X,A1/1X,A43
C      + /1X,A43/1X,A25)
C-----
C
C----- TEST TO ENSURE WINDOW LENGTH IS APPROPRIATE -----
C      I=N-1
C      IF ((BWLEN .GT. I) .OR. (EWLEN .GT. I)) THEN
C          WRITE(*,69)
C          GO TO 99
C      ENDIF

```

```

      I=MOD(BWLEN,2)
      K=MOD(WINC,2)
      IF (I .EQ. 0) THEN
        IF (K .EQ. 1) THEN
          WRITE(*,68)
          GO TO 99
        ELSE
          WRITE(*,67)
          GO TO 99
        ENDIF
      ENDIF
69  FORMAT (1X,'WINDOW LENGTH EXCEEDS LENGTH OF THE DATA')
68  FORMAT (1X,'WINDOW INCREMENT MUST BE EVEN')
67  FORMAT (1X,'INITIAL WINDOW LENGTH MUST BE ODD')
C
C-----
C
C----- PLOTTING DEVICE CALL -----
      IF (PLTR .EQ. 0) THEN
        CALL COMPR5
      ELSE
        CALL IBM79
      ENDIF
C-----
C
      PI=4*ATAN(1.)
      NX=512
      READ(4,*)(X(J),J=1,2*N,2)
C
C----- DATA INTERPOLATION -----
      DO 5 J=2,2*N,2
        X(J)=(0.,0.)
5     CONTINUE
      CALL FFT(2*N,X,FT)
      DO 10 J=N/2+2,2*N-N/2+1
        FT(J)=(0.,0.)
10    CONTINUE
      DO 20 J=1,2*N
        FT(J)=CONJG(FT(J))
20    CONTINUE
      CALL FFT(2*N,FT,X)
      DO 30 J=1,2*N
        X(J)=CONJG(X(J))/N
30    CONTINUE
C-----
C
C
      DO 111 Z=BWLEN,EWLEN,WINC
        WRITE(61,600)TTL,SIGNAL,TSMTH,WTYPE,Z
600  FORMAT(1X,A43/1X,A37/1X,A25/1X,A19,I3,' POINTS')
      M=(Z-1)/2
      AMAX=0
      AMIN=AMAX
      DO 40 I=1,2*N,2
        DO 50 K=0,512
          SAMP=(0.,0.)

```

```

        SAM=(0.,0.)
        IF ( (I+K) .LE. 2*N ) THEN
            SAMP=X(I+K)
        ENDIF
        IF ( (I-K) .GT. 0 ) THEN
            SAM=CONJG(X(I-K))
        ENDIF
C
C
        IF (K .LE. 2*M) THEN
            C(K+1)=SAMP*SAM*(0.54+0.46*COS(2*PI*K/(4*M)))
        ELSE
            C(K+1)=0
        ENDIF
C
C
        C(1024-K+1)=CONJG(C(K+1))
50    CONTINUE
        C(513)=(0.,0.)
        CALL FFT(1024,C,FT)
        DO 60 K=1,MODE*512,MODE
            IF (REAL(FT(K)) .GT. AMAX) THEN
                AMAX=REAL(FT(K))
            ENDIF
            IF (REAL(FT(K)) .LT. AMIN) THEN
                AMIN=REAL(FT(K))
            ENDIF
            IF ( (K.LT.514) .AND. (MODE .EQ. 2) ) THEN
                OUT(INT((K+1)/2+255),(I+1)/2)=REAL(FT(K))
            ELSE
                IF( MODE .EQ. 2 ) THEN
                    OUT(INT((K+1)/2-257),(I+1)/2)=REAL(FT(K))
                ELSE
                    OUT(K,(I+1)/2)=REAL(FT(K))
                ENDIF
            ENDIF
60    CONTINUE
40    CONTINUE
C
C-----FOR TIME SMOOTHING PURPOSES -----
        DO 48 K=1,512
            DO 46 I=1,N-2
                OUT(K,I)=(OUT(K,I)+OUT(K,I+1)+OUT(K,I+2))/3
46    CONTINUE
            DO 47 I=N,3,-1
                OUT(K,I)=(OUT(K,I)+OUT(K,I-1)+OUT(K,I-2))/3
47    CONTINUE
C
C----- DATA OUTPUT -----
        IF((K.GT.285).AND.(K.LT.310))THEN
            WRITE(61,601)
            DO 81 I=1,N
                WRITE(61,602)K,I,OUT(K,I)
81    CONTINUE
            ENDIF
601  FORMAT('FREQ BIN=',8X,'TIME BIN=',7X,'AMPLITUDE=')

```

```

602  FORMAT(10X,I4,13X,I4,14X,E14.7)
C-----
C
48  CONTINUE
C-----
C
C ----- PLOTTING -----
      IF (CONTR.EQ. 'C') THEN
        GO TO 52
      ENDIF
      CALL BSHIFT ( -0.2 , -0.25)
      CALL AREA2D(8,9)
      CALL VOLM3D(10,10,8)
      CALL HEADIN(TTL,100,1.,3)
      CALL HEADIN(SIGNAL,100,1.,3)
      CALL HEADIN(TSMTH,100,1.,3)
      CALL ANGLE(0.,0.)
      CALL MESSAG(WTYPE,100,2.5,9.3)
      CALL INTNO(Z,'ABUT','ABUT')
      CALL MESSAG(' POINTS ')$,100,'ABUT','ABUT')
      CALL X3NAME('FREQUENCY AXIS$',100)
      CALL Y3NAME('TIME AXIS$',100)
      CALL Z3NAME(' ',100)
      CALL VUANG(-65,70,700)
      CALL XNONUM
C     CALL ZNONUM
      CALL MX1ALF('STANDARD',' #')
      CALL MX2ALF('L/CGREEK','+')
      CALL ANGLE(-25.0)
      IF ( MODE.EQ. 2 ) THEN
        CALL MESSAG(' +-P# ',6,0.,2.3)
      ELSE
        CALL MESSAG(' +0# ',5,0.,2.3)
      ENDIF
      CALL ANGLE(-25.0)
      CALL MESSAG(' +P# ',5,4.9,0.15)
      CALL GRAF3D(-256,256,256,1,N,N,1.0*AMIN,.5*(AMAX-AMIN),
+1.0*AMAX)
      CALL SURMAT(OUT,512,512,1,N,0.)
      CALL ENDPL(0)
C
52  IF(CONTR.NE. 'A') THEN
      DO 49 I=1,N
        DO 51 K=1,512
          IF((OUT(K,I).LT. 5.0).AND.(OUT(K,I) .GT. -5.0)) THEN
            OUT(K,I)=0
          ENDIF
61      CONTINUE
49      CONTINUE
      CALL CONTOR(OUT,NX,N,TTL,SIGNAL,WTYPE,TSMTH,Z)
      ENDIF
C-----
C
      WRITE(61,603)AMAX,AMIN
603  FORMAT(1X,'MAXIMUM AMPLITUDE=',E14.7
+ /1X,'MINIMUM AMPLITUDE=',E14.7)

```



```

S = N/ISPACE
IWIDTH = ISPACE/2
DO 40 J=0,(IWIDTH-1)
  R = S*J
  ALPHA = 2.*PI*R/EN
  WTFAC = CMPLX( COS(ALPHA), -SIN(ALPHA))
  DO 30 ITOP=J,N-2,ISPACE
    IBOT = ITOP + IWIDTH
    TMP = X(IBOT+1)*WTFAC
    X(IBOT+1) = X(ITOP+1) - TMP
    X(ITOP+1) = X(ITOP+1) + TMP
30    CONTINUE
40    CONTINUE
50    CONTINUE
  RETURN
END

```

```

FFT00620
FFT00630
FFT00670
FFT00720
FFT00730
FFT00740
FFT00750
FFT00800
FFT00810
FFT00820
FFT00830
FFT00840
FFT00850
FFT00860
FFT01000
FFT01010

```

5. $|RD,|^2$

```

C**      THIS FORTRAN FILE COMPUTES THE SQUARED MAGNITUDE OF THE      ****
C**      RIHACZEK DISTRIBUTION                                         ****
C
C      INPUT DATA SEQUENCE IS READ USING FILEDEF 4, AS THE COMPLEX
C      ARRAY X(N).
C
C      N IS THE LENGTH OF THE DATA SEQUENCE AND IS ADJUSTED FROM THE
C      PARAMETER STATEMENT.  N MUST NOT EXCEED 128.
C
C      ANALYSIS PARAMETERS ARE READ USING FILEDEF 41.  THE PARAMETERS
C      ARE:
C
C          ARGUMENT TYPE      ALLOWED VAULUES
C
C      MODE - I1
C          1  PLOT 0 TO PI
C          2  PLOT PI TO PI
C
C      PLTR - I1
C          0  SHERPA LASER PRINTER
C          1  IMB79 GRAPHICS TERMINAL
C
C      BWLEN- I3
C          3  DIGIT INITIAL WINDOW LENGTH,
C             MUST BE AN ODD INTEGER
C      EWLEN- I3
C          3  DIGIT FINAL WINDOW LENGTH
C      WINC - I2
C          2  DIGIT WINDOW INCREMENT, MUST
C             BE AN EVEN INTEGER
C
C      WTYPE- A19
C          19 CHARACTER STRING USED IN THE
C             PLOT HEADER DISCRIBING THE
C             WINDOW USED.  THE CURRENT
C             WINDOW LENGTH IS AUTOMATICALLY
C             INCLUDED
C
C      CONTR- A1
C          1  CHARACTER STRING INDICATING
C             TYPE OF PLOT DESIRED
C
C             A  AMPLITUDE PLOT ONLY
C             C  CONTOUR PLOT ONLY
C             B  BOTH AMPLITUDE AND CONTOUR
C
C      TTL - A43
C          43 CHARACTER STRING USED IN THE
C             HEADING WHICH DESCRIBES THE
C             ALGORITHM AND THE CLASS OF
C             SIGNAL USED
C
C      SIGNAL- A43
C          43 CHARACTER STRING DESCRIBING
C             TEST SIGNAL
C
C      TSMTH- A25
C          25 CHARACTER STRING DESCRIBING
C             TYPE OF TIME SMOOTHING USED
C
C      OUTR  REAL
C            INITIALLY USED AS STORAGE FOR THE TIME SMOOTHED IPS, THEN
C            AS OUTPUT ARRAY OF DIMENSION 512 BY N

```



```

C      OUTI  REAL
C          ARRAY USED TO HOLD THE THE TIME SMOOTHED IMRD
C
C      SAMP  COMPLEX
C          SHIFTED VERSION OF X
C
C      SAM   COMPLEX
C          SHIFTED AND CONJUGATED VERSION OF X
C
C      RE    COMPLEX
C          ARRAY OF SUM OF PRODUCTS OF DIMENSION 1 BY 1025,
C          POSITIONS 1 - 512 ARE CONJUGATE SYMMETRIC WITH
C          POSITIONS 514 - 1025,  POSITION 513 = (0.,0.).
C
C      IM    COMPLEX
C          ARRAY OF DIFFERENCE OF PRODUCTS OF DIMENSION 1 BY 1025,
C          POSITIONS 1 - 512 ARE CONJUGATE SYMMETRIC WITH
C          POSITIONS 514 - 1025,  POSITION 513 = (0.,0.).
C
C      FTR   COMPLEX
C          ARRAY OF THE 1024 POINT TRANSFORM RE
C
C      FTI   COMPLEX
C          ARRAY OF THE 1024 POINT TRANSFORM IM
C
C      Z     INTEGER
C          LENGTH OF CURRENT WINDOW
C
C      M     INTEGER
C          MID-POINT OF THE CURRENT WINDOW
C
C      AMAX  REAL
C          MAXIMUM AMPLITUDE, USED TO SCALE VERTICAL AXIS
C
C      AMIN  REAL
C          MINIMUM AMPLITUDE, USED TO SCALE VERTICAL AXIS
C
C      NX    HORIZONTAL DIMENSION OF OUT WHICH IS ALWAYS 512
C
C      DATA CAN BE OUTPUT USING FILEDEF 61.  POINTS OF INTEREST MUST
C          BE DEFINED IN THE APPROPRAITE SECTION OF CODE.  BECAUSE
C          OF SPACE CONSTRAINTS, THE DATA OUTPUT FILE IS WRITTEN TO
C          THE B DISK.
C
C*****
C
C      PARAMETER(N= 64)
C      COMPLEX X(N),RE(1025),SAMP,SAM,FTR(1024)
C      COMPLEX IM(1025),FTI(1024)
C      REAL OUTR(512,N),OUTI(512,N),AMAX,AMIN
C      INTEGER NX,K,1,J,MODE,Z,M,BWLEN,EWLEN,WINC,PLTR
C      CHARACTER WTYPE*19,TTL*43,SIGNAL*37,TSMTH*25,CONTR*1
C      CALL EXCMS('FILEDEF 4 DISK TEST IN (PERM')
C      CALL EXCMS('FILEDEF 41 DISK PARAM IN (PERM')

```

```

PARAMETER(N= 64)
COMPLEX X(N),RE(1025),SAMP,SAM,FTR(1024)
COMPLEX IM(1025),FTI(1024)
REAL OUTR(512,N),OUTI(512,N),AMAX,AMIN
INTEGER NX,K,1,J,MODE,Z,M,BWLEN,EWLEN,WINC,PLTR
CHARACTER WTYPE*19,TTL*43,SIGNAL*37,TSMTH*25,CONTR*1
CALL EXCMS('FILEDEF 4 DISK TEST IN (PERM)')
CALL EXCMS('FILEDEF 41 DISK PARAM IN (PERM)')

```

```

CALL EXCMS('FILEDEF 61 DISK DATA OUT B (PERM')
C
C-----READ IN PARAMETER LISITNG-----
  READ (41,400)MODE,PLTR,BWLEN,EWLEN,WINC,WTYPE,CONTR,TTL,
  + SIGNAL,TSMTH
  400 FORMAT (1X,I1,3X,I1,3X,I3,3X,I3,3X,I2/1X,A19/1X,A1/1X,A43
  + /1X,A37/1X,A25)
C-----
C
C----- TEST TO ENSURE WINDOW LENGTH IS APPROPRIATE -----
  I=N-1
  IF ((BWLEN .GT. 1) .OR. (EWLEN .GT. 1)) THEN
    WRITE(*,69)
    GO TO 99
  ENDIF
  I=MOD(BWLEN,2)
  K=MOD(WINC,2)
  IF (I .EQ. 0) THEN
    IF (K .EQ. 1) THEN
      WRITE(*,68)
      GO TO 99
    ELSE
      WRITE(*,67)
      GO TO 99
    ENDIF
  ENDIF
  69 FORMAT (1X,'WINDOW LENGTH EXCEEDS LENGTH OF THE DATA')
  68 FORMAT (1X,'WINDOW INCREMENT MUST BE EVEN')
  67 FORMAT (1X,'INITIAL WINDOW LENGTH MUST BE ODD')
C-----
C
C----- PLOTTING DEVICE CALL -----
  IF (PLTR.EQ.0)THEN
    CALL COMPRS
  ELSE
    CALL IBM79
  ENDIF
C-----
C
  PI=4*ATAN(1.)
  NX=512
  READ (4,*)(X(J),J=1,N)
  DO 111 Z= BWLEN,EWLEN,WINC
  WRITE (61,600)TTL,SIGNAL,TSMTH,WTYPE,Z
  600 FORMAT (1X,A43/1X,A37/1X,A25/1X,A19,I3,' POINTS')
  CALL ANGLE(0.,0.)
  M=(Z-1)/2
  AMAX=0.
  AMIN=AMAX
  DO 10 I=1,N
    DO 20 K=0,512
      SAMP=(0.,0.)
      SAM=SAMP
      IF ( (I+K) .LE. N ) THEN

```



```

DO 200 K=1,512
DO 201 I=1,N
OUTR(K,I)=ABS(OUTR(K,I))
OUTI(K,I)=ABS(OUTI(K,I))
OUTR(K,I)=OUTR(K,I) + OUTI(K,I)
C
      IF (OUTR(K,I) .GT. AMAX) THEN
        AMAX=OUTR(K,I)
      ENDIF
      IF (OUTR(K,I) .LT. AMIN) THEN
        AMIN=OUTR(K,I)
      ENDIF
201      CONTINUE
200      CONTINUE
C+ - + - + - + - + - + - + - + - + - + - + - + - + - + - +
C-----
C
C----- PLOTTING -----
      IF (CONTR.EQ. 'C') THEN
        GO TO 50
      ENDIF
C
      CALL HEIGHT(0.28)
      CALL BSHIFT ( -0.2, -.25)
      CALL AREA2D(8,9)
      CALL VOLM3D(10,10,8)
      CALL HEADIN(TTL,100,1.,3)
      CALL HEADIN(SIGNAL,100,1.,3)
      CALL HEADIN(TSMTH,100,1.,3)
      CALL MESSAG(WTYPE,100,2.5,9.3)
      CALL INTNO(Z, 'ABUT', 'ABUT')
      CALL MESSAG('POINTS$',100, 'ABUT', 'ABUT')
      CALL X3NAME('FREQUENCY AXIS$',100)
      CALL Y3NAME('TIME AXIS$',100)
      CALL Z3NAME(' ',100)
      CALL VUANGL(-65,70,700)
      CALL XNONUM
      CALL ZNONUM
C
      CALL MX1ALF('STANDARD', '#')
      CALL MX2ALF('L/CGREEK', '+')
      CALL ANGLE(-25.0)
      IF ( MODE .EQ. 2 ) THEN
        CALL MESSAG(' +-P# ',6,0.,2.3)
      ELSE
        CALL MESSAG(' +0# ',5,0.,2.3)
      ENDIF
      CALL ANGLE(-25.0)
      CALL MESSAG(' +P# ',5,4.9,0.15)
      CALL GRAF3D(-256,256,256,1,N,N,1.0*AMIN,0.5*(AMAX-AMIN),
+ 1.0*AMAX)
      CALL SURMAT(OUTR,512,512,1,N,0.)
      CALL ENDPL(0)
      CONTINUE
50      IF (CONTR.NE. 'A') THEN
        CALL CONTOR(OUTR,NX,N,TTL,SIGNAL,WTYPE,TSMTH,Z)
      ENDIF
C-----

```


	X(NEWADR+1) = XTMP(K+1)	FFT00400
10	CONTINUE	FFT00410
	DO 50 L=1,M	FFT00530
	ISPACE = 2**L	FFT00610
	S = N/ISPACE	FFT00620
	IWIDTH = ISPACE/2	FFT00630
	DO 40 J=0,(IWIDTH-1)	FFT00670
	R = S*J	FFT00720
	ALPHA = 2.*PI*R/EN	FFT00730
	WTFAC = CMPLX(COS(ALPHA), -SIN(ALPHA))	FFT00740
	DO 30 ITOP=J,N-2,ISPACE	FFT00750
	IBOT = ITOP + IWIDTH	FFT00800
	TMP = X(IBOT+1)*WTFAC	FFT00810
	X(IBOT+1) = X(ITOP+1) - TMP	FFT00820
	X(ITOP+1) = X(ITOP+1) + TMP	FFT00830
30	CONTINUE	FFT00840
40	CONTINUE	FFT00850
50	CONTINUE	FFT00860
	RETURN	FFT01000
	END	FFT01010

APPENDIX B. CROSS IPS

Up to this point only autospectra have been discussed. Analysis of cross spectral characteristics of nonstationary phenomena can provide valuable information about the process. Equivalent to (1), a cross power spectral density is defined

$$P_{x_i x_j}(f) = \int_{-\infty}^{\infty} R_{x_i x_j}(\tau) e^{-j2\pi f\tau} d\tau. \quad (63)$$

For the case when x_i and x_j are uncorrelated then

$$\begin{aligned} P_{x_i x_j}(f) &= 2\pi\mu_i\mu_j\delta(f) \\ &= P_{x_j x_i}(f), \end{aligned} \quad (64)$$

where μ_i is the mean value. If the data is correlated the energy resulting from cross spectral analysis can be complex. By examining Parseval's theorem in a more general context,

$$\begin{aligned} \int_{-\infty}^{\infty} x_i(t)x_j^*(t)dt &= \int_{-\infty}^{\infty} X_i(f)X_j^*(f)df \\ &= \int_{-\infty}^{\infty} P_{x_i x_j}(f)df \\ &= R_{x_i x_j}(0), \end{aligned} \quad (65)$$

where $R_{x_i x_j}(0)$ is not necessarily real nor is the cross correlation function (CCF) necessarily conjugate symmetric about $R_{x_i x_j}(0)$. [Ref. 1]

All the spectral estimators previously discussed are applicable if the ACF estimate is replaced by with the CCF estimate. The bias for cross spectra may be much larger than an equivalent autospectra where the point of maximum overlap occurs at lag zero. In practice, the location of maximum overlap is unknown for CCF's. One interpretation of cross PSD are of importance, the case where x_i and x_j are two channels of a multi-channel system. The $|P_{x_i x_j}(f)|$ contains information concerning relative amplitudes at specific frequencies where the $\angle P_{x_i x_j}$ contains information concerning the lead or lag in phase between the two channels. [Ref. 3]

Applying IPS in a multi-sensor environment leads to the following defining equation,

$$IPS_{xy}(f,t) = \frac{1}{2} \int_{-\infty}^{\infty} (x(t)y^*(t-\tau) + x^*(t)y(t+\tau)) e^{-j2\pi f\tau} d\tau, \quad (66)$$

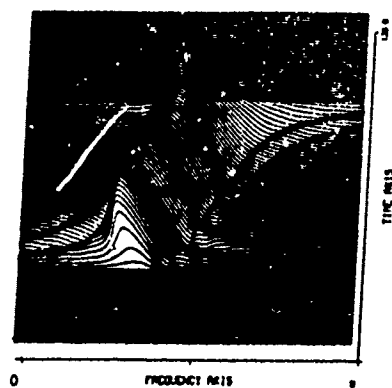
where signal y could be a delayed, noisy version of signal x . Using a rapidly changing, linearly chirped pulse $e^{j2\pi(\frac{10}{128}t + 20(\frac{t}{128})^2)}$ and implementing a windowed version of IPS_{xy} , two sample cross spectra are shown in Figure 50 and Figure 51.

The first spectra was created by beating the pulsed chirp $x(t)$ against a delayed version of itself. The cross spectrum is shown in Figure 50 (a). In this case the delay is 18 samples for a pulse 63 samples in duration. The cross spectrum can be seen in Figure 50 (b) and (c), where the spectral ridge over the interval corresponding to the absolute time of overlap. The maximum amplitude achieved on the cross-spectral surface is nearly the same as for the autospectra. The minimum however, is approximately 44% greater in magnitude than that found on the corresponding auto-spectral surface. IPS_{xy} does not appear to provide information which can estimate delay in reception for this class of signal.

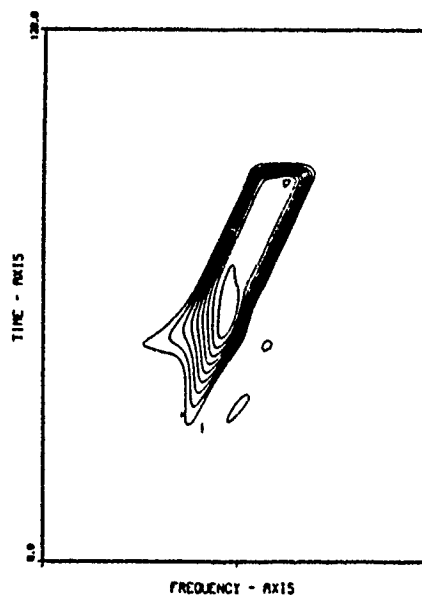
The second cross spectrum considered examines the ability of IPS_{xy} to indicate correlation between a pulsed chirp and a Doppler-shifted version of itself. In this case,

$$\begin{aligned} x(t) &= e^{j2\pi(\frac{10}{128}t + 20(\frac{t}{128})^2)} \\ y(t) &= e^{j2\pi(\frac{15}{128}t + 20(\frac{t}{128})^2)}, \end{aligned} \quad (67)$$

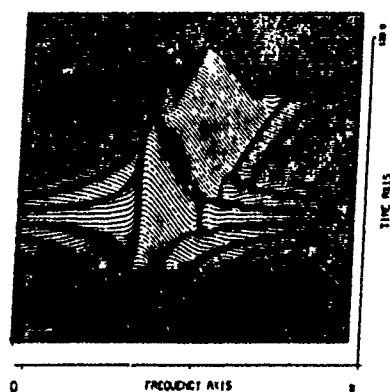
representing a shift of 50%. Figure 51 (c) shows an overlay of the two pulses. Figure 51 (b) is the contour for the cross spectrum. The peaks of the characteristically modulated ridge correspond to the line of overlap shown in (c). It is not clear if the cross spectrum of a linear chirp with a Doppler shifted version of itself yields information concerning the degree of coherence. The cross spectrum in Figure 51 could easily be interpreted as an autospectrum in which two, closely-spaced parallel chirps are present. This initial investigation into the behavior of IPS_{xy} suggests that a more detailed examination of its behavior is in order.



(a) IPS_y amplitude plot of original pulse

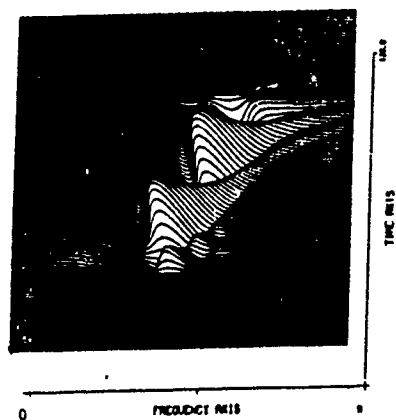


(b) IPS_{xy} contour plot

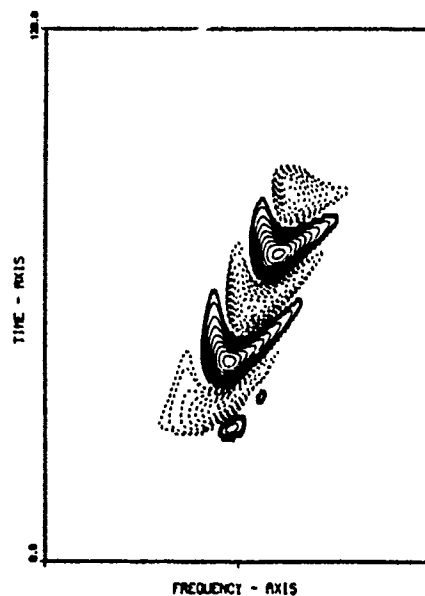


(c) IPS_{xy} amplitude plot

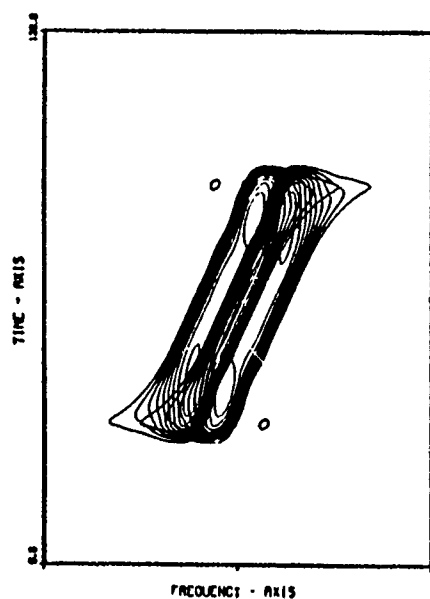
Figure 50. Cross spectral analysis of a pulsed linear chirp



(a) $IPS_{x,y}$ amplitude plot



(b) $IPS_{x,y}$ contour plot



(c) $IPS_{x,y}$ overlaid contour plots of the original and Doppler-shifted pulse

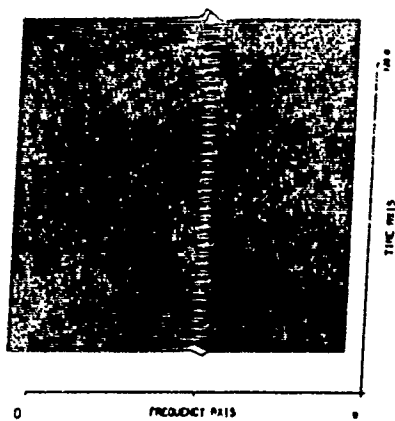
Figure 51. Cross spectral analysis for a Doppler-shifted linear pulse

APPENDIX C. CUMULANT

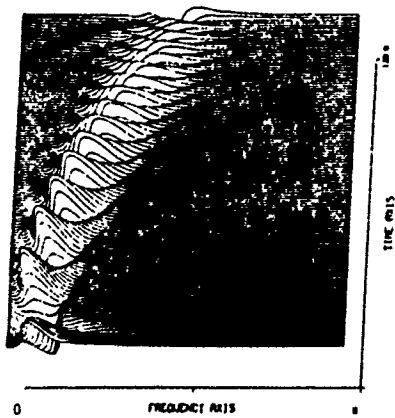
Assuming the received signal is corrupted by zero mean, Gaussian noise, examining the third-order moment or cumulant may yield information about the signal while suppressing the contributions of the noise. This potential processing gain is realized because the odd moments of a Gaussian process are identically zero. One way to implement IPS as an estimator of the cumulant is

$$\text{Cum. } IPS_{|RD|}(f, t) = \frac{1}{2} \int_{-\infty}^{\infty} \left(|x(t)|^2 x(t - \tau) + |x^*(t)|^2 x(t + \tau) \right) e^{-j2\pi f \tau} d\tau.$$

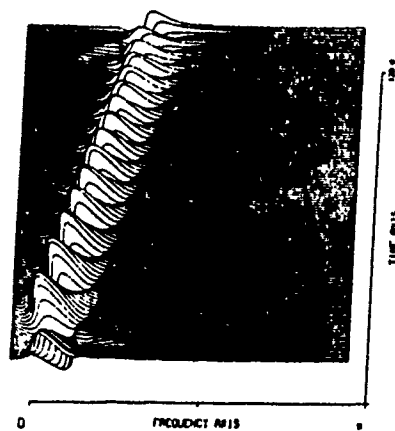
Looking only at the effect on noiseless signal data, some preliminary results can be seen in Figure 52. All signals are analytic, therefore the magnitude squared term is always unity. A comparison of the treatment of IPS , can be made by referring to Chapter IV, Section C (3): Test Case Results. This method of processing the cumulant of an analytic signal does not appear to provide any useful results. Further research should examine the behavior using real signals or possibly forming the approximation of the cumulant in a different fashion.



(a) Stationary signal



(c) Quadratic chirp



(b) Linear chirp



(d) FSK

Figure 52. The cumulant of various analytic signals

LIST OF REFERENCES

1. P. B. Peebles, Jr., "Spectral characteristics of random processes," in *Probability, Random Variables and Random Signal Principles*, pp. 172-204, McGraw Hill, New York, 1980.
2. Athanasios Papoulis, "Correlation and power spectrum of stationary processes," in *Probability, Random Variables and Stochastic Processes*, pp. 336-384, McGraw Hill, New York, 1965.
3. Steven M. Kay, *Modern Spectral Estimation: Theory and Application*, McGraw Hill, New York, 1980.
4. Fredric J. Harris, "On the Use of Windows for Harmonic Analysis with the Discrete Fourier Transform," *IEEE Proc.*, Vol. 66, No. 1 pp. 51-83, January 1978.
5. M. H. Ackroyd, "Instantaneous and Time-Varying Spectra: an Introduction," *The Radio and Electronic Engine*, Vol. 39, No. 3, pp. 142-152, March 1980.
6. O. D. Grace, "Instantaneous Power Spectra," *J. Acoust. Soc. Amer.*, Vol. 39, No. 3, pp. 191-197, January 1981.
7. W. Mecklenbräuker, "A Tutorial on Non-Parametric Bilinear Time-Frequency Signal Representations," *Les Houches, Session XLV, 1985*, J.L. Lacoume and R. Stora, eds., pp. 276-236, Elsevier Science Publishers B.V., 1987.
8. Richard B. Altes, "Detection, Estimation, and Classification with Spectrograms," *J. Acoust. Soc. Amer.*, Vol. 67, No. 4, pp. 1232-1246, April 1980.
9. Leon Cohen, "Generalized Phase-Space Distribution Functions," *J. Math Physics*, Vol. 7, No. 5, pp. 781-786, May 1966.

10. Leon Cohen, "Time-frequency Distributions - a Review," *Proc. IEEE*, Vol. 77, No. 7, pp. 941-981, July 1989.
11. C. H. Page, "Instantaneous Power Spectra," *J Appl. Phys.*, Vol. 23, pp. 103-106, 1952.
12. Morris J. Levin, "Instantaneous Spectra and Ambiguity Functions," *Trans. IEEE on Information Theory*, Vol. IT-10, pp. 95-96, January 1964.
13. R.M. Fano, "Short-Time Autocorrelation Functions and Power Spectra," *J. Acoust. Soc. Amer.*, Vol. 22, No. 5, pp. 546-550, September 1950.
14. M.R. Schroeder and B.S. Atal, "Generalized Short-Time Power Spectra and Autocorrelation Functions," *J. Acoust. Soc. Amer.*, Vol. 34, No. 11, pp. 1679-1683, November 1962.
15. Paulo M. D. Mónica de Oliveira, "Instantaneous Power Spectrum," Engineer's Thesis, Naval Postgraduate School, Monterey, California, March 1989.
16. August W. Rihaczek, "Signal Energy Distribution in Time," *Trans. IEEE on Information Theory*, Vol. 14, No. 3, pp. 369-374, May 1968.
17. E. P. Wigner, "On the Quantum Correction for Thermodynamic Equilibrium," *Phys. Rev.*, Vol. 40, No. pp. 749-759, 1932.
18. J. Ville, "Théorie et Applications de la Notion de Signal Analytique," *Câbles et Transmission*, Vol. 2, No. pp. 61-74, 1948.
19. T.A.C.M. Claasen and W.F.G. Mecklenbräuker, "The Wigner Distribution - a Tool for Time Frequency Signal Analysis, Part III: Relations with other Time-Frequency Signal Transforms," *Phillips J. Research*, Vol. 35, No. 6, pp. 372-389, 1980.

20. Boualem Bouashash "Notes on the use of the Wigner Distribution for Time-Frequency Signal Analysis," *Trans. IEEE ASSP*, Vol. 36, No. 9, pp. 1518-1521, September 1988.
21. Cornelis P. Janse and Arie J.M. Kaiser "Time-Frequency Distribution of Loudspeakers: the Application of the Wigner Distribution," *J. Audio Eng. Soc.*, Vol. 31, No. 4, pp. 198-216, April 1983.
22. H.I. Choi and W.J. Williams, "Improved Time-Frequency Representations of Multicomponent Signals Using Exponential Kernels," *Trans IEEE on Acoust., Speech and Signal Processing*, Vol. ASSP-37, 1989.

BIBLIOGRAPHY

Allard, Jean F. and Valiere, Jean C. and Bourdier R., "Broadband Signal Analysis with the Smoothed Pseudo-Wigner Distribution," *J. Acoust. Amer.*, Vol. 83, No. 3, pp. 1041-1044, March 1988.

Amin, Moeness G., "Sliding Spectra: A New Perspective," *Fourth Annual ASSP Workshop on Spectrum Estimation and Modeling*, pp. 55-59, IEEE Press, New York, 1988.

T.A.C.M. Claasen and W.F.G. Mecklenbräuker, "The Wigner Distribution - a Tool for Time Frequency Signal Analysis, Part I: Continuous Time Signals," *Phillips J. Research*, Vol. 35, No. 6, pp. 217-250, 1980.

T.A.C.M. Claasen and W.F.G. Mecklenbräuker, "The Wigner Distribution - a Tool for Time Frequency Signal Analysis, Part II: Discrete Time Signals," *Phillips J. Research*, Vol. 35, No. 6, pp. 276-300, 1980.

Cohen, Leon and Posch, Theodore E., "Positive Time-Frequency Distribution Functions," *Trans. IEEE on Acoustics, Speech and Signal Processing*, Vol. ASSP 33, No. 1, pp. 31-38, February 1985.

Flaska, M.,D., "Cross Correlation of Short Time Spectral Histories," *Acoust. Soc. Amer.*, Vol. 59, No. 2, pp. 381-388, February 1976.

Lampard, D.G., "Generalization of the Wiener-Khintchine Theorem to Nonstationary Processes," *J. App. Physics*, Vol. 25, No. 6, pp. 802-803, June 1954.

Mark, W.,D., "Spectral Analysis of the Convolution and Filtering of Nonstationary Stochastic Processes," *J. Sound Vib.*, Vol. 11, pp. 19-63, 1970.

Martin, W. and Flandrin, P., "Analysis of Nonstationary Processes: Short time Periodograms versus a Pseudo-Wigner Estimator," *Signal Processing II: Theories and Applications*, edited by H.W. Schüssler, pp. 455-458, Elsevier Science Publishers B.V., 1983.

Stutt, Charles A., "Some Results on Real-Part/Imaginary-Part and Magnitude/Phase Relations in Ambiguity Functions," *Trans. IEEE on Information Theory*, pp. 321-327, October 1964.

Urkowitz, Harry, "Pre-envelopes of Nonstationary Bandpass Processes," *J. Franklin Institute*, Vol. 277, No. 1, pp. 31-36, January 1964.

INITIAL DISTRIBUTION LIST

		No. Copies
1.	Defense Technical Information Center Cameron Station Alexandria, VA 22304-6145	2
2.	Library, Code 0142 Naval Postgraduate School Monterey, CA 93943-5002	2
3.	Professor Ralph D. Hippenstiel, Code EC/Hi Department of Electrical and Computer Engineering Naval Postgraduate School Monterey, CA, 93943-5004	3
4.	Professor Roberto Cristi, Code EC/Cx Department of Electrical and Computer Engineering Naval Postgraduate School Monterey, CA, 93943-5004	1
5.	Chairman, Code EC Department of Electrical and Computer Engineering Naval Postgraduate School Monterey, CA, 93943-5004	1
6.	Professor Charles W. Therrien, Code EC/Th Department of Electrical and Computer Engineering Naval Postgraduate School Monterey, CA, 93943-5004	1
7.	Professor Murali Tummala, Code EC/Tu Department of Electrical and Computer Engineering Naval Postgraduate School Monterey, CA, 93943-5004	1
8.	Naval Ocean Systems Center Attn: Dr. C. E. Persons, Code 732 San Diego, CA, 92152-5000	1
9.	Naval Ocean Systems Center Attn: LT E.H. Stitz, Code 30 San Diego, CA, 92152-5000	3